

MICROSCALE PROPERTIES OF THE ANNULUS FIBROSUS IN THE DISC: EFFECT OF DEGENERATION

By

Abraham Jacob

Thesis
Submitted to Flinders University
for the degree of

Masters Biomedical Engineering

Flinders University
16.10.2023

TABLE OF CONTENTS

TABLE OF CONTENTS	I
ABSTRACT	III
DECLARATION	IV
ACKNOWLEDGEMENTS	V
LIST OF FIGURES	VI
LIST OF TABLES	VIII
INTRODUCTION	1
LITERATURE REVIEW	3
Intervertebral disc and anulus fibrosis lamellae	3
Effects of region on micro-mechanical properties	4
Degenerative Grade of intervertebral disc	4
Micro-mechanical testing and effect of strain rate.....	4
Gaps in research.....	6
METHODOLOGY	6
Segmenting the IVD.....	8
Gripping the specimen	10
Transporting the specimen.....	12
Micromechanical testing	12
Data analysis and Quality control.....	13
RESULTS	15
Sandpaper fixation gripping outcome.....	15
Viscoelasticity	16
Average Hysteresis loss coefficient – tensile test.....	16
Average hysteresis loss coefficient – shear test.....	17
Average stiffness – Tensile test	18
Average stiffness – Shear test	19
Median stiffness and hysteresis loss coefficient.....	20
Failure load.....	21
Average failure load – Tensile.....	22
Average energy absorbed at failure – Tensile	22
Average failure load – Shear.....	23
Average energy absorbed at failure - Shear.....	24
Median failure load	25
Median energy absorbed	26
DISCUSSION	27
Hysteresis loss coefficient.....	27
Modulus.....	28
Failure load.....	30

Limitations	31
CONCLUSION AND FUTURE WORKS	32
BIBLIOGRAPHY	33
APPENDICES	35
Appendix A	35
Appendix B	35
Appendix C	36
Appendix D	39
Appendix E	54

ABSTRACT

The main region of focus in this study is the interlamellar matrix (ILM), which is situated between neighbouring lamellae of the annulus fibrosus (AF) and has a complicated pattern of elastic fibres, while elastic fibres of the intra-lamellar region are primarily parallel to the collagen fibres. Researchers have focused on the fundamental biomechanical functions of the interlamellar matrix, and its role in load distribution, shock absorption, and spinal flexibility are discussed, emphasising the importance of maintaining their integrity, thus establishing their clinical relevance. Studying the nature of the ILM can also help in tissue engineering methods to develop biomaterials that can help to alleviate pain and promote tissue healing.

The thesis investigates the impacts of intervertebral disc (IVD) degeneration, a multidimensional phenomenon driven by genetic, mechanical, and environmental variables, on the mechanical properties of the IVD. This was done by isolating and testing the non-destructive mechanical properties of the circumferential regions of healthy and degenerated discs and comparing them. Samples from various circumferential (anterior, anterolateral, lateral, posterolateral, and posterior) regions within the disc were used to assess variations, and the viscoelastic properties (stiffness and hysteresis loss coefficient) was evaluated by applying the load at three different strain rates. While similar studies to determine the delamination thresholds have been done before, this is the first time it has been done on human discs and analyzing all the regions. Future research into the numerous molecular and cellular mechanisms involved in degeneration will provide insight into potential treatment targets for reducing or stopping the degenerative cascade. Additionally, failure mechanics were studied using ultimate failure load and energy absorbed analysis. Prior to working with human tissue, extensive practice testing was done on ovine specimens to ensure the procedure's repeatability, and then the results were confirmed by pilot testing on human specimen.

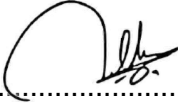
Higher modulus and strength were found in the anterior regions, as opposed to the posterior and lateral regions, while degeneration grade had a noticeable effect on the ultimate strength of some regions but not all. A strong strain rate dependency supported the human ILM's viscoelastic characteristics. The modulus and ultimate stress were also influenced by the loading direction. These findings offer a new perspective on human ILM mechanics and serve as a solid foundation for further research in the area.

The findings of this study hold great promise for furthering our understanding of intervertebral disc health and aiding the development of novel treatment strategies, potentially transforming spinal disease therapy and improving patients' quality of life.

DECLARATION

I certify that this thesis:


1. does not incorporate without acknowledgment any material previously submitted for a degree or diploma in any university
2. and the research within will not be submitted for any other future degree or diploma without the permission of Flinders University; and
3. to the best of my knowledge and belief, does not contain any material previously published or written by another person except where due reference is made in the text.

Signature of student.....

Print name of student.....Abraham Jacob.....

Date : 16/10/2023

I certify that I have read this thesis. In my opinion it is is not (please circle) fully adequate, in scope and in quality, as a thesis for the degree of <Degree Name>. Furthermore, I confirm that I have provided feedback on this thesis and the student has implemented it minimally/partially/fully (please circle).


Signature of Principal Supervisor.....

Print name of Principal Supervisor.....John Costi

Date.....16/10/2023

ACKNOWLEDGEMENTS

I would like to express my sincere gratitude to my primary supervisor Associate Professor John J. Costi for mentoring me. He instilled the confidence in me to see it through till the end. In spite of his hectic schedule, he always found time to respond to my concerns and doubts in the most constructive manner. I would especially like to thank my secondary supervisor, Michael P. Russo for all the support he has provided me. He always went out of his own way to tend to my troubles in the lab. He also taught me some valuable technical skills that helped me to complete this thesis in a professional manner. I will always be grateful for the time and expertise that Michael and John have given me through their constructive feedback was invaluable expertise.

I would also like to extend my thanks to my mother and father. If it was not for their love and prayers, I would not have been able to reach this far in this endeavour. My partner has been a source of moral support for me during the last few weeks of this course and I am grateful to her for it.

Special thanks to my friend Radhwa who has been with me every step of this journey. Her cheerful nature inspired me to keep going to the lab every day while working on this thesis. Also Maddy and Nelufer deserve special praise for their encouraging words and made the time in the lab less stressful.

LIST OF FIGURES

Fig. 1 Schematic representation of spinal anatomy (left) and the heterogeneous tissue composition of the intervertebral disc (IVD) (right).....	1
Fig. 2 Anterior schematic of the annulus fibrosus, showing the coordinate system with the radial, circumferential, and axial directions, which corresponds to the 1, 2, and 3 directions, respectively..	2
Fig. 3 Sections of the annulus fibrosus used to define their different properties (modified from Jo and Chae 2021)	6
Fig. 4 Three testing phases in the study.....	7
Fig. 5 The sheep intervertebral disc (b) was separated from the FSU (a). 5mm wide segments are separated from the disc (c)	8
Fig. 6 A 3D printed platform (a) lined with tape to contain the sample and OCT (a) is loaded onto the microtome (b) and the specimen segment is placed in it (c)	9
Fig. 7 The specimen is set at -20°C (b) with OCT fluid filled in it (a). A feather blade (c) was used to slice the specimen measuring 1mm height.....	9
Fig. 8 Two slices (1mm thickness) are obtained (a). Sandpaper strips (b) and glue are used for gripping the specimen.....	10
Fig. 9 Functional lamellae unit consisting of two adjacent lamellae and ILM in between is gripped using sandpaper and glue.....	10
Fig. 10 Preparing specimen for micromechanical testing in shear (a) and tensile (b) directions. Specimens are clamped between two slides for fixing the glue and for transportation (c,d).	11
Fig. 11 The specimen prepared was loaded on the cellscale device for micromechanical testing in shear direction.	11
Fig. 12 The specimen prepared was loaded on the cellscale device for micromechanical testing in tensile direction.....	12
Fig. 13 CellScale micromechanical testing device used for uniaxial testing.....	13
Fig. 14 Stress vs strain graph – slow, medium, and fast strain rate.....	14
Fig. 15 Stress vs strain graph – final cycle with young’s modulus calculated by linear regression	14
Fig. 16 Pictures taken at different points of the testing cycle shows no evidence of slippage.	15
Fig. 17 plot of final cycle showing loading and unloading curve.....	16
Fig. 18 Median (interquartile range) hysteresis loss coefficient for tensile tests – comparing healthy and degenerated discs at three strain rates (slow, medium and fast).....	17
Fig. 19 Median (interquartile range) hysteresis loss coefficient for shear tests – comparing healthy and degenerated discs at three strain rates (slow, medium and fast).....	18
Fig. 20 Median (interquartile range) stiffness for tensile tests – comparing healthy and degenerated discs at three strain rates (slow, medium and fast).....	19
Fig. 21 Median (interquartile range) stiffness for tensile tests – comparing healthy and degenerated discs at three strain rates (slow, medium and fast).....	20
Fig. 22 Comparison of median values calculated and plotted showing quartile errors	21
Fig. 23 Force vs displacement graph showing maximum failure load.....	21
Fig. 24 Average failure loads – comparing healthy and degenerated discs in tensile testing	22
Fig. 25 Average energy absorbed at failure – comparing healthy and degenerated discs in tensile test.....	23
Fig. 26 Average failure loads comparing healthy and degenerated discs in shear testing	24

Fig. 27 Average energy absorbed at failure – comparing healthy and degenerated discs in shear test.....	25
Fig. 28 Median failure loads comparing healthy and degenerated discs in both tensile and shear testing.....	26
Fig. 29 Median energy absorbed comparing healthy and degenerated discs in both tensile and shear testing.	26
Fig. 30 Specimen number 4696 excluded from results.....	28
Fig. 31 Specimen number GL406	28
Fig. 32 GL471 sample showed much higher stiffness in the slow strain rate test	29
Fig. 33 Comparison of the effect of the extra tissue on GL471 compared to another specimen from same region and degradation grade (medium strain rate)	29

LIST OF TABLES

Table 1 Human discs taken from different levels of the lumbar spine, graded according to Thompson scale and segmented into regions. Regions – ANT – anterior, ALT – anterolateral, POS – posterior, PLT – posterolateral, LAT - lateral.....	7
--	---

INTRODUCTION

Intervertebral disc herniation is one of the most frequent root causes of chronic low back and neck pain and it has been found that patients with lumbar and cervical disc herniation were more likely to suffer from mood and anxiety disorders as well (Finneson and Schmidek, 2000). According to the AIHW, 2023, back pain and related problems contributed to the leading cause of burden on the economy due to disease, accounting for 4.2% of Australia's total disease burden. Financially, it costs the health system approximately \$3.4 billion a year that translates to 2.4% of total health expenditure (AIHW, 2023,). These findings very well indicate that lower back pain has considerable effect on the socioeconomic problem that effects 1 in 6 people in the country, as a result of hospitalization and loss of productivity.

The intervertebral discs (IVDs) are made up of three parts: the nucleus pulposus (NP), the annulus fibrosus (AF), and the endplate. Its configuration is such that the AF surrounds the NP and is encompassed between the endplates (figure 1). The primary role of the IVD is to give structural support and movement (Bogduk, 2002). It is positioned between neighbouring vertebrae in the spine and functions as a cushion, stress absorber, and spacer between the vertebrae. It is principally supported by the annulus fibrosus.

Figure removed due to copyright restriction

Fig. 1 Schematic representation of spinal anatomy (left) and the heterogeneous tissue composition of the intervertebral disc (IVD) (right). Insets (right) show matrix organization (scanning electron microscopy, gray) and cell organization (fluorescence) for anulus fibrosus (AF) and nucleus pulposus (NP) regions. AF matrix is composed of aligned collagen I fiber bundles, while a much random distribution of collagen II bundles and proteoglycan is observed in the NP. Fluorescence insets are rat IVD cells stained for collagen VI (green) and nucleus (red) revealing the different cellular arrangement in each tissue area (Adapted from Cao et al, 2007)

IVD herniation does not always progress linearly via the annulus fibrosus (AF) but might migrate circumferentially due to localised AF delamination due to the characteristic rostral-caudal orientation of the fibres, the AF restricts spinal flexion, extension, and torsion (Waxenbaum et al., 2017). As a result, resistance to delamination is a significant determinant in defining herniation progression risk. Delamination of the AF lamellae has been found to be related to failure of the ILM, and quite possibly

could be resulting in IVD degeneration (Bruehlmann S. B. et al., 2002). Because of this deformation, the inter-lamellar matrix (ILM) and the AF layers are both susceptible to shear and tensile strain. Shear strain in a deteriorated disc can induce lamellae to separate, and Tavakoli et al. (2016) discovered that the ILM has the highest probability of failure beginning. It is probable that the onset of this failure will cause or hasten disc degeneration. To understand the loading parameters that place the AF at risk of delamination and subsequent disc disruption and herniation, the ILM structure and mechanics of delamination must be understood. This knowledge of the ILM could contribute to the development of better clinical techniques for disc herniation and painful degenerative disc diseases. When discs that are prone to degeneration become more irregular as lamellae structure deteriorates with age, diseases like scoliosis develop, which results in the loss of the structural boundaries between lamellae. This correlation between the ILM disorganization and disc degeneration has been demonstrated by Tavakoli and Costi, 2018. The methodology used in the current study is adapted from the research done by Tavakoli, that focused on determining the mechanical characteristics of the AF in both the microscale and nanoscale levels. This experiment delves into the effects that degeneration of the AF has on the mechanical properties of the IVD, with the region of study being the interlamellar matrix. This was a significant gap in Diana Pham's research as it focused mainly on testing the AF lamellae.

The purpose of this research was to ascertain how degeneration affected the micromechanical characteristics of the human ILM. A validated testing approach was created using a micromechanical testing instrument (BioTester, CellScale, Waterloo, ON, Canada) to characterize the viscoelastic (non-destructive) and failure (destructive) properties of the ILM in ovine discs (Tavakoli et al., 2018). The discs were loaded at three distinct strain rates in both the radial and circumferential directions (figure 2) to determine the viscoelastic characteristics. It was deduced that even in a degenerated state, the ILM exhibits viscoelastic behaviour, with a rise in modulus but a decrease in strength and peak stress.

Figure removed due to copyright restriction

Fig. 2 Anterior schematic of the annulus fibrosus, showing the coordinate system with the radial, circumferential, and axial directions, which corresponds to the 1, 2, and 3 directions, respectively. The fiber angle is measured from the spine axis. The fiber directions are indicated by and while and are perpendicular to the fibers.

LITERATURE REVIEW

The intervertebral disc is an important part of the human musculoskeletal system. It has attracted significant attention from researchers over the years, making it a subject of considerable examination. The interlamellar matrix plays a vital role to the disc's function, and therefore, understanding the mechanical and biological elements of spinal health and degeneration is dependent on the interaction between the intervertebral disc and its interlamellar matrix. This section aims to shed light on the distinct interdependence of the intervertebral disc and its interlamellar matrix, bridging the gap between structure and function.

Intervertebral disc and anulus fibrosis lamellae

The IVD is made up of a central nucleus that is initially gelatinous but gradually loses moisture as it ages and an outer fibrous anulus that is inserted into the rim of each vertebral body. The anulus fibrosis and a layer of hyaline cartilage covering the face of each vertebral body endplate work together to prevent the tendency for the nucleus to be ejected under the very high stresses sustained by the disc (Cassidy et al., 1989). Around the NP, the lamellae that make up the AF create continuous layers in the shape of cylindrical walls, with collagen fibres running parallel to one another in each layer. In each succeeding layer, the fibre orientation changes in relation to the axis (Cassidy et al., 1989). It can be inferred that the mechanical character of the AF is influenced by this structure. According to Cassidy et al. (1989), the AF's X-ray diffraction under compression revealed an increase in the interlamellar angle. The stress-strain curve under compression would therefore produce a low modulus toe zone, a linear region would suggest fibre expansion, and a yield region, according to the hierarchical structure's response. For the disc to operate normally, the AF's integrity is crucial. (Thompson, R.E. *et al.*, 2000).

Studies done by Guerin and Elliott, 2006, and O'Connell et al., 2009 explored the toe modulus (E_T) of multiple lamellae in the AF in the circumferential direction, while Fujita et. al, 1997, and Smith et al., 2008, observed it in the radial direction. From Guerin and Elliott's observation of the fibre angle, using Fast Fourier Transform (FFT) image processing tools, it was evident that the angle of orientation of the collagen fibres and mechanical properties were correlated to the age and grade of the disc samples. AF fibres reoriented towards the direction of loading, with at least 17° reduction in fibre angle for the healthy disc samples and 9.5° for degenerated samples, indicating that fibre reorientation as a result of degeneration may significantly affect the mechanical properties. Therefore, degenerated disc undergoes bulging and decrease in stability due to the inability of fibres to reorient (Guerin and Elliott, 2006, and O'Connell et al., 2009).

Effects of region on micro-mechanical properties

For research, the AF is broken down into circumferential regions which run parallel to the outer circumference of the IVD – these regions are anterior, anterolateral, lateral, posterolateral and posterior, and in the radial direction they are divided into inner (closer to the NP) and outer regions (closer to the periphery). This division of the AF allows to better understand the anatomical variations in the disc as forces generated by different loading conditions of the spine are not distributed evenly across the disc.

Studies done by Fujita et al., 1997, demonstrated that the specimen's deformation was focused within the interlamellar matrix between the lamellae when it was extended. When the ILM was loaded, the radial tensile modulus increased by 250% before failing under greater strain, although specimens from the centre of the AF were stiffer and failed at lower strain rates than those from the inner and outer regions. The anisotropic nature of the AF was clearly confirmed in this work. Moreover, the specimens from the middle AF were found to be stiffer and failed at lower strains than those from the inner and outer areas.

Degenerative Grade of intervertebral disc

The Thompson Scale technique (Table 1) has been employed as a benchmark in various degeneration research (Thompson, J.P. et al., 1990). Acaroglu, 1985, for example, categorized the discs into five groups: grade I (normal), grades II and III (mildly degenerated), and grades IV and V (severely degenerated). See appendix A.

Micro-mechanical testing and effect of strain rate

Research done by Tavakoli et al, 2018 found that when IVD was tested under stress, in comparison to the control group, the ILM failure stress under radial and circumferential loading was significantly lower in the pre-herniation and herniation groups. The pre-herniated group is a group of discs in which microstructural damage was induced, as compared to the herniated disc that was already herniated. The lamella, however, showed no difference in failure stress across the three groups. This implied that the delamination of the lamellae initiated at the ILM. This observations at the lamellae signifies a relation to degeneration and the presence of disc tears in degenerated discs. Tavakoli also demonstrated that the failure stress under both radial and circumferential loading conditions was affected considerably by pre-herniation as well as in herniated group of specimen used. Moreover, after pre herniation it was found that there was not much difference in failure stress when compared to the herniated group, which led the researchers to conclude that at loads below those required to cause herniation, the ILM was at risk of mechanical injury. The lamella, however, showed no difference in failure stress across the three groups. The anterior and posterolateral regions tested in the pre herniated and herniated discs both resulted in a loss of distinction between the lamellae and ILM boundaries. In addition, it was also found that the ILM in the posterolateral region of the pre

herniated disc had a lower failure stress when compared to the anterior. These findings suggested that the lamellae and ILM have a dependency on the region. The higher mechanical strength in the outer lamellae of the anterior region is likely because of the highly packed collages and elastic fibres, whereas the ILM consists mostly of elastic fibres.

Porcine AF samples were examined in the circumferential and axial directions by Gregory & Callaghan, 2010, under three different strain rates: 1, 2 and 4%/s. However, stiffness and maximum stress did not differ between strain rates, as expected given that the three strain rates used in these trials were not significantly different. This was true for specimens taken from inner and outer regions of the AF's posterior and anterior regions. J. Tavakoli and J.J Costi., 2018, on the other hand, studied various strain rates of 1 Hz, 10 Hz, and 100 Hz, a wider range of speeds when compared to Gregory & Callaghan, 2010, and discovered that as the strain rate increased, so did the stiffness in all specimens undergoing compression, taken from all circumferential regions. Therefore, it was concluded that intervertebral disc cells exhibit viscoelastic solid behaviour.

The ILM's structure has been studied by several researchers using techniques such as light microscopy (Cassidy et al., 1989), layer by layer peeling method employing stereo microscopy (Marchand et al., 1990) and histological and immune histochemical detection (Yu et al, 2002). Cassidy et al., 1989, established that the lamellae of the AF are distinct and separate from each other, but there was no visible interconnection between them. The lamellae varied in thickness at different radial locations, where it averaged 100-130um at the periphery, and 260 um as the lamellae moved 2.2 mm towards the centre of the disc. This division of the lamellae according to thickness divides the anterior part of the IVD into peripheral and transitional regions. It is mainly made up of a non-fibrillar matrix, elastic fibres, and cells, with cross bridges transversing in the radial direction across the ILM and lamellae of the AF. The matrix is mainly composed of proteoglycans, lipids and elastic fibres (Sivan et al, 2014). Compressive loads are always applied to the IVD and it results in high intradiscal pressure. Though the peel test represents a tensile loading process that's consistent with compressive loads, further experimenting was required to measure the mechanical and viscoelastic behaviour of the ILM under direct tensile and shear loading. This direct testing of the mechanical properties of the ILM was done by Tavakoli and Costi, 2018, by experimenting on an ovine model. The research found that the overall effects of strain had no significant effect on the loading direction. Extensibility was also found to be insignificantly affected by the strain rate and loading direction. Moreover, the average stiffness of the ILM samples was found to increase with increasing strain rate.

Marchand et al, 1990 peeled the AF layer-by-layer and examined the cut surfaces through a microscope to establish how the structure of the annulus varied depending on the circumferential and radial positions. It was concluded that the AF comprises 15 to 25 layers and the thickness of the

layers varied throughout the AF, from minimum 0.14 mm to 0.52mm, depending on the distance from the nucleus.

Gaps in research

Tavakoli et al., 2018 effectively investigated the micromechanical parameters of an ovine model, but the effects of degeneration on the human ILM were not validated. Former master's research student's Ushmita Reebye and Ali Kaisi too had adapted Tavakoli's methodology to study the mechanical properties of the ILM, but this is the first study that focuses on all the regions together and comparing both degenerated and healthy discs. Therefore, the main aims of this research were to study the mechanical properties of the ILM taken from all 5 regions of the AF, obtained from two groups of healthy and degenerated IVD, and to do a comparison of their hysteresis loss coefficient, stiffness, as well as failure properties

METHODOLOGY

The human discs required for the study were obtained from the Biomechanics and Implants Laboratory at Flinders University, Tonsley. Three of these were grade 2 (healthy discs) and the other two grade 4 (degenerated discs) (Table 2). The sample preparation and gripping method used was adopted from Tavakoli and Costi, 2018 (figure 3). For this experiment the IVDs were defined in the regions as shown in figure 6. The regions are abbreviated as ANT – anterior, ALT - antero-lateral, LAT – lateral, PLT – posterolateral, and POS - posterior.

Figure removed due to
copyright restriction

Figure removed due to copyright restriction

Fig. 3 Sections of the annulus fibrosus used to define their different properties (modified from Jo and Chae 2021)

There were three testing groups that all utilise the same methods: Practise (n=6, on sheep) to acquire the necessary skills; Pilot (n=1, healthy human) (Table 2) to formalise the skills on a human specimen; Pilot testing was done on one human IVD sample (GL191447). This testing phase was conducted to validate the testing methodology laid out by Tavakoli et al., 2018. Two slices each (1mm thickness) was taken from each circumferential region of the disc with the help of a handheld microtome (Figure 6b). During the pilot testing phase it was found that the ideal width of a human ILM segment is 5 mm as it provided enough length and avoided curvature of the outer ILM in the radial direction, making it easier to prepare the specimen for micromechanical testing. (Figure a,b,c). Formal testing (n=2 healthy, and n=2 degenerated) (Table 2). After each of the testing phase, quality control checks were made to ensure that the data was appreciable.

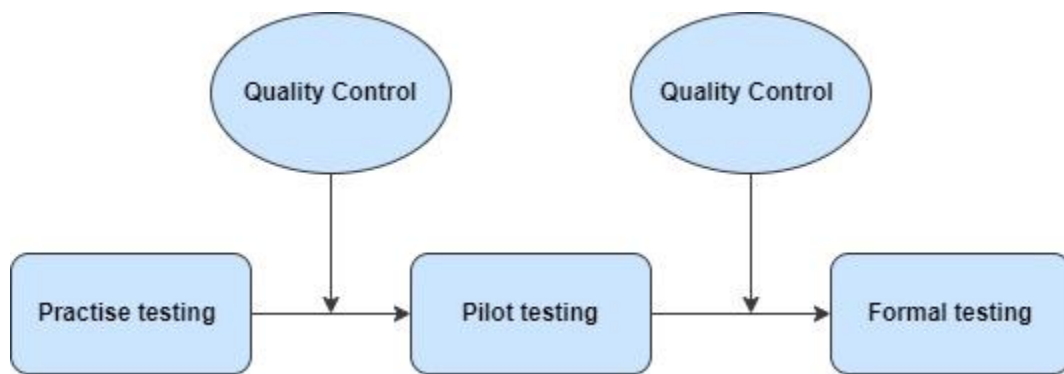


Fig. 4 Three testing phases in the study

Table 1 Human discs taken from different levels of the lumbar spine, graded according to Thompson scale and segmented into regions. Regions – ANT – anterior, ALT – anterolateral, POS – posterior, PLT – posterolateral, LAT - lateral

Sample number (test phase)	Age/Gender	Level	Grade	Regions
4696 (Formal study)	58/M	L5-S1	Grade 2	ALT, LAT, POS
GL406 (Formal study)	53/M	L3-L4	Grade 2	ANT, LAT, PLT
5194 (Formal study)	55/M	L2-L3	Grade 4	ANT, ALT, LAT
GL471 (Formal study)	65/M	L4-L5	Grade 4	ANT, ALT, LAT, PLT, POS
GL191447 (Pilot study)	34/M	L2-L3	Grade 2	ANT, ALT, LAT, PLT, POS

Samples 4969, GL406 and 5194 did not have all 5 regions on the disc available for creating specimen as the non-available parts were used by other researchers prior to this study. The detailed steps and methodologies used are presented in sections below in the order at which they were applied. Pilot testing was done on one human IVD sample (GL191447). This testing phase

was conducted to validate the testing methodology laid out by Tavakoli et al., 2018. Two slices each (1mm thickness) was taken from each circumferential region of the disc with the help of a handheld microtome. During the pilot testing phase it was found that the ideal width of a human ILM segment is 5 mm as it provided enough length and avoided curvature of the outer ILM in the radial direction, making it easier to prepare the specimen for micromechanical testing. (Figure a,b,c).

Segmenting the IVD

Practise was done on sheep IVD samples (n=12) that were isolated from sheep functional spine units (FSUs) (Figure 5 a, b). Due to the difficulty in obtaining cadaver material, sheep are increasingly being used as a model for spine research.

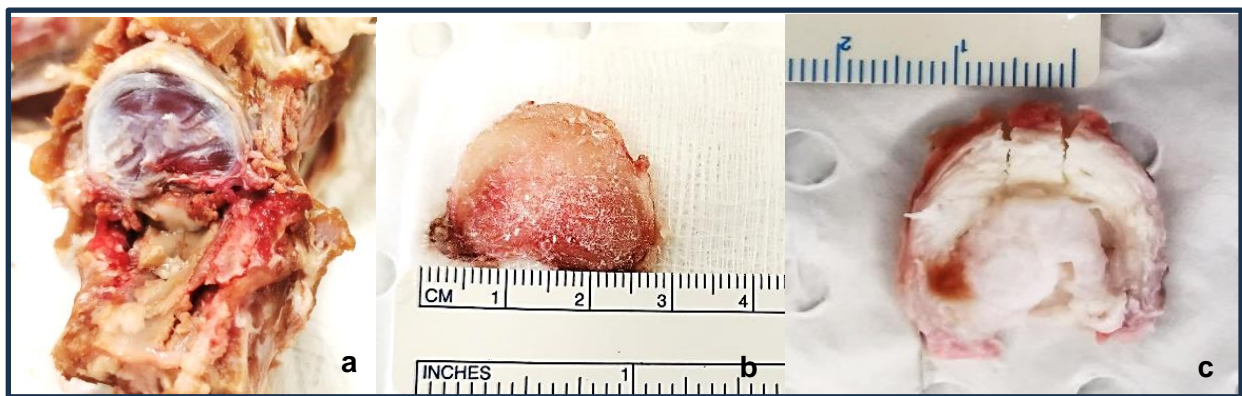


Fig. 5 The sheep intervertebral disc (b) was separated from the FSU (a). 5mm wide segments are separated from the disc (c)

According to study, sheep and human spines have biomechanical and molecular similarities (Wilke et al., 1997). The isolated ovine discs were then segmented into the respective circumferential regions (5mm wide blocks) with 1 mm thickness - anterior (ANT), anterolateral (ALT), lateral (LAT), and posterolateral (PLT) (Figure 5c). In the ovine disc, the AF was lacking in thickness at the posterior region and couldn't be sliced using a handheld microtome. The IVD to be tested was first frozen at -20°C . The frozen disc was then segmented into its regions for testing (Figure 6), using a scalpel blade. Care was taken to make dissecting cuts at 90° angles to the ILM and immediately after taking them out of the freezer. The 5 mm wide segment were wrapped in gauze and sprayed with Phosphate buffered saline (PBS) solution, then wrapped with cling wrap and stored in labelled airtight containers till the time for testing

The handheld microtome (Figure 6 b) consists of a rotating dial for raising/lowering the stage, and a platform (Figure 6 a) for placing the sample in (Figure 6 c).

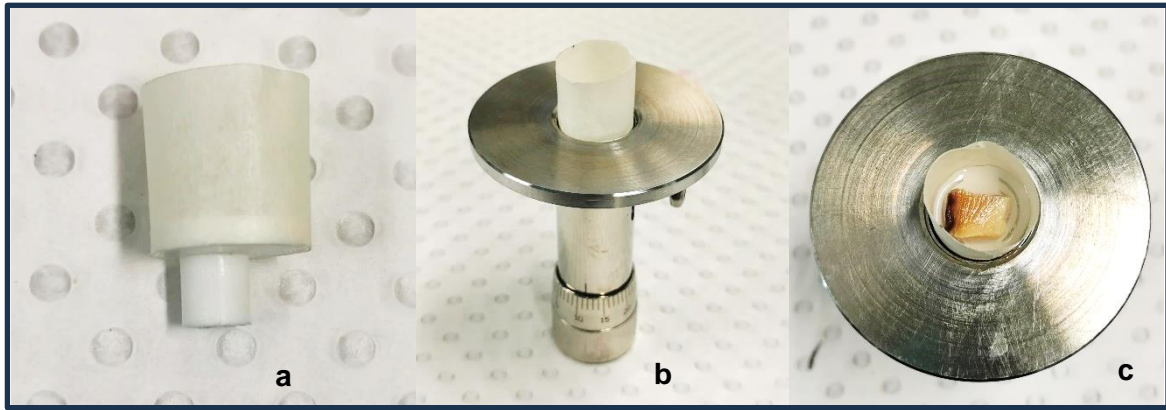


Fig. 6 A 3D printed platform (a) lined with tape to contain the sample and OCT (a) is loaded onto the microtome (b) and the specimen segment is placed in it (c)

To define the transverse cutting plane, each AF tissue was moulded using optimal cutting temperature (OCT, Tissue-Tek, Sakura, Japan) compound. The segment of the disc when ready for testing is thawed and set in within the prepared microtome, in the freezer at -20°C , for at least 45 minutes (Figure 7b).



Fig. 7 The specimen is set at -20°C (b) with OCT fluid filled in it (a). A feather blade (c) was used to slice the specimen measuring 1mm height.

Once this is set, two 1 mm slices were obtained from the frozen sample using a feather blade (Figure 7c). The specimen slices were then sprayed with Phosphate buffered saline (PBS) again to dissolve the OCT surrounding it (Figure 8a). Two slices were taken from each sample, one for tensile test (S01) and the other for shear test (S02). A total of 48 slices were obtained from six IVDs.

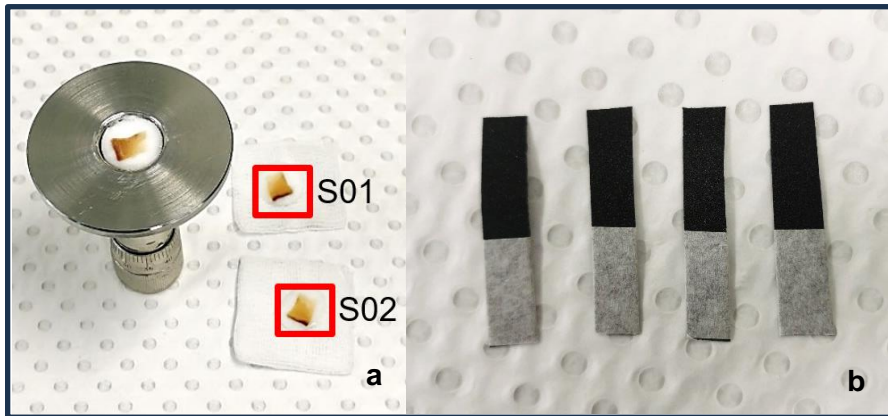


Fig. 8 Two slices (1mm thickness) are obtained (a). Sandpaper strips (b) and glue are used for gripping the specimen

Gripping the specimen

The specimen is then placed on a slide in preparation for gripping. Four sandpaper strip (wet and dry, 180 grit) of 7 mm width and 45-60mm length are required (Figure 8 b). Using a magnifying glass, a functioning lamellae unit was identified from the specimen's adjacent lying lamellae, that consisted of two adjacent lamellae and the ILM between them (Figure 8.).

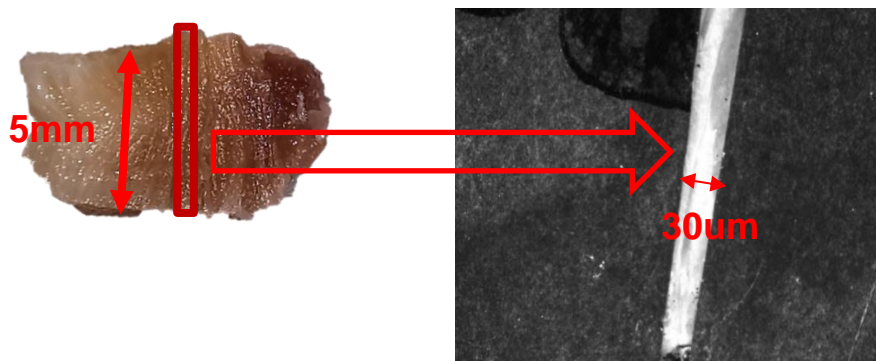


Fig. 9 Functional lamellae unit consisting of two adjacent lamellae and ILM in between is gripped using sandpaper and glue

The glue used for gripping is Loctite 480, which is a slow setting (approximately 2 minutes), black coloured glue. The dyed glue was selected so that any leakage of the glue onto the ILM can be observed. This ensured that the mechanical properties being measured were not a result of the altered ILM mechanics. The glue was spread evenly on the strips using a needle and then while observing under the magnifying glass, it was pressed onto the sample with precision, such that it grips the periphery of the ILM from either side on the top and bottom. Therefore, the only region of the specimen that isn't gripped by the sandpaper is the ILM and any force applied to the sandpaper

is directly propagated onto the ILM. The second slice from the specimen was wrapped in gauze, rehydrated with a spray of PBS, then covered with cling wrap and stored on ice packs (0°-5°C) while the first slice is being prepared and tested. The slices were not frozen again, but tested on the same day so that the micromechanical properties were not affected by repeated freeze thawing cycles. The specimens are prepared to test them firstly in the tensile stress direction (Figure 11), and the second slice is glued such that the force applied by the cellscale is acting in the shear (Figure 10) direction.

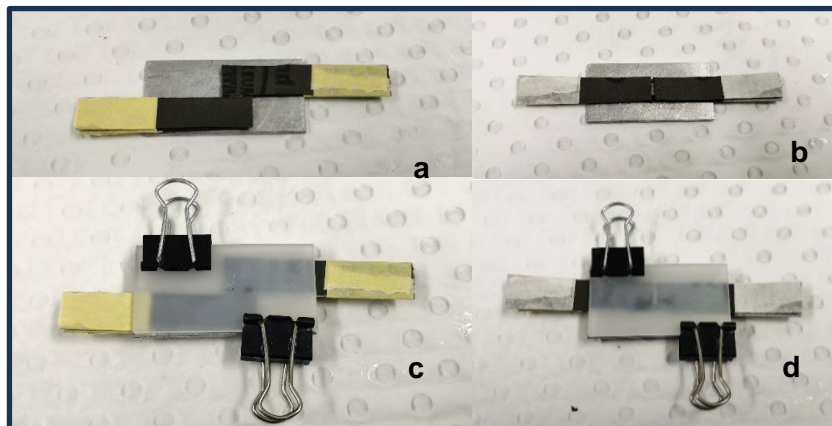


Fig. 10 Preparing specimen for micromechanical testing in shear (a) and tensile (b) directions. Specimens are clamped between two slides for fixing the glue and for transportation (c,d).

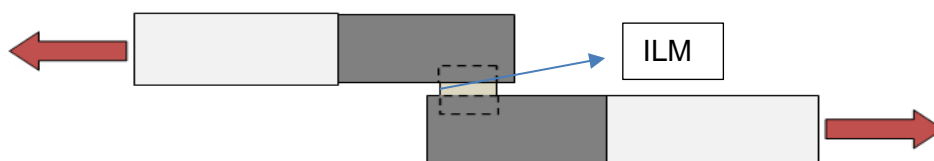
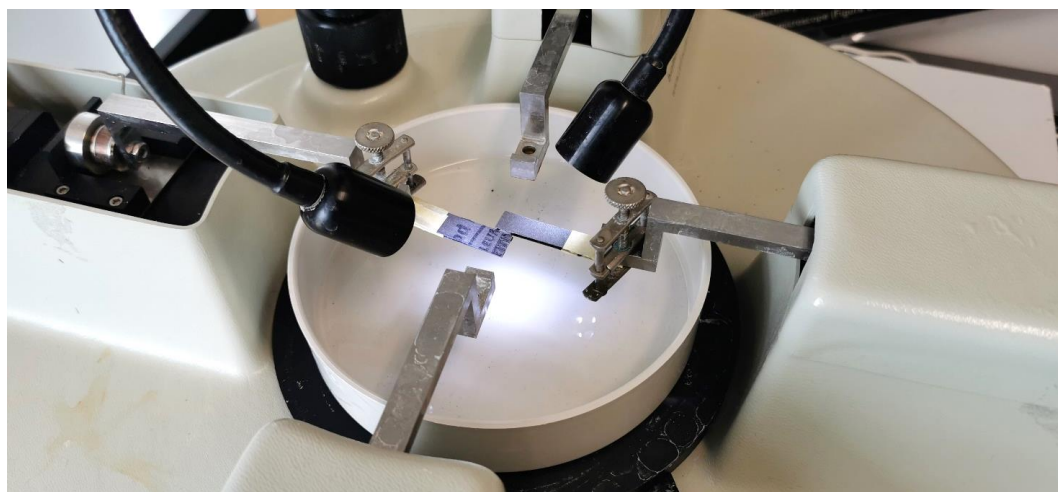


Fig. 11 The specimen prepared was loaded on the cellscale device for micromechanical testing in shear direction.



Fig. 12 The specimen prepared was loaded on the cellscale device for micromechanical testing in tensile direction.

Transporting the specimen

The specimen after gripping must be transported from the sample preparation area of the laboratory to the cellscale device, for micromechanical testing. The prepared specimen is quite delicate, and transportation can cause damage to the tissue if not handled with care. In order to hold the specimen intact in position, the gripped specimen is sandwiched in between two plates and clamped at two opposite sides (Figure 9 c, d). This will ensure that the mechanical property of the specimen is not disturbed till the time of testing. The specimen is unclipped once it is placed in the water bath of the cellscale (Figure 12). The prepared functional lamellae unit is hydrated in PBS in the water bath at room temperature (37°C).

Micromechanical testing

The ends of the sandpaper strips are taped (Figure 8 b) to allow the micromechanical test specimen to float in the water bath. The samples are attached to the Cellscale device with the help of clamps attached provided with the device. The specimen was then subjected to dynamic testing followed by a failure test. To reduce creep between tests, a preload of 100mN was applied. The gripper-to-gripper distance was used as the initial length for strain calculation after applying preload to all samples. The data acquisition frequency was set at 1, 5, and 100 Hz for slow, medium, and fast strain rates, respectively. Displacement control is applied using the Cellscale, and five cycles of dynamic loading with a triangle waveform were performed to stretch the samples to 40% of their initial length at strain rates of 0.1%/s (slow), 1%/s (medium), and 10%/s (fast). In the final stage of the test, for both tensile and shear loading direction, a ramp test to failure was performed at a strain rate of 10% and 100 Hz data recording.



Fig. 13 CellScale micromechanical testing device used for uniaxial testing

Data analysis and Quality control

Along with biaxial and uniaxial mechanical testing, the cellscale also has the ability to record pictures which could be played back. This provided the ability to examine the fixation closely. Prior to formal testing, the practise and pilot tests conducted in sheep and human IVD respectively, both returned desired results as the viscoelastic and failure properties of the IVD could be confirmed. The testing methodology was also validated as there was no slippage observed in the recorded video of the tests. The force curves were steady and no sharp drop in the force was observed. The recording also allowed to verify that no glue overflowed from the sandpaper strip onto the specimen, to impede its mechanics.

The micromechanical testing done on the cellscale provides force vs time and force vs displacement data that was then plotted with the help of templates created on Microsoft Excel. The area of gripping for the specimen was calculated by measuring the ILM width, with the help of a vernier caliper, and thickness (1mm) were sliced using a handheld microtome . The stress and strain for each data point was thus calculated and plotted. This stress and strain data of the last loading unloading cycle was used to calculate Young's modulus and the hysteresis loss coefficient (The hysteresis area, which is a measure of the toughness of the material was calculated as the area between the loading and unloading curve, calculated by using a trapezoid formula). The area of hysteresis region (energy absorbed) divided by the area under the loading curve provides the hysteresis loss coefficient. Hysteresis loss coefficient for all the samples are plotted for the destructive and non-destructive tests. The Young's modulus on the other hand, was calculated by

inserting a best fit line to the linear region of the loading curve and measuring its slope using linear regression. From Tavakoli et al., 2018 the linear region was selected to be from 25% to 35% strain rate on the loading curve of the last cycle. The force displacement data for the failure test was plotted to obtain the peak stress or failure load.

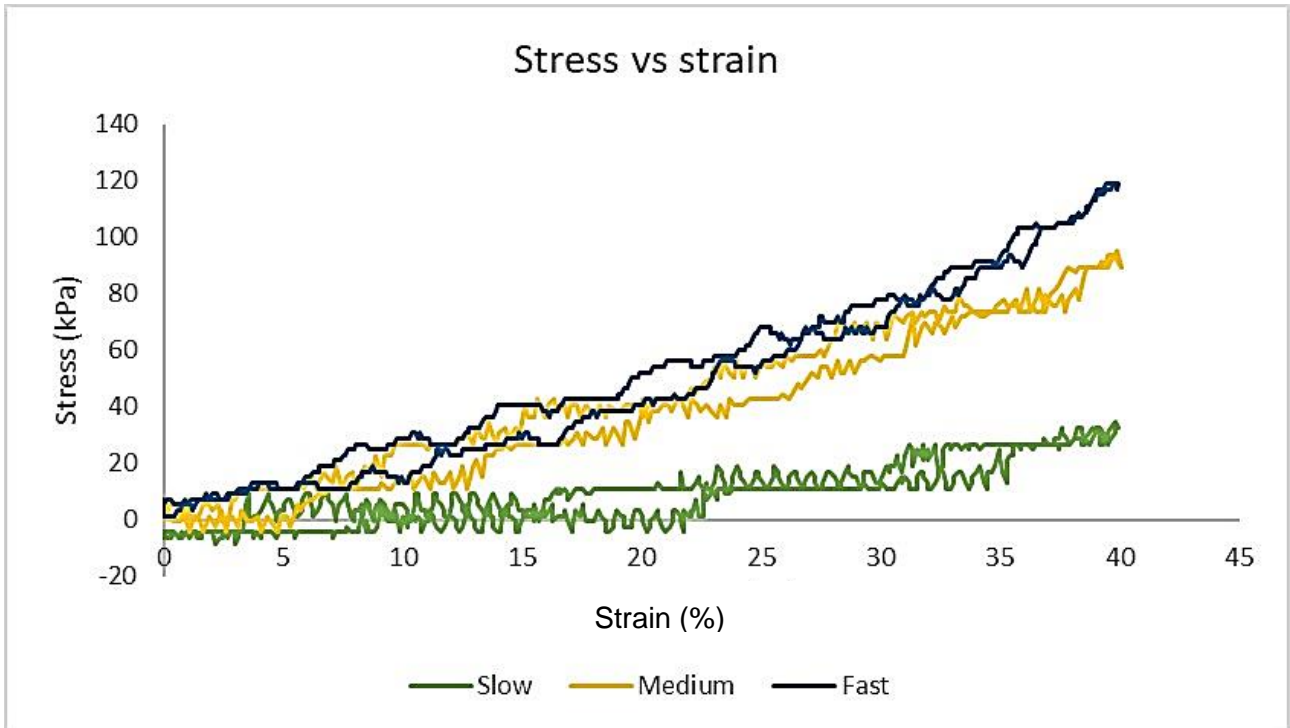


Fig. 14 Stress vs strain graph – slow, medium, and fast strain rate

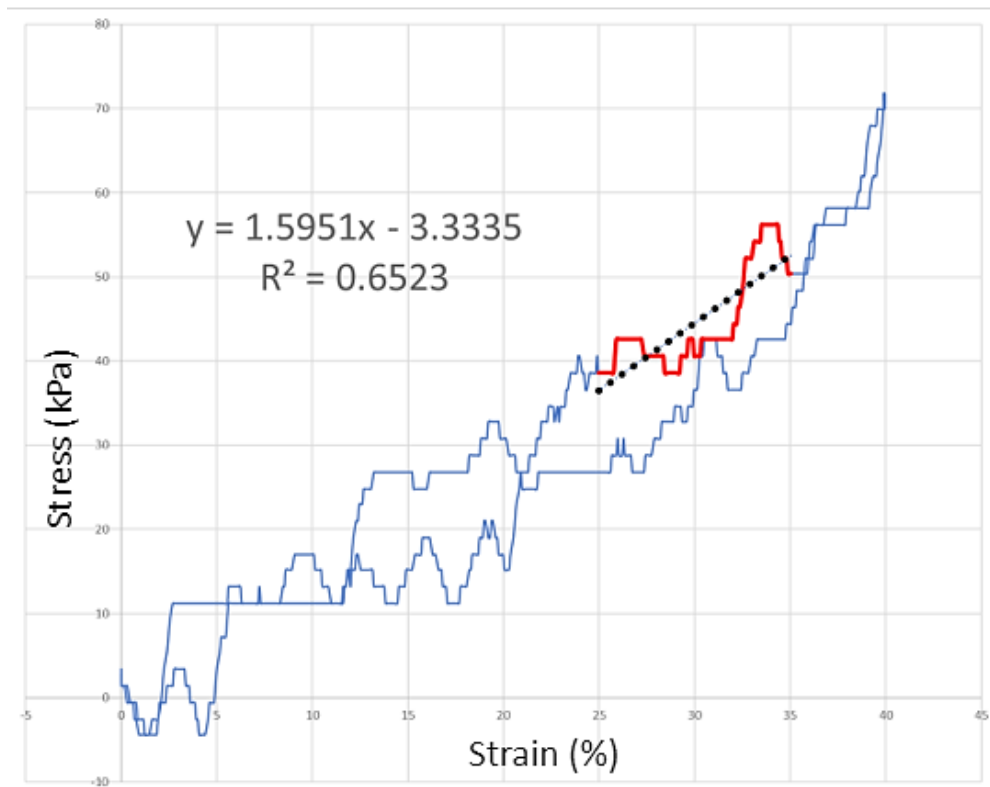


Fig. 15 Stress vs strain graph – final cycle with young’s modulus calculated by linear regression

RESULTS

The formal study consisted of minimum of three region, taken from two each healthy and degenerated discs (refer table 2). This summed up to a total of 112 tests conducted to obtain data for the formal test results. Since each data group consists of not more than 2 specimens, statistical analyses, such as an Analysis of Variance (ANOVA), was not able to be performed. This is because ANOVA method assumes that the data within each group is distributed normally and should be having equal variances. Since the sample size for each group is only two at the most, the assumptions would not be met. Therefore, the differences between each group would not be detected, and possibly giving rise to false negatives. In this study, thus the results are directly analysed from the graphs plotted on excel, and viable trends are discussed. For the test results to be admissible for data analysis, the specimen used had to be checked with the quality control measures: the specimen is of uniform thickness (1mm), there is no slippage in the gripping, there is glue spilled over onto the ILM region, the sample should not tear and provide an undesirable force displacement response. After reviewing the data, out of the 112 tests done, 16 tests were found to be inadmissible. Therefore, 96 tests were accepted for formal analysis.

Sandpaper fixation gripping outcome

From the images recorded on the cellscale it was evident that there was no slippage while micromechanical testing was carried out. Thus, confirming the reliability of the sandpaper fixation method (Figure 16.).

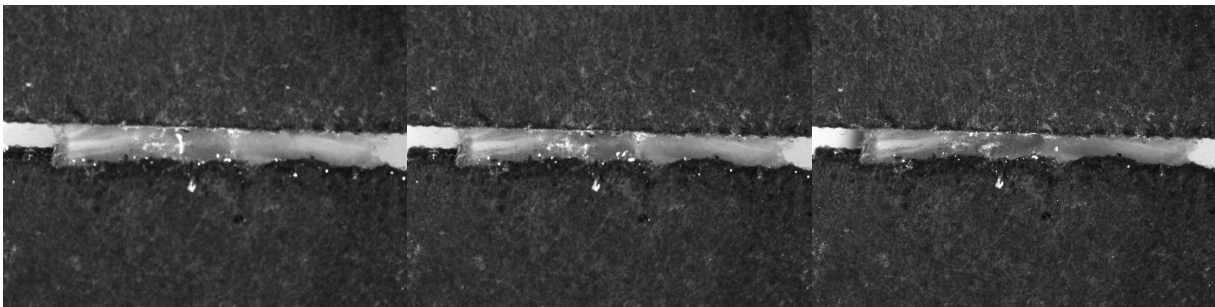


Fig. 16 Pictures taken at different points of the testing cycle shows no evidence of slippage.

Viscoelasticity

Non-destructive testing done on each sample through the cellscale device returned a viscoelastic response as it was observed during the loading phase, when a displacement was applied to the sample and the force response was measured. During the unloading phase, the displacement is returned to its starting phase while continuing to measure the force. Figure 17 depicts the viscoelasticity of the ILM.

The average hysteresis loss coefficient and the average stiffness are calculated using MS Excel and plotted. Pivot charts were used to observe trends in the variables.

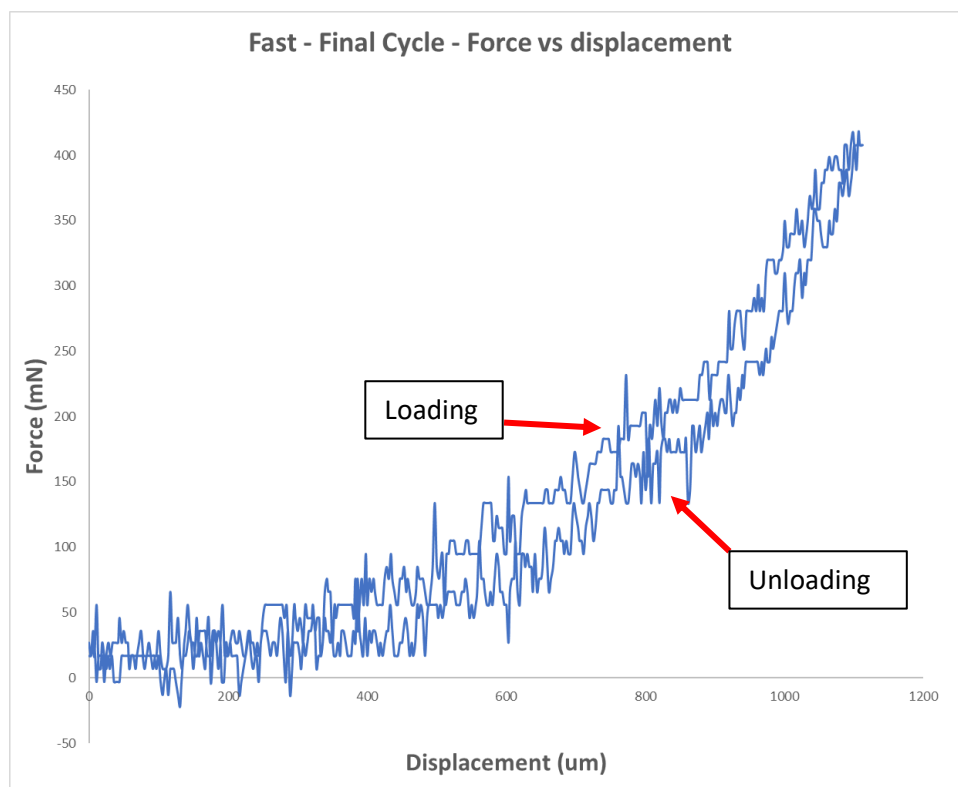


Fig. 17 plot of final cycle showing loading and unloading curve

Hysteresis loss coefficient – tensile test

The average hysteresis loss coefficient for tensile test for all strain rates were tabulated (refer Appendix E). Standard deviation was not a good measure of error in this case since the sample size was only two, and moreover some of the specimen data had to be excluded. Hence, the median for each data set was calculated and the interquartile range plotted using MS Excel. The difference between the degenerated and healthy set of samples are observed. The interquartile range (IQR) calculated (Appendix E) is a good indication of the spread of the data. Error bars were added to the bar graphs to identify the variations associated with the data points. It is beneficial because the IQR

is less affected by extreme values that has occurred in some of the data points. Moreover, the data obtained is non-parametric or doesn't follow a normal distribution, in which case the IQR is beneficial. For the tensile test, hysteresis loss coefficient IQR was 0.036 for all the healthy disc tissue across all strain rates and regions, and 0.0369 for degenerated discs.

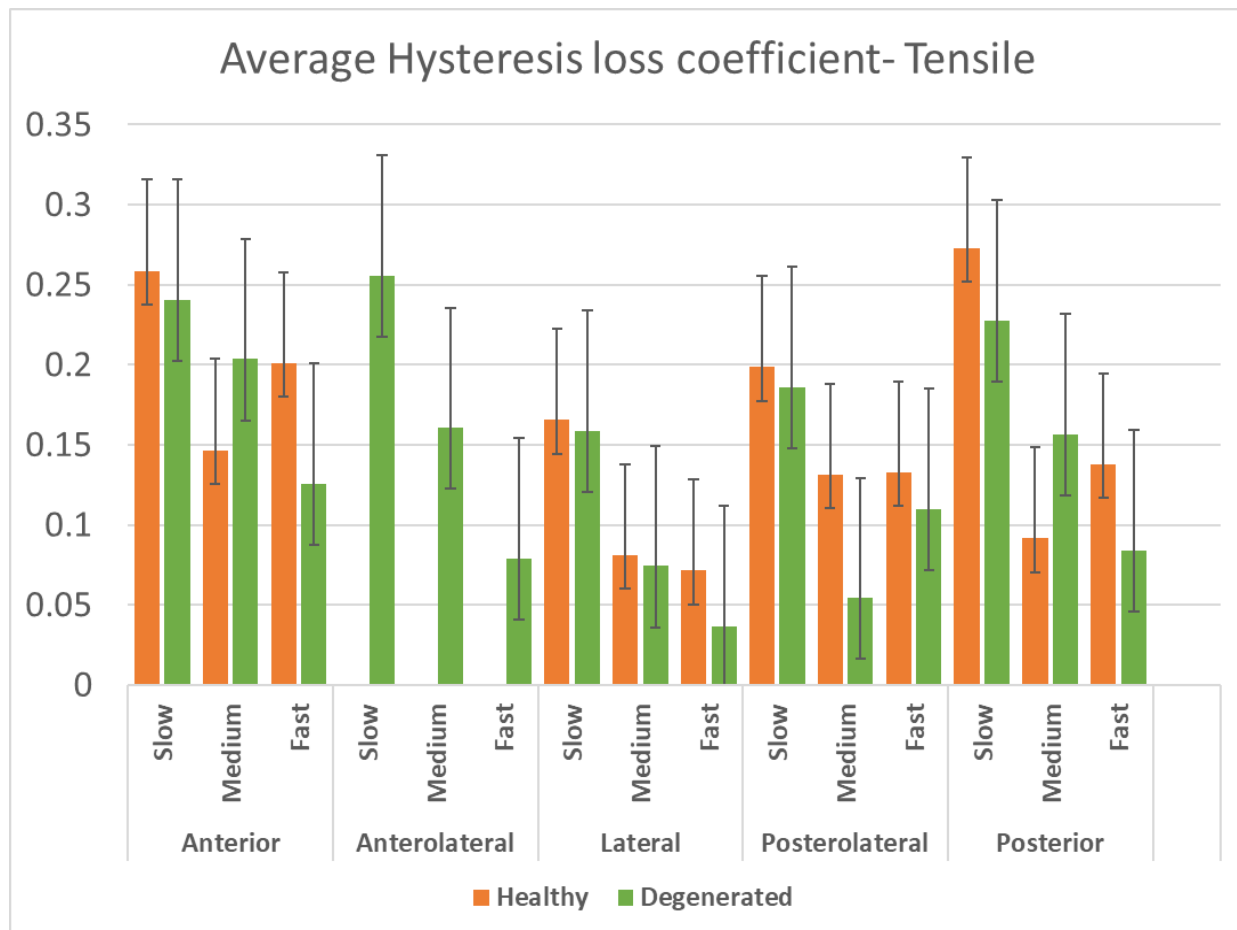


Fig. 18 Median (interquartile range) hysteresis loss coefficient for tensile tests – comparing healthy and degenerated discs at three strain rates (slow, medium and fast)

Hysteresis loss coefficient – shear test

The average hysteresis loss coefficient for shear testing was tabulated in the similar manner to the tensile test. The difference between the degenerated and healthy set of samples are observed. For the shear test, hysteresis loss coefficient IQR was 0.090 for the healthy discs, and 0.062 for degenerated discs

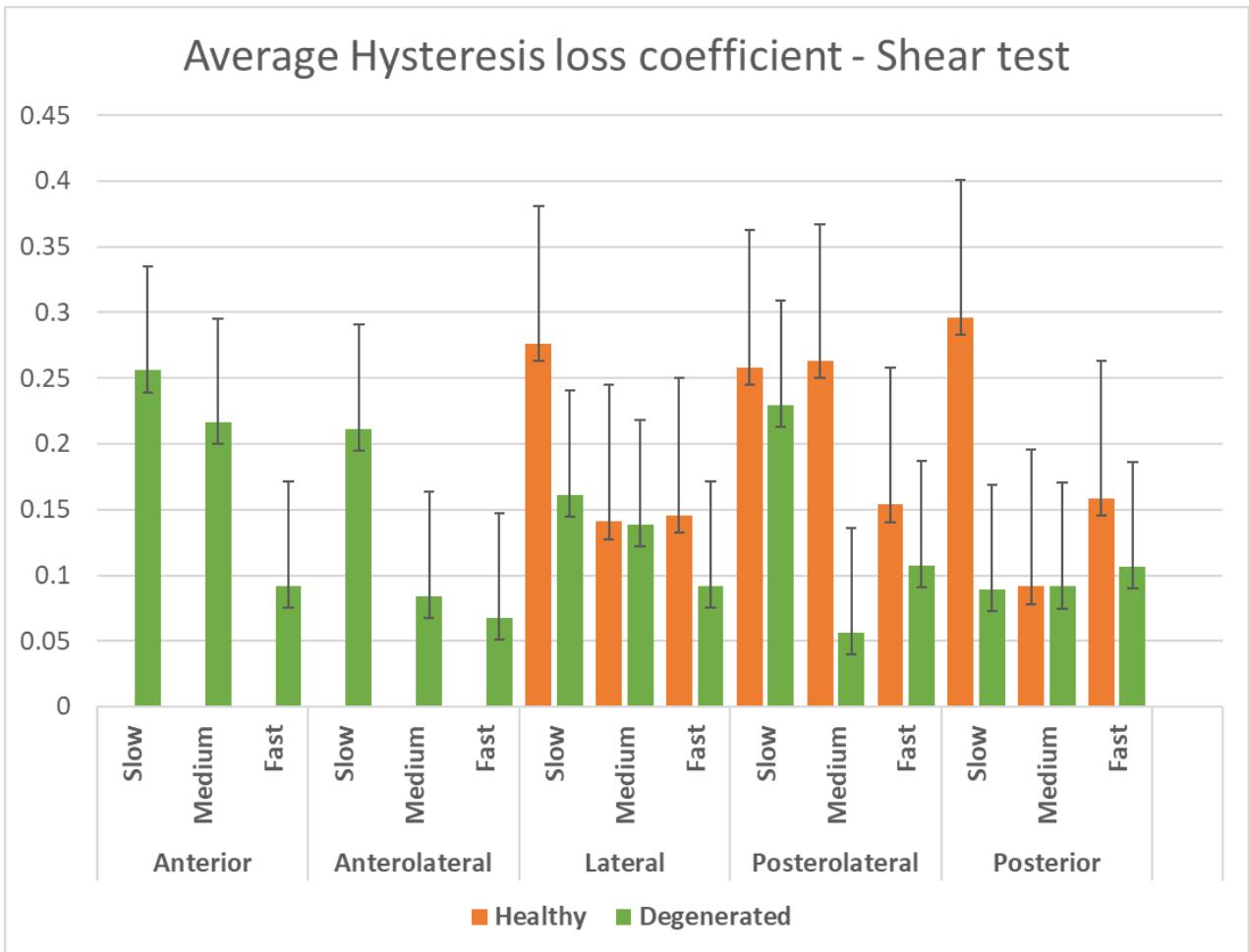


Fig. 19 Median (interquartile range) hysteresis loss coefficient for shear tests – comparing healthy and degenerated discs at three strain rates (slow, medium and fast)

Stiffness – Tensile test

The average stiffness for tensile testing was tabulated. The difference between the degenerated and healthy set of samples are observed. For the tensile test, stiffness IQR was 0.471 for the healthy discs, and 0.99 for unhealthy discs.

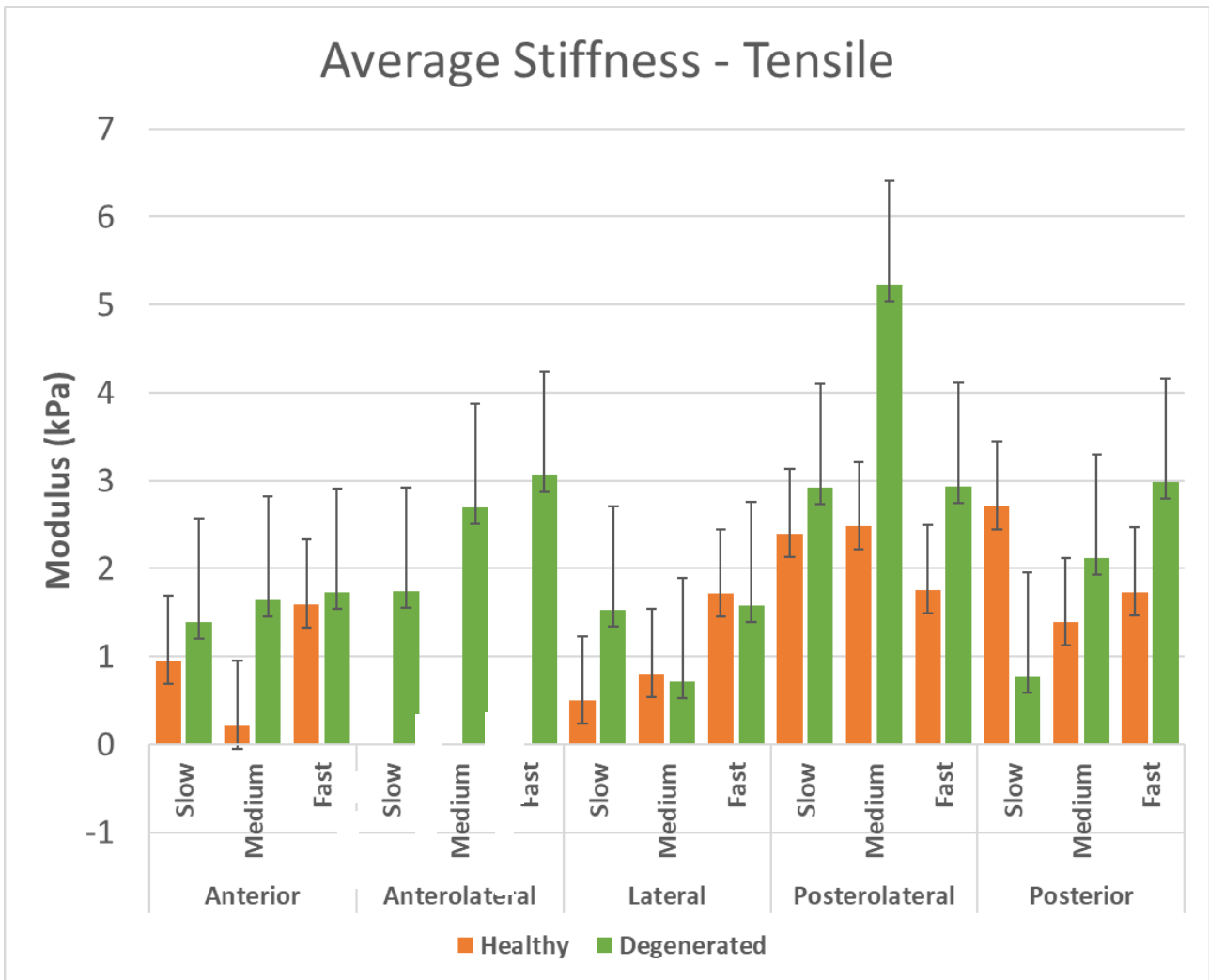


Fig. 20 Median (interquartile range) stiffness for tensile tests – comparing healthy and degenerated discs at three strain rates (slow, medium and fast)

Stiffness – Shear test

The average stiffness for shear testing was tabulated. The difference between the degenerated and healthy set of samples are observed. For the shear test, stiffness IQR 0.08625 for the healthy discs, and 0.283 for unhealthy discs

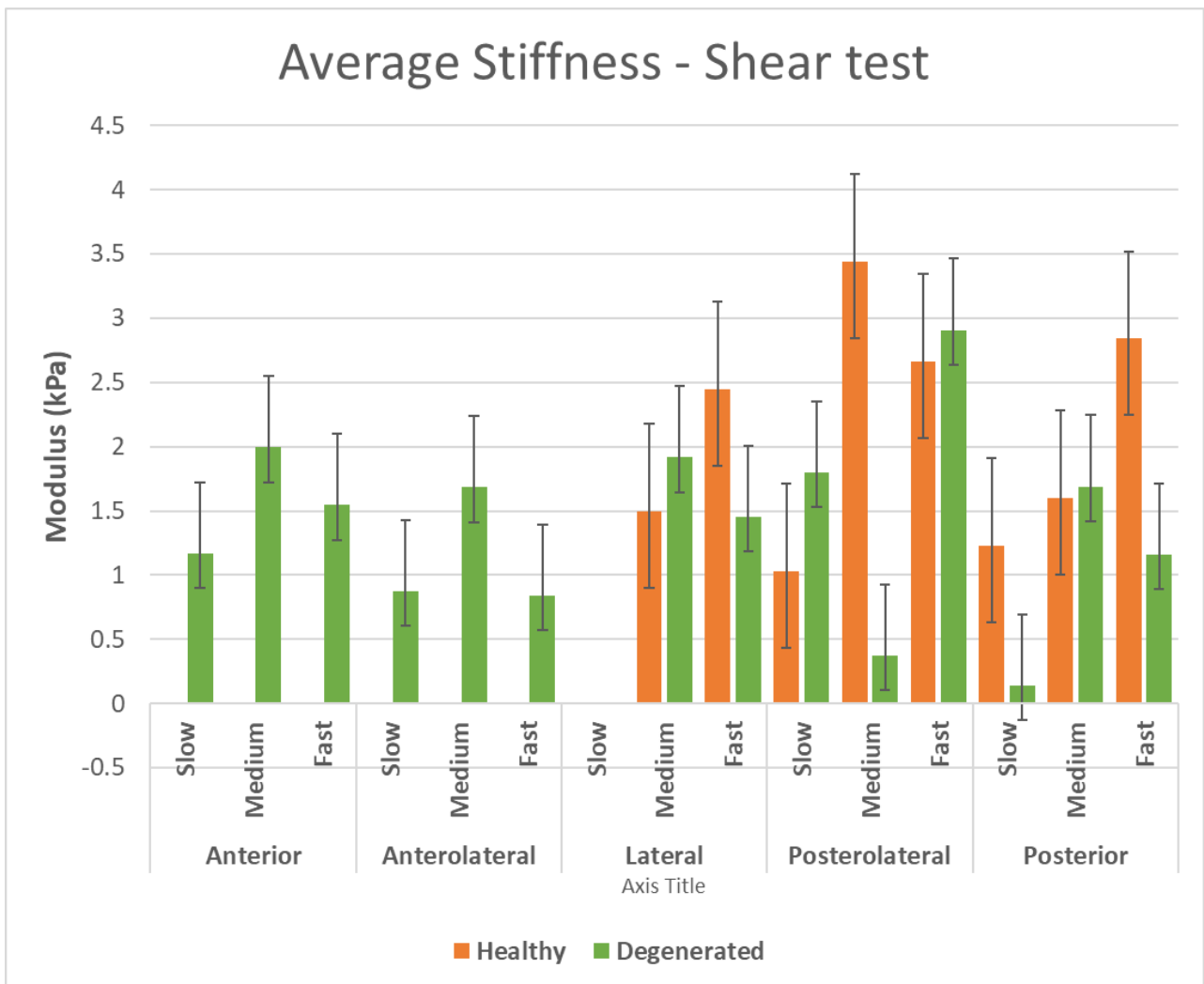


Fig. 21 Median (interquartile range) stiffness for tensile tests – comparing healthy and degenerated discs at three strain rates (slow, medium and fast)

Median stiffness and hysteresis loss coefficient

To make a further broad comparison of the hysteresis loss coefficient, the median values of tests ranging across three strain rates for all the regions were calculated and the 25% and 75% quartile errors were added to the plots. .

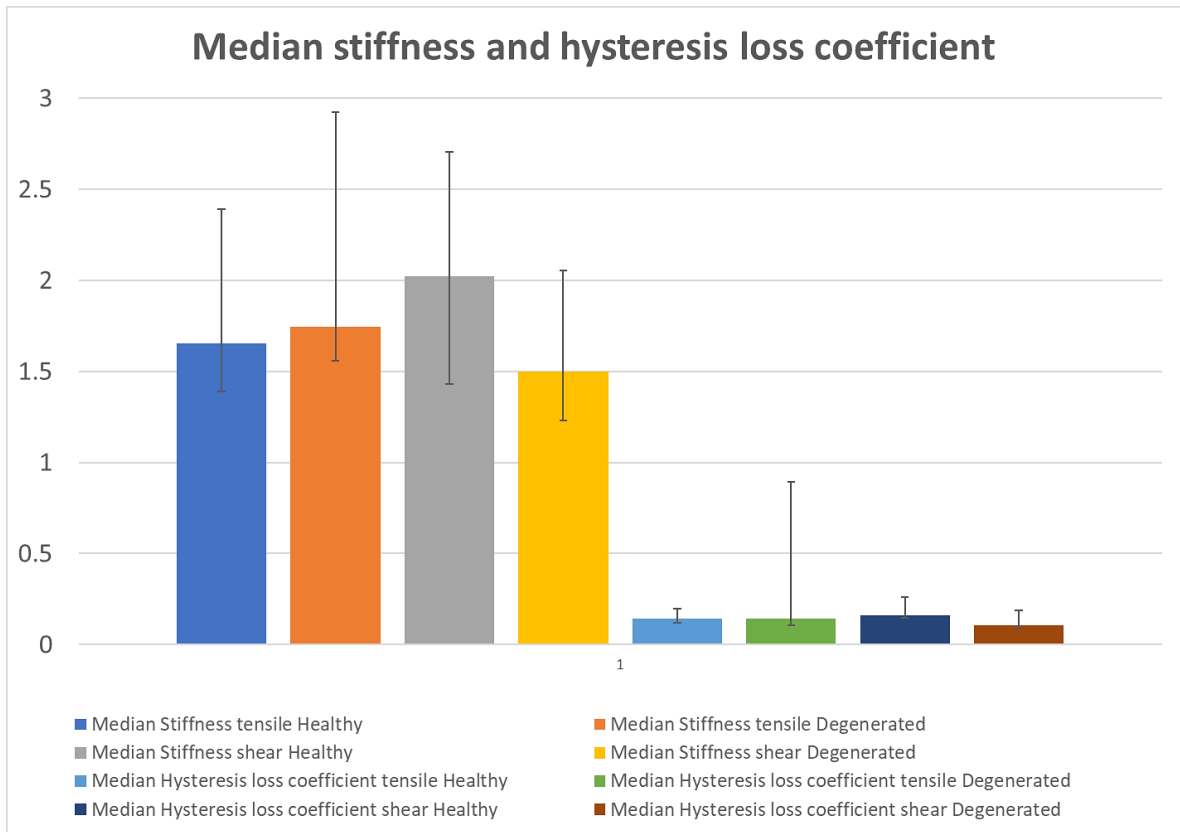


Fig. 22 Comparison of median values calculated and plotted showing quartile errors

Failure load

The failure load was determined for each sample under both the tensile and shear direction. The maximum force observed before the ILM failed and deformed substantially was noted. The picture inset in Figure 23 shows the deterioration and pulling apart of the ILM in the tensile test.

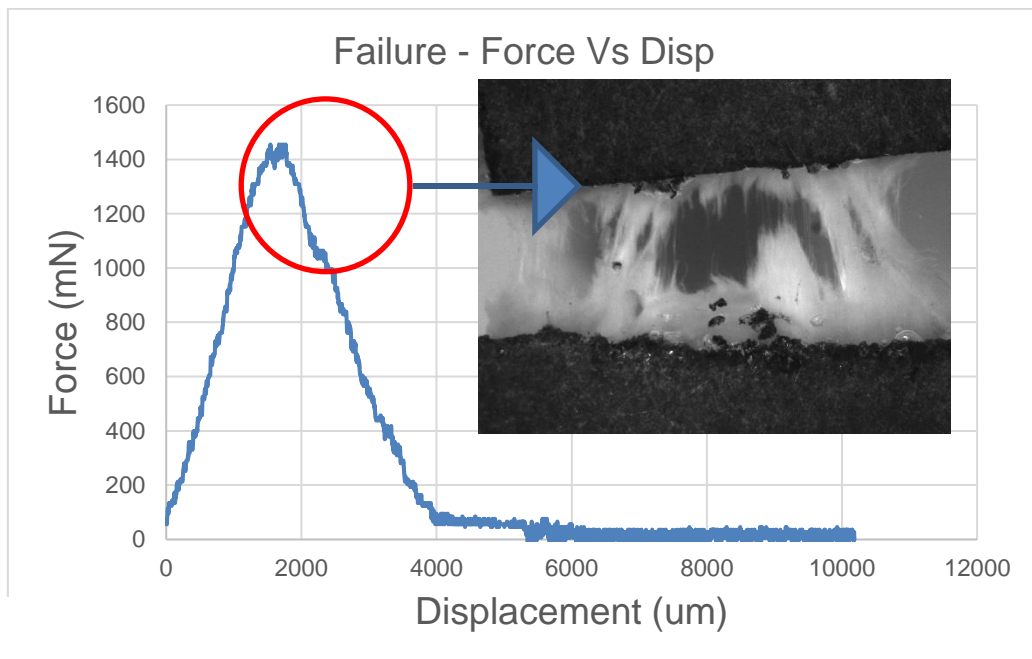


Fig. 23 Force vs displacement graph showing maximum failure load

Average failure load – Tensile

The average failure load for tensile testing was tabulated. The difference between the degenerated and healthy set of samples are observed. For the tensile test, failure load IQR is 1.85 for the healthy discs, and 7.39 for unhealthy discs.

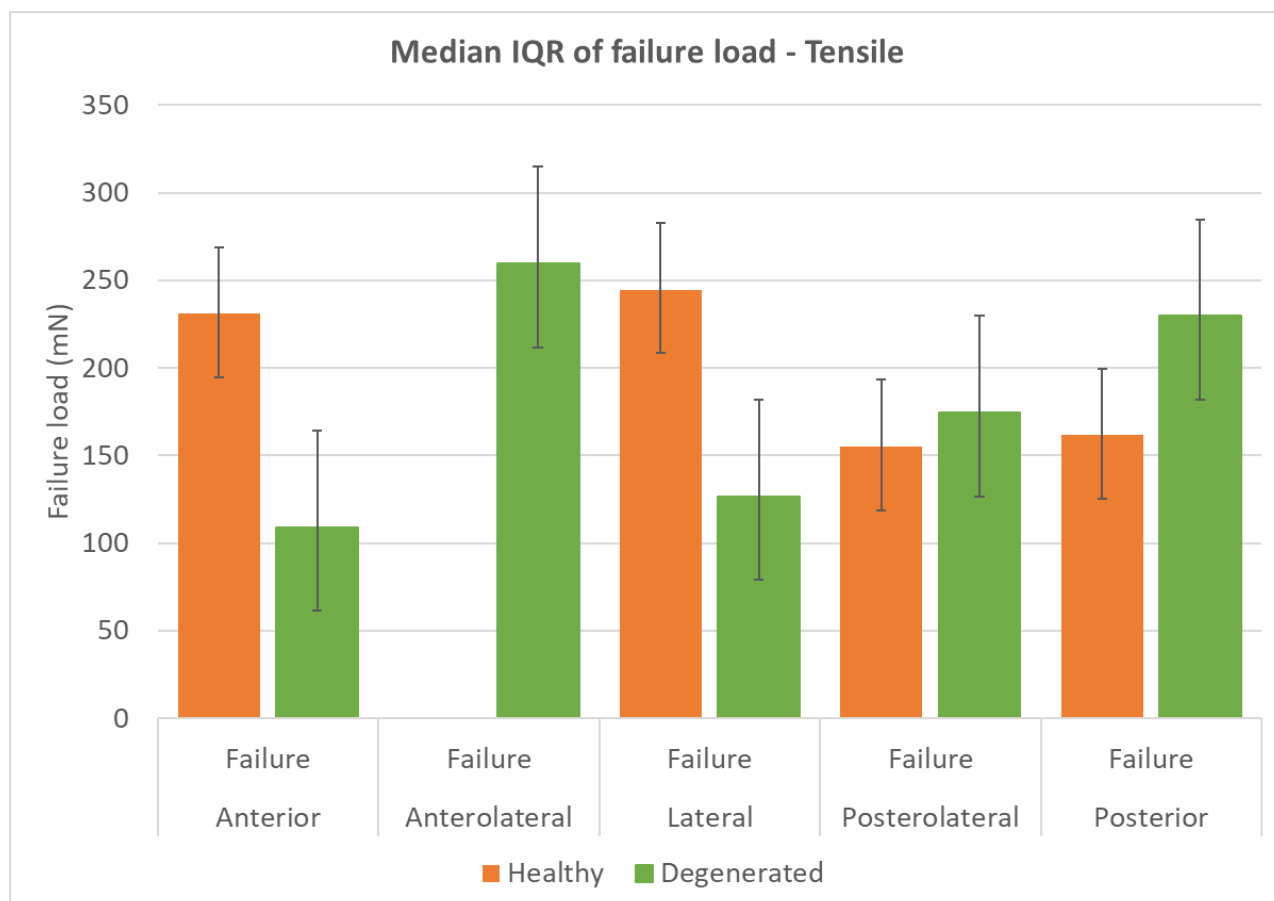


Fig. 24 Average failure loads – comparing healthy and degenerated discs in tensile testing

Average energy absorbed at failure – Tensile

The average energy absorbed at failure for tensile testing was tabulated. The difference between the degenerated and healthy set of samples are observed. For the tensile test, failure load IQR is 9653 for the healthy discs, and 7389 for unhealthy discs

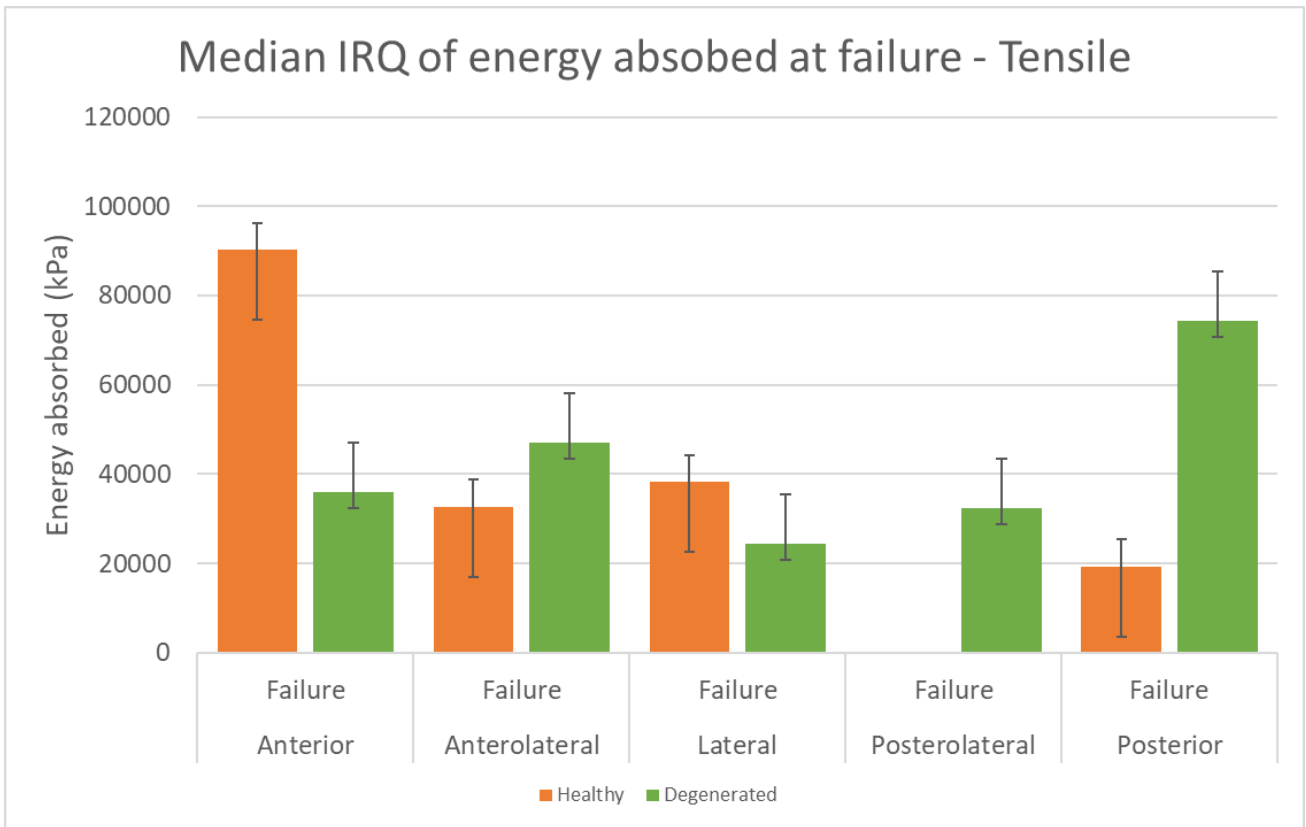


Fig. 25 Average energy absorbed at failure – comparing healthy and degenerated discs in tensile test

Average failure load – Shear

The average failure load for shear testing was tabulated. The difference between the degenerated and healthy set of samples are observed. For the tensile test, failure load IQR is 2.062 for the healthy discs, and 15.88 for unhealthy discs

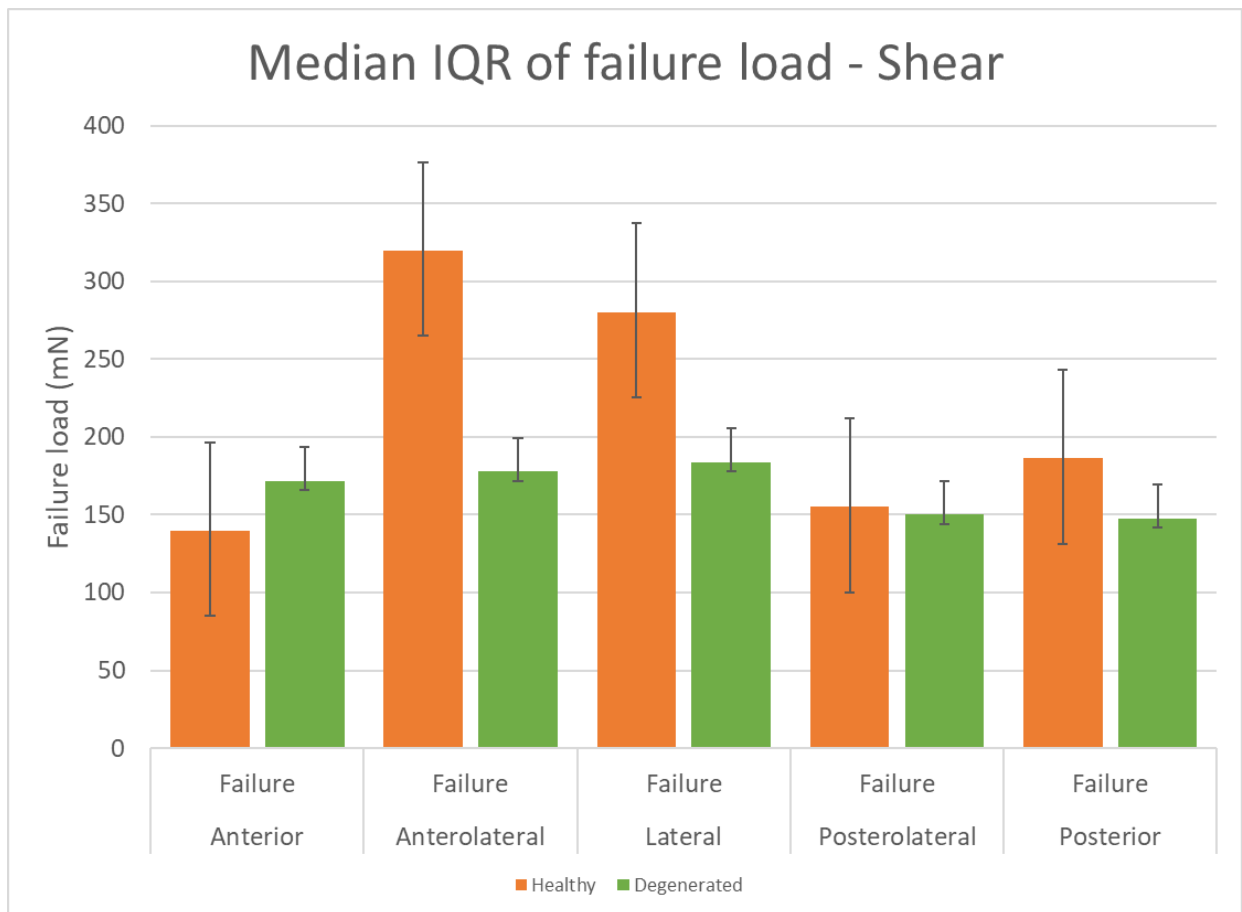


Fig. 26 Average failure loads comparing healthy and degenerated discs in shear testing

Average energy absorbed at failure - Shear

The average energy absorbed at failure for shear testing was tabulated. The difference between the degenerated and healthy set of samples are observed. For the shear test, failure load IQR is 67.893 for the healthy discs, and 11926.5 for unhealthy discs.

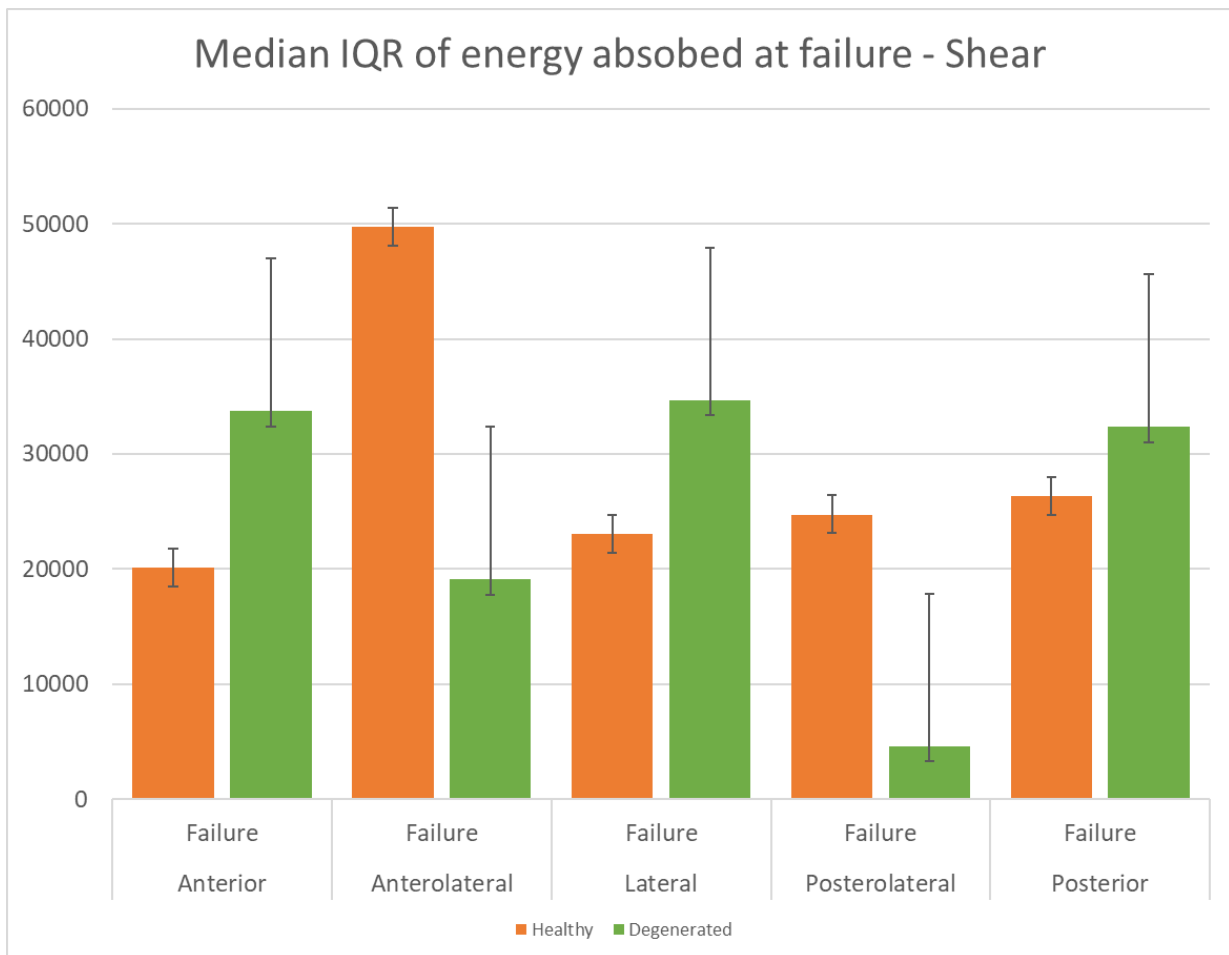


Fig. 27 Average energy absorbed at failure – comparing healthy and degenerated discs in shear test

Median failure load

To make a further broad comparison of the failure loads across the varying strain rates and regions, the median values of tests ranging across three strain rates for all the regions were calculated and plotted. The median values provide a good summary of the dataset acquired. The spread of the data is summarised through these graphs.

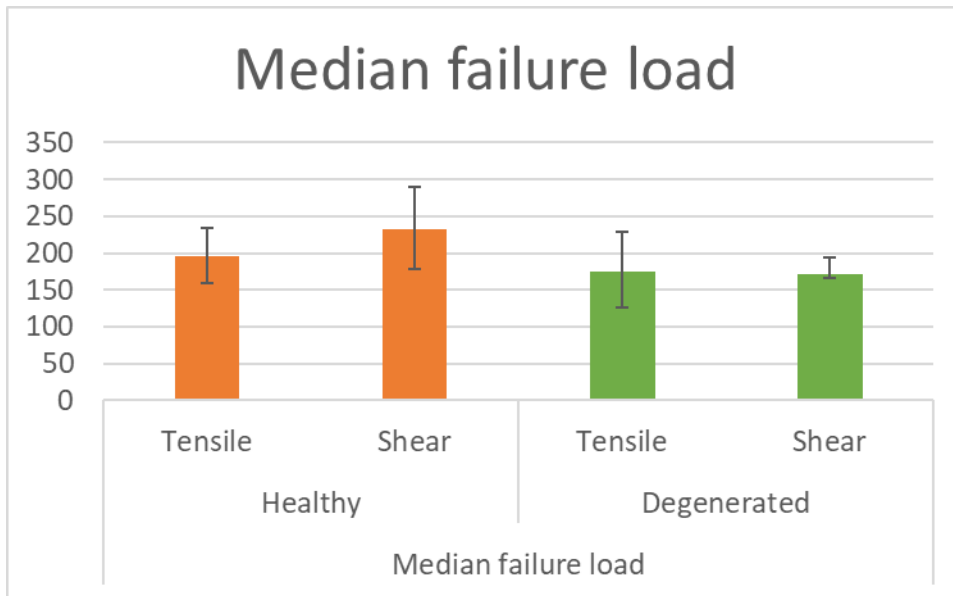


Fig. 28 Median failure loads comparing healthy and degenerated discs in both tensile and shear testing

Median energy absorbed

To make a further broad comparison of the energy absorbed, the median values of tests ranging across three strain rates for all the regions were calculated and plotted. The median values provide a good summary of the dataset acquired, especially because of the outlying datapoints. The spread of the data is summarised through these graphs.

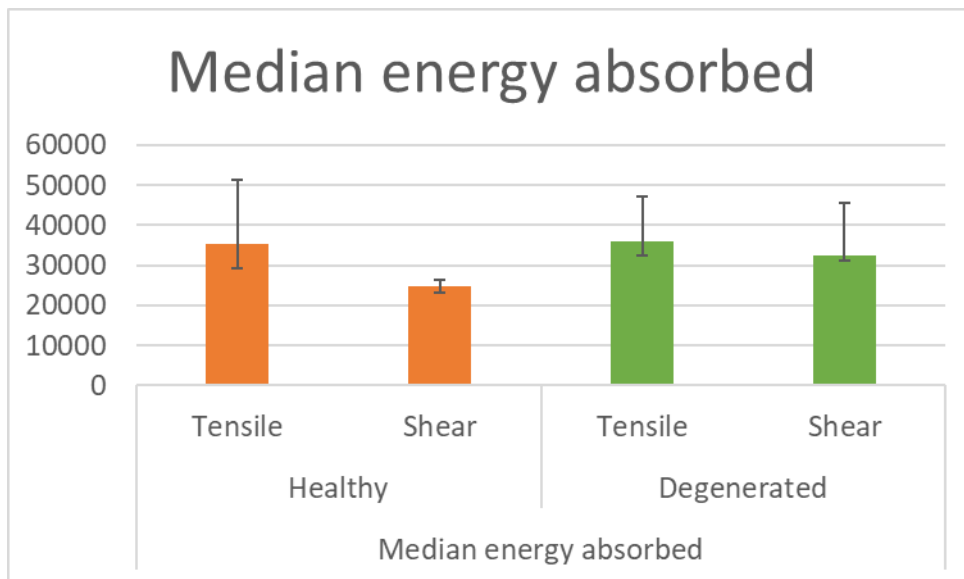


Fig. 29 Median energy absorbed comparing healthy and degenerated discs in both tensile and shear testing.

DISCUSSION

The last cycles when plotted for all the lamella-ILM-lamella complex specimen exhibited viscoelastic characteristics. There were noticeable trends in the collected data. However, some observations were not according to hypothesis and further observation into the video recorded for the test was able to shed some light on the unexpected results. These unexpected results are discussed in detail in the following section.

Hysteresis loss coefficient

It was observed that the hysteresis loss coefficient was higher for the slow strain rate and reduced with increasing strain rate, which is characteristic of viscoelastic tissue. This observation was true for majority of the regions in both degenerated and healthy groups. Measuring this property of the AF provides a measure of the energy absorption during the loading and unloading phase. Overall from the medians plotted, it could be observed that there was a slight reduction in the hysteresis loss coefficient of degenerated disc in tensile direction when compared to healthy discs, and a considerable reduction for the same in shear direction.

Hysteresis loss coefficient in case of both tensile and shear test are in the same IQR of 0.090944 – 0.035 healthy and 0.06269 - 0.036 for degenerated discs. So, it may be observed that the range for healthy is higher across all the regions. The trends indicated a similar energy absorption under ILM delaminating conditions such as rotation and torsion. Moreover, the highest hysteresis loss coefficient is observed in the anterior region and lowest in the lateral region. The specimen shows the characteristics of a viscoelastic fluid where the applied strain does show a linear elastic region and returned to its original state when the strain was removed. In addition, the force response that occurred over the three strain rates were different, increasing with the strain rate which is also characteristic of a viscoelastic material. Additionally testing including stress relaxation or creep tests might be beneficial in understanding if the material is behaving more like a viscoelastic fluid or solid. The slow strain rate tensile test conducted on the anterolateral region of sample 4696 (Grade 2) and the fast strain rate shear test done on the anterior GL406 (Grade 2) returned a hysteresis coefficient of -0.071 and -0.044 respectively. These results were contradictory to our hypothesis as a negative number would indicate that energy is being gained rather than being lost/absorbed. This may have been a result of delaminated ILM in the tissue that occurred in the specimen as seen in Fig. So, these specimen tests had to be excluded from the formal results.

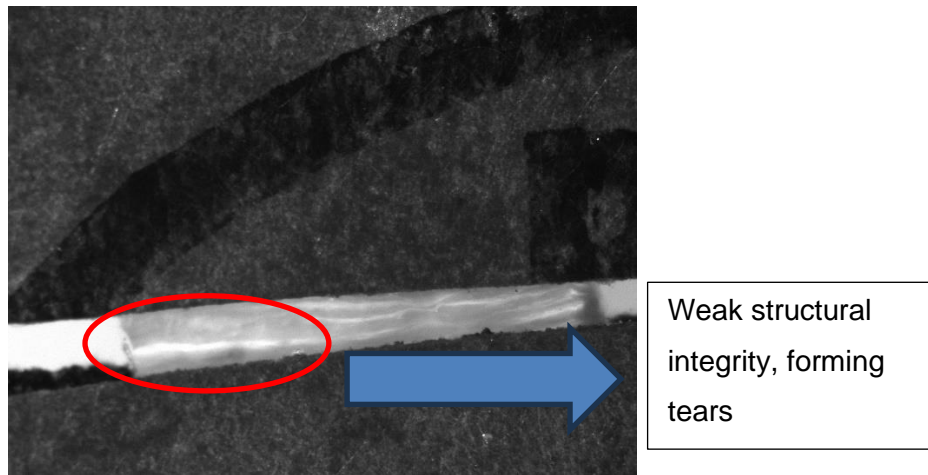


Fig. 30 Specimen number 4696 excluded from results

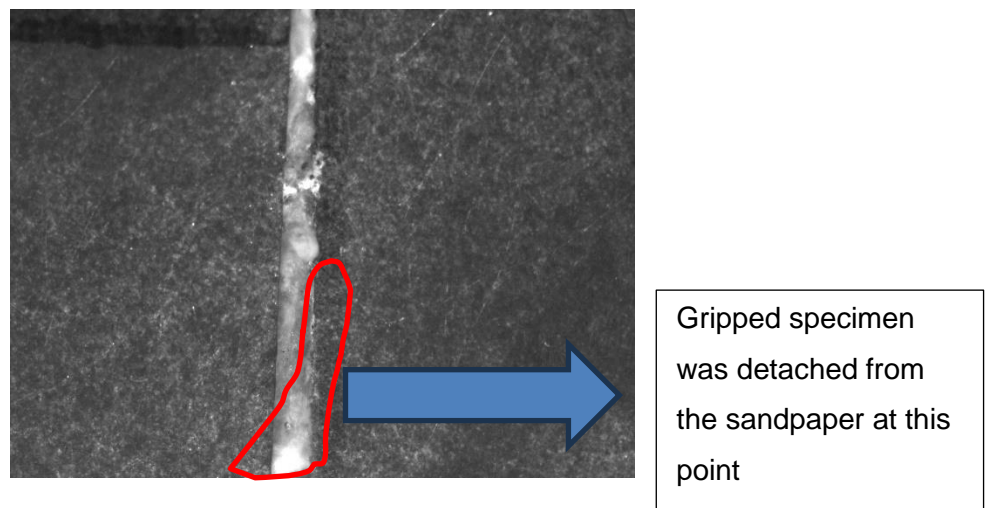


Fig. 31 Specimen number GL406 excluded from results

Modulus

It was consistently observed that the Young's modulus in the shear direction indicated that the specimens were stiffer, which made them more prone to failure in shear loading. It's worth noting that this result contradicts previous research, where the shear modulus in ovine (sheep) intervertebral discs was found to be significantly lower than the tensile modulus, and shear failure stress was equivalent to tensile failure stress (Tavakoli et al., 2018). The difference could be attributed to variations in the behaviour of collagen and elastic fibers in the annulus fibrosus between humans and sheep.

It may be interesting to note that the stiffness is higher in one of the degenerated samples in the tensile test, but only in the medium strain-rate test. This could be because of a piece of tissue that was attached to the specimen (GL471) as observed in the figure, the presence of which made the

stress response extremely stiff, and in the subsequent fast strain rate test we observe the tissue breaking away and equilibrating in the fast cycle.

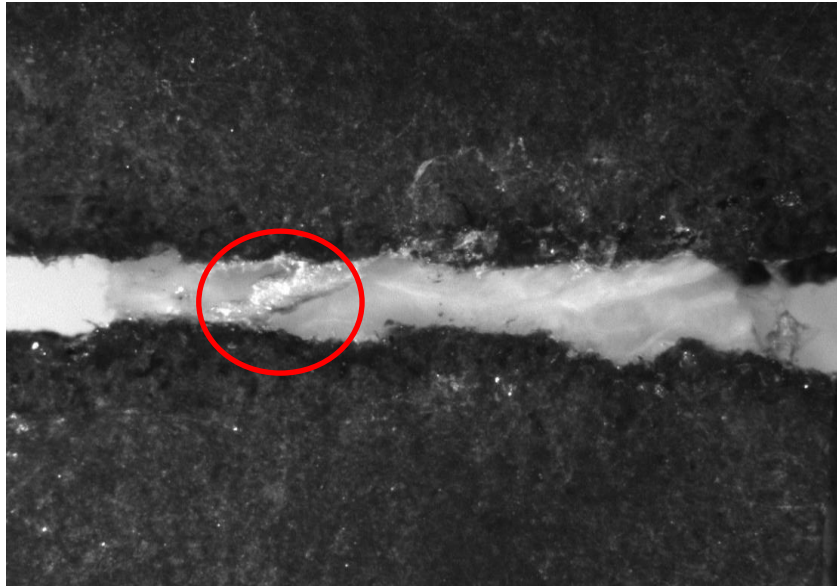


Fig. 32 GL471 sample showed much higher stiffness in the slow strain rate test

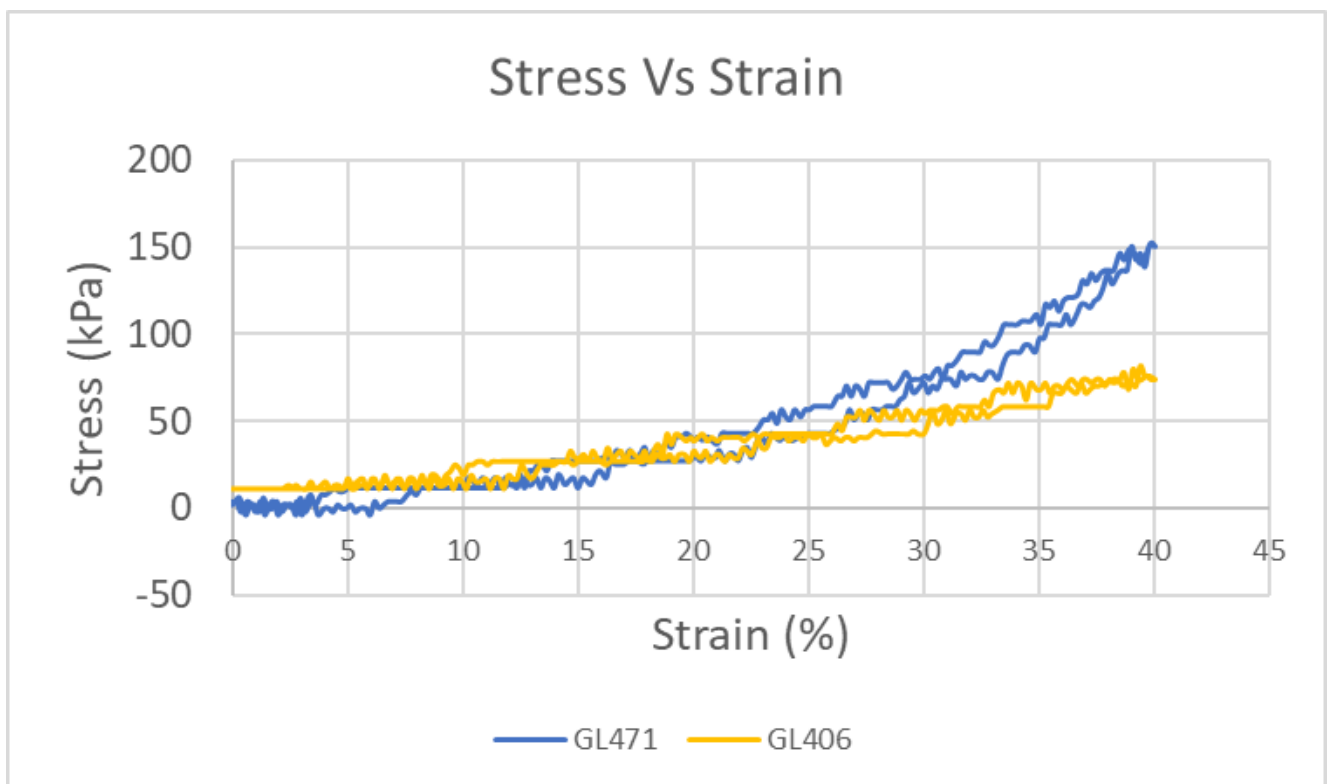


Fig. 33 Comparison of the effect of the extra tissue on GL471 compared to another specimen from same region and degradation grade (medium strain rate)

When comparing the difference between stiffness of healthy and degenerated discs, it can be noticed that during tensile loading, degenerated discs show a higher stiffness when compared to healthy discs, but in contrast, for shear testing healthy discs are stiffer than degenerated discs.

On comparing the regions, it was found that for healthy discs, the stiffness decreases from posterior region to the anterior region, and was stiffer during tensile loading, which could be an indication that delamination and failure of the ILM is more possible during shear loading. However, in the degenerated disc, the variance among regions is not so evident, indicating a more random arrangement of the collagen fibres. An overview of the median values across all regions and strain rates suggest that the stiffness in shear direction is considerably higher in healthy discs than in degenerated. On the other hand, in tensile testing, the degenerated specimen showed slightly higher stiffness.

Failure load

For the shear test, in the ANT and LAT regions there was a visible difference in the maximum stress between the degenerated and healthy specimen. The difference was not so evident in the ALT, PLT and POS regions. Consequently, the POS and PLT region may be more prone to failure, which can be explained by the region's proximity to the nucleus within the disc. On the other hand, during tensile testing, ANT, PLT and POS regions were not noticeably different in the maximum stress between degenerated and healthy specimen. The maximum stress for the regions were found to be independent of the direction of loading.

When comparing different degeneration grades, it was noticed that the trend for failure stress was lower in Grade 4 specimens compared to Grade 2 specimens, both in tension and shear. This trend aligns with the understanding that degenerated specimens, which are already less effective at swelling and withstanding compressive loads, would exhibit lower failure stress (Tavakoli and Costi, 2018), and may also be more likely to undergo additional tissue structural disruption, or loss of ILM connectivity, due to degeneration. Additionally, ultrastructural studies suggested that the elastic fiber network within the annulus fibrosus is more likely to be recruited under tension, whereas in shear, only fibers oriented in the direction of loading would likely be recruited (Tavakoli and Costi, 2018). Therefore, given that the discs were degenerated, it was expected that shear failure stress would be lower in degenerated specimens compared to healthy specimens. This observation is in agreement to when a comparison of the medians for failure load was done, as it was noticed that the failure load is higher for healthy specimen.

Energy absorbed at failure

Among all the specimens tested, the direction in which the load was applied had a significant impact on energy absorption. There was an effect of degeneration on the energy absorbed. During tensile

loading the posterior region was This increase in stiffness may result from a lower water content in the nucleus pulposus (NP), which in turn enhances energy absorption. Conversely, when the specimens were loaded in shear, the opposite trend was observed, affirming the anisotropic (direction-dependent) nature of the annulus fibrosus (AF). The median range of the energy absorbed remained almost constant in the tensile direction for healthy ad degenerated, while a good variance is observed in the shear direction with degenerated disc showing a considerably higher value than healthy.

Limitations

The main aim of the study that was to do a comparison of the stiffness, hysteresis loss coefficient, as well as failure properties of ILM from healthy and degenerated disc was successfully completed, however, there were some limitations to the study. The sample size (n=2) for each of healthy and degenerated disc did not provide an opportunity for a statistical analysis of the data, and additionally some of the tested data could not be included for the formal results. There was huge variability in some of the data because only one specimen per data group was available for some samples, if not two. Therefore, comparing the results to the results obtained by other researchers was having its limitations.

Human IVD specimen were not easy to obtain and therefore care was taken to ensure that the specimens are not damaged while preparing and handling them. Some of the measures included slicing the specimen by running it in the direction perpendicular to that of the lamellae and running the fingers around the periphery of the frozen OCT holding the specimen, to make it easier for the feather blade to cut into the specimen. Initially, the screw mechanism of the microtome used in the experiment was difficult to adjust and had to be serviced during the practise phase. This ensured that it operated well during the pilot and formal testing phases.

Specimen's freeze-thawing cycles may also have had its effect on the hydration state and was mitigated by hydrating the specimen in the PBS bath for at least 2 minutes prior to each test series. Moreover, care was taken to always keep the specimen hydrated while waiting to be tested. It must be borne in mind that that mechanical properties of IVD samples are better studied by comparing under the same freeze/thaw cycles (Azarnoosh, M. et al., 2017). So, it may be beneficial to conduct testing on the same batch of specimen that have been thawed and frozen the same number of times.

CONCLUSION AND FUTURE WORKS

The research conducted for this study adopted a rigorous methodology that can be explored further to deepen our understanding of the mechanical characteristics of the ILM of the AF in humans. The main goal of this research was to compare the micromechanical properties of healthy and degenerated human ILM, and this goal was achieved by using the force-displacement data obtained to calculate the modulus, hysteresis loss coefficient, failure load and energy absorbed at failure, in different regions of the disc, while observing the effects at different strain rates. Overall, it could be noted that for the shear test, in the ANT and LAT regions there was a visible difference in the maximum stress between the degenerated and healthy specimen. Therefore, given that the discs were degenerated, it was expected that shear failure stress would be lower in degenerated specimens compared to healthy specimens.

Future studies would benefit from a larger specimen and should ensure all regions of the discs are available to be tested. The radial regions – outer and inner for each of the circumferential regions can also be a decisive factor. Incorporating these factors into a study would require a lot of time and planning. Furthermore, the effect of elastic fibres in the ILM can be examined by isolating different components using enzymatic digestion techniques, followed by mechanical testing, and comparing the outcomes to the performance of the entire ILM. It was also noticed that some of the specimens were having odour coming from them, raising suspicion of putrefaction. The effect of breakdown of protein due to this factor may be considered in future studies.

BIBLIOGRAPHY

- Australian Institute of Health and Welfare. (2023). Back problems. Retrieved from <https://www.aihw.gov.au/reports/chronic-musculoskeletal-conditions/back-problems>
- Azarnoosh, M., et al. (2017). A comparative study of mechanical properties of fresh and frozen-thawed porcine intervertebral discs in a bioreactor environment. *Journal of the mechanical behavior of biomedical materials*, 69169–177.
- Cao, L., Guilak, F., and Setton, L. A. (2007). Three-dimensional morphology of the pericellular matrix of intervertebral disc cells in the rat. *Journal of Anatomy*, 0(0). doi:10.1111/j.1469-7580.2007.00784.x.
- Costi, J. J., Hearn, T. C., and Fazzalari, N. L. (2002). The effect of hydration on the stiffness of intervertebral discs in an ovine model. *Clinical Biomechanics*, 17(6), 446–455. doi:10.1016/s0268-0033(02)00035-9.
- Costi, J. J., Stokes, I. A., Gardner-Morse, M., Laible, J. P., Scoffone, H. M., & Iatridis, J. C. (2007). Direct measurement of intervertebral disc maximum shear strain in six degrees of freedom: Motions that place disc tissue at risk of injury. *Journal of Biomechanics*, 40(11), 2457–2466. <https://doi.org/10.1016/j.jbiomech.2006.11.006>.
- Fearing, B. V., et al. (2018). Mechanotransduction and cell biomechanics of the intervertebral disc. *JOR SPINE*, 1(3). doi:10.1002/jsp2.1026.
- Fujita, Y., Duncan, N., & Lotz, J. (1997). Radial tensile properties of the lumbar annulus fibrosus are site and degeneration dependent. *Journal of Orthopaedic Research*, 15(6), 814–819.
- Fujita, Y. et al. (2000) Anisotropic shear behavior of the annulus fibrosus: effect of harvest site and tissue prestrain. *Medical engineering & physics*. [Online] 22 (5), 349–357.
- Ghezelbash, F., et al. (2021). Modeling of human intervertebral disc annulus fibrosus with complex multi-fiber Networks. *Acta Biomaterialia*, 123, 208–221. doi:10.1016/j.actbio.2020.12.062.
- Jo, M., & Chae, S.-W. (2021). Development of L4-L5 lumbar spine finite element model to estimate spine loads. *Journal of the Korean Society for Precision Engineering*, 38(6), 461–467. doi:10.7736/jkspe.020.107.
- Kaissi, A. (2022). Micromechanical assessment of regional variation in the human lumbar interlamellar matrix. Flinders University, College of Science and Engineering.
- MARCHAND, F., & AHMED, A. M. (1990). Investigation of the laminate structure of lumbar disc anulus fibrosus. *Spine*, 15(5), 402–410. doi:10.1097/00007632-199005000-00011.
- Reebye, U. D. (2022). Assessing the effect of degeneration on the human lumbar inter-lamellar matrix. Flinders University, College of Science and Engineering.

Sivan, S. S., et al. (2013). Biochemical composition and turnover of the extracellular matrix of the normal and degenerate intervertebral disc. *European Spine Journal*, 23(S3), 344–353. doi:10.1007/s00586-013-2767-8.

Thompson, R. E., et al. (2000). Disc lesions and the mechanics of the Intervertebral Joint Complex. *Spine*, 25(23), 3026–3035. doi:10.1097/00007632-200012010-00010.

Wilke, H.-J., Kettler, A., & Claes, L. E. (1997). Are sheep spines a valid biomechanical model for human spines? *Spine*, 22(20), 2365–2374. doi:10.1097/00007632-199710150-00009.

Yu, J., et al. (2002). Elastic fibre organization in the intervertebral discs of the bovine tail. *Journal of Anatomy*, 201(6), 465–475. doi:10.1046/j.1469-7580.2002.00111.x.

APPENDICES

Appendix A

Table 2 The Thompson Scale. This grading system can be used for determining the morphologic grade of the disc in experimental investigations. NP = nucleus pulposus; AF = anulus fibrosus; V_E = vertebral endplate; V_B = vertebral body (From Thompson (1990))

Grade	Nucleus Pulposus	Annulus Fibrosis	V _E (Vertebral body)		V _B (Vertebral endplate)
I	Bulging gel	Discrete fibrous bundles	Hyaline, uniformly thick		Margins rounded
II	White fibrous tissue peripherally	Mucinous material between lamellae	Thickness irregular		Margins pointed
III	Consolidated fibrous tissue	Extensive mucinous infiltrate; loss of annular nuclear demarcation	Focal defects in cartilage		Early chondrocytes or osteophytes at margins
IV	Horizontal clefts parallel to endplate	Focal disruption	Fibrocartilage extending from subchondral bone; irregularity and focal sclerosis on subchondral bone		Osteophytes less than 2 mm
V	Clefts extend through nucleus and anulus		Diffuse sclerosis		Osteophytes greater than 2mm

Appendix B

Calculations

1) Modulus

Strain $\epsilon = \Delta L / L_0$, where

ΔL - change in length

L_0 - original length

Stress, $\sigma = F/A$, where

F - resultant force after displacement is applied

A - cross sectional area of the specimen after displacement is applied

Modulus, $E = \sigma / \epsilon$

2) Hysteresis loss coefficient

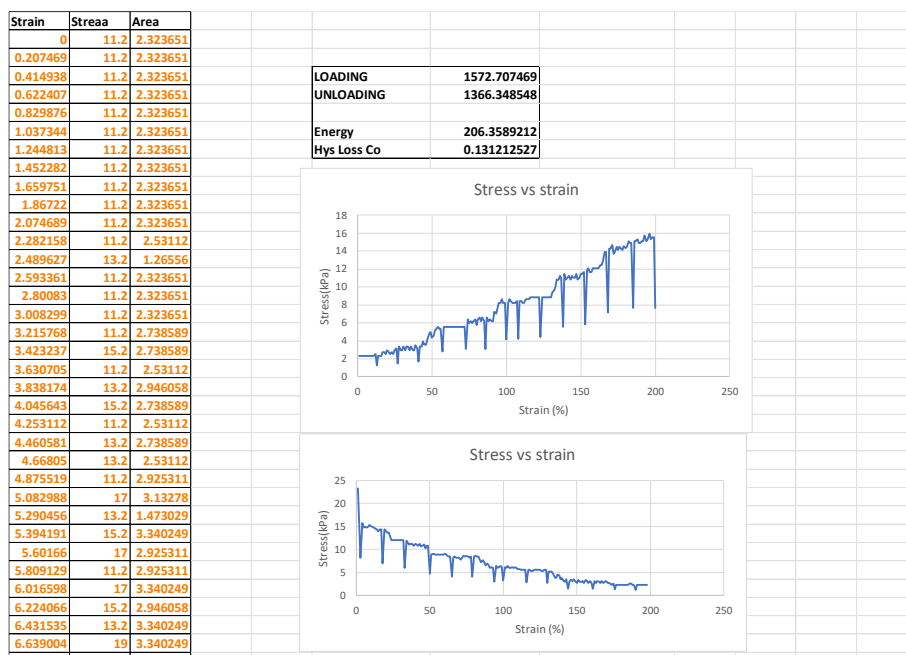
Energy absorbed or hysteresis area is measured as the difference between the area under the loading curve of the graph and unloading curve of the graph.

Hysteresis loss coefficient is the ratio between the energy absorbed and the area of the loading curve.

The area under the curve was found as the sum of the datapoints under the stress strain curve using the trapezoid formula $=((B2+B3)/2)*(A3-A2)$ in the template

Appendix C

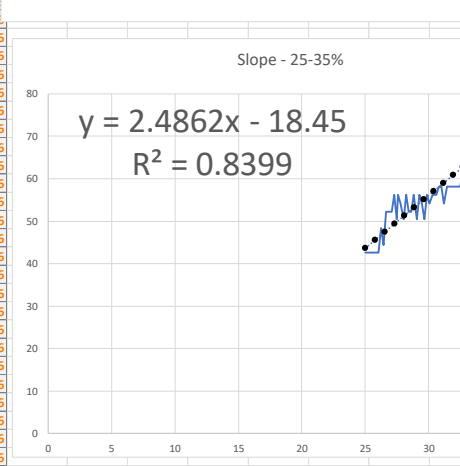
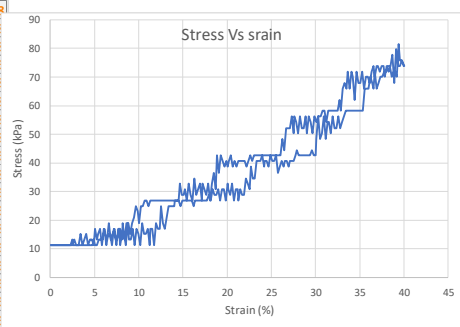
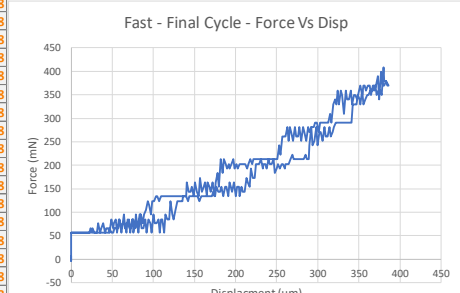
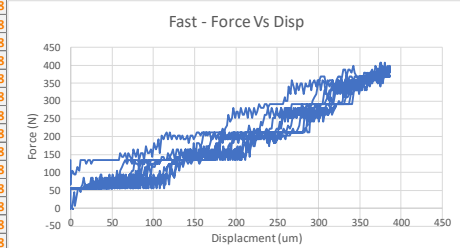
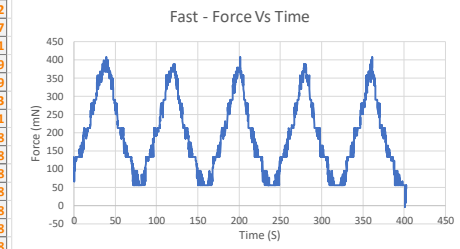
Template for calculating hysteresis loss coefficient :



Template for Calculating modulus :

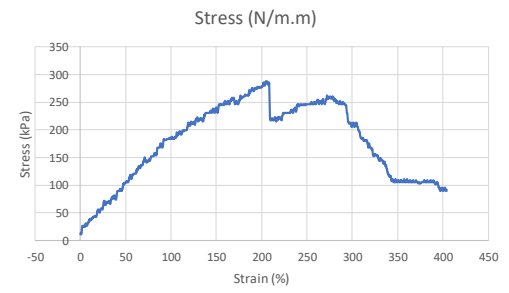
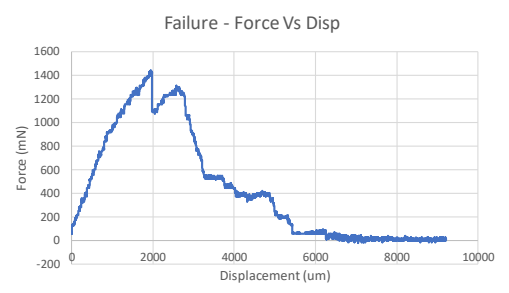
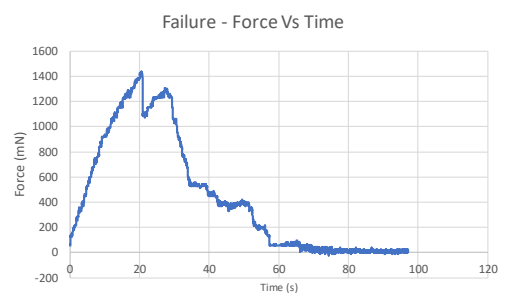
SetName	Cycle	Time_S	Temperat	XSize_um	YSize_um	YDisplac	Force_mN	STRAIN	Stress (N/m.m)	specimen width	5000	5
Medium	1-Preload	0	23.5	4699	964	0	134	0	26.8			
Medium	1-Preload	0.2	23.5	4699	964	0	105	0	21			
Medium	1-Preload	0.4	23.5	4699	964	0	66	0	13.2			
Medium	1-Stretch	0.44	23.5	4699	964	0	85	0	17			
Medium	1-Stretch	0.64	23.5	4699	966	2	105	0.207469	21			
Medium	1-Stretch	0.84	23.5	4699	968	4	95	0.414938	19			
Medium	1-Stretch	1.04	23.5	4699	970	6	95	0.622407	19			
Medium	1-Stretch	1.24	23.5	4699	972	8	115	0.829876	23			
Medium	1-Stretch	1.44	23.5	4699	974	10	105	1.037344	21			
Medium	1-Stretch	1.64	23.5	4699	976	12	134	1.244813	26.8			
Medium	1-Stretch	1.84	23.5	4699	977	13	134	1.348548	26.8			
Medium	1-Stretch	2.04	23.5	4699	979	15	134	1.556017	26.8			
Medium	1-Stretch	2.24	23.5	4699	981	17	134	1.763485	26.8			
Medium	1-Stretch	2.44	23.5	4699	983	19	124	1.970954	24.8			
Medium	1-Stretch	2.64	23.5	4699	985	21	134	2.178423	26.8			
Medium	1-Stretch	2.84	23.5	4699	987	23	134	2.385892	26.8			
Medium	1-Stretch	3.04	23.5	4699	989	25	124	2.593361	24.8			
Medium	1-Stretch	3.24	23.5	4699	991	27	134	2.80083	26.8			
Medium	1-Stretch	3.44	23.6	4699	993	29	134	3.008299	26.8			
Medium	1-Stretch	3.64	23.6	4699	995	31	134	3.215768	26.8			
Medium	1-Stretch	3.84	23.6	4699	997	33	134	3.423237	26.8			
Medium	1-Stretch	4.04	23.6	4699	999	35	134	3.630705	26.8			
Medium	1-Stretch	4.24	23.6	4699	1001	37	134	3.838174	26.8			
Medium	1-Stretch	4.44	23.6	4699	1003	39	134	4.045643	26.8			
Medium	1-Stretch	4.64	23.6	4699	1005	41	134	4.253112	26.8			
Medium	1-Stretch	4.84	23.6	4699	1007	43	134	4.460581	26.8			
Medium	1-Stretch	5.04	23.6	4699	1008	44	134	4.564315	26.8			
Medium	1-Stretch	5.24	23.6	4699	1010	46	134	4.771784	26.8			
Medium	1-Stretch	5.44	23.6	4699	1012	48	134	4.979253	26.8			
Medium	1-Stretch	5.64	23.6	4699	1014	50	134	5.186722	26.8			
Medium	1-Stretch	5.84	23.6	4699	1016	52	134	5.394191	26.8			
Medium	1-Stretch	6.04	23.6	4699	1018	54	134	5.60166	26.8			
Medium	1-Stretch	6.24	23.6	4699	1020	56	134	5.809129	26.8			
Medium	1-Stretch	6.44	23.6	4699	1022	58	134	6.016598	26.8			
Medium	1-Stretch	6.64	23.6	4699	1024	60	154	6.224066	30.8			
Medium	1-Stretch	6.84	23.6	4699	1026	62	144	6.431535	28.8			
Medium	1-Stretch	7.04	23.6	4699	1028	64	144	6.639004	28.8			
Medium	1-Stretch	7.24	23.6	4699	1030	66	154	6.846473	30.8			
Medium	1-Stretch	7.44	23.6	4699	1032	68	134	7.053942	26.8			
Medium	1-Stretch	7.64	23.6	4699	1034	70	154	7.261411	30.8			
Medium	1-Stretch	7.84	23.6	4699	1036	72	144	7.46888	28.8			
Medium	1-Stretch	8.04	23.6	4699	1038	74	134	7.676349	26.8			
Medium	1-Stretch	8.24	23.6	4699	1040	76	164	7.883817	32.8			
Medium	1-Stretch	8.44	23.6	4699	1041	77	154	7.987552	30.8			
Medium	1-Stretch	8.64	23.6	4699	1043	79	144	8.195021	28.8			
Medium	1-Stretch	8.84	23.6	4699	1045	81	164	8.40249	32.8			
Medium	1-Stretch	9.04	23.6	4699	1047	83	134	8.609959	26.8			
Medium	1-Stretch	9.24	23.6	4699	1049	85	154	8.817427	30.8			
Medium	1-Stretch	9.44	23.6	4699	1051	87	154	9.024896	30.8			
Medium	1-Stretch	9.64	23.6	4699	1053	89	134	9.232365	26.8			
Medium	1-Stretch	9.84	23.6	4699	1055	91	173	9.439834	34.8			
Medium	1-Stretch	10.04	23.6	4699	1057	93	154	9.647303	30.8			
Medium	1-Stretch	10.24	23.6	4699	1059	95	154	9.854772	30.8			
Medium	1-Stretch	10.44	23.6	4699	1061	97	164	10.06224	32.8			
Medium	1-Stretch	10.64	23.6	4699	1063	99	144	10.26971	28.8			
Medium	1-Stretch	10.84	23.6	4699	1065	101	183	10.47718	36.8			
Medium	1-Stretch	11.04	23.6	4699	1067	103	164	10.68465	32.8			
Medium	1-Stretch	11.24	23.6	4699	1069	105	173	10.89212	34.8			
Medium	1-Stretch	11.44	23.6	4699	1070	106	193	10.99585	38.8			
Medium	1-Stretch	11.64	23.6	4699	1072	108	154	11.20332	30.8			
Medium	1-Stretch	11.84	23.6	4699	1074	110	203	11.41079	40.8			
Medium	1-Stretch	12.04	23.6	4699	1076	112	193	11.61826	38.8			
Medium	1-Stretch	12.24	23.6	4699	1078	114	203	11.82573	40.8			
Medium	1-Stretch	12.44	23.6	4699	1080	116	213	12.0332	42.8			
Medium	1-Stretch	12.64	23.6	4699	1082	118	193	12.24066	38.8			
Medium	1-Stretch	12.84	23.6	4699	1084	120	213	12.44813	42.8			
Medium	1-Stretch	13.04	23.6	4699	1086	122	193	12.6556	38.8			
Medium	1-Stretch	13.24	23.6	4699	1088	124	203	12.86307	40.8			
Medium	1-Stretch	13.44	23.6	4699	1090	126	203	13.07054	40.8			
Medium	1-Stretch	13.64	23.6	4699	1092	128	193	13.27801	38.8			
Medium	1-Stretch	13.84	23.6	4699	1094	130	203	13.48548	40.8			
Medium	1-Stretch	14.04	23.6	4699	1096	132	203	13.69295	40.8			
Medium	1-Stretch	14.24	23.6	4699	1097	133	193	13.79668	38.8			
Medium	1-Stretch	14.44	23.6	4699	1099	135	203	14.00415	40.8			
Medium	1-Stretch	14.64	23.6	4699	1101	137	193	14.21162	38.8			
Medium	1-Stretch	14.84	23.6	4699	1103	139	193	14.41909	38.8			
Medium	1-Stretch	15.04	23.6	4699	1105	141	203	14.62656	40.8			
Medium	1-Stretch	15.24	23.6	4699	1107	143	183	14.83402	36.8			
Medium	1-Stretch	15.44	23.6	4699	1109	145	203	15.04149	40.8			
Medium	1-Stretch	15.64	23.6	4699	1111	147	203	15.24896	40.8			
Medium	1-Stretch	15.84	23.6	4699	1113	149	193	15.45643	38.8			
Medium	1-Stretch	16.04	23.6	4699	1115	151	203	15.6639	40.8			
Medium	1-Stretch	16.24	23.6	4699	1117	153	213	15.87137	42.8			
Medium	1-Stretch	16.44	23.6	4699	1119	155	213	16.07884	42.8			
Medium	1-Stretch	16.64	23.6	4699	1121	157	203	16.28631	40.8			
Medium	1-Stretch	16.84	23.6	4699	1123	159	213	16.49378	42.8			
Medium	1-Stretch	17.04	23.6	4699	1124	160	213	16.59751	42.8			
Medium	1-Stretch	17.24	23.6	4699	1126	162	213	16.80498	42.8			
Medium	1-Stretch	17.44	23.6	4699	1128	164	213	17.01245	42.8			
Medium	1-Stretch	17.64	23.6	4699	1130	166	213	17.21992	42.8			
Medium	1-Stretch	17.84	23.6	4699	1132	168	213	17.42739	42.8			

specimen width 5000 5
Slice 1
ARFA 5



Template for Calculating Max load :

SetName	Cycle	Time_S	Temperat	XSize_um	YSize_um	YDisplac	YForce_m	STRAIN	Stress (N/m.m)	specimen width	5000	5	Max	1436
Failure	1-Stretch	0	22	4699	949	0	66	0	13.2	Slice		1	Min	-22
Failure	1-Stretch	0.01	22	4699	949	0	66	0	13.2	AREA		5		
Failure	1-Stretch	0.02	22	4699	949	0	66	0	13.2					
Failure	1-Stretch	0.03	22	4699	949	0	56	0	11.2					
Failure	1-Stretch	0.04	22	4699	950	1	56	0.105374	11.2					
Failure	1-Stretch	0.05	22	4699	951	2	56	0.210748	11.2					
Failure	1-Stretch	0.06	22	4699	952	3	56	0.316122	11.2					
Failure	1-Stretch	0.07	22	4699	953	4	56	0.421496	11.2					
Failure	1-Stretch	0.08	22	4699	954	5	56	0.52687	11.2					
Failure	1-Stretch	0.09	22	4699	955	6	56	0.632244	11.2					
Failure	1-Stretch	0.1	22	4699	956	7	56	0.737619	11.2					
Failure	1-Stretch	0.11	22	4699	957	8	56	0.842993	11.2					
Failure	1-Stretch	0.12	22	4699	958	9	66	0.948367	13.2					
Failure	1-Stretch	0.13	22	4699	959	10	66	1.053741	13.2					
Failure	1-Stretch	0.14	22	4699	960	11	76	1.159115	15.2					
Failure	1-Stretch	0.15	22	4699	961	12	76	1.264489	15.2					
Failure	1-Stretch	0.16	22	4699	962	13	85	1.369863	17					
Failure	1-Stretch	0.17	22	4699	962	13	95	1.369863	19					
Failure	1-Stretch	0.18	22	4699	963	14	95	1.475237	19					
Failure	1-Stretch	0.19	22	4699	964	15	105	1.580611	21					
Failure	1-Stretch	0.2	22	4699	965	16	115	1.685985	23					
Failure	1-Stretch	0.21	22	4699	966	17	124	1.791359	24.8					
Failure	1-Stretch	0.22	22	4699	967	18	124	1.896733	24.8					
Failure	1-Stretch	0.23	22	4699	968	19	134	2.002107	26.8					
Failure	1-Stretch	0.24	22	4699	969	20	134	2.107482	26.8					
Failure	1-Stretch	0.25	22	4699	970	21	134	2.212856	26.8					
Failure	1-Stretch	0.26	22	4699	971	22	134	2.31823	26.8					
Failure	1-Stretch	0.27	22	4699	972	23	134	2.423604	26.8					
Failure	1-Stretch	0.28	22	4699	973	24	134	2.528978	26.8					
Failure	1-Stretch	0.29	22	4699	974	25	124	2.634352	24.8					
Failure	1-Stretch	0.3	22	4699	975	26	124	2.739726	24.8					
Failure	1-Stretch	0.31	22	4699	976	27	124	2.8451	24.8					
Failure	1-Stretch	0.32	22	4699	977	28	124	2.950474	24.8					
Failure	1-Stretch	0.33	22	4699	978	29	124	3.055848	24.8					
Failure	1-Stretch	0.34	22	4699	979	30	124	3.161222	24.8					
Failure	1-Stretch	0.35	22	4699	980	31	124	3.266596	24.8					
Failure	1-Stretch	0.36	22	4699	981	32	124	3.37197	24.8					
Failure	1-Stretch	0.37	22	4699	982	33	134	3.477345	26.8					
Failure	1-Stretch	0.38	22	4699	982	33	134	3.477345	26.8					
Failure	1-Stretch	0.39	22	4699	983	34	134	3.582719	26.8					
Failure	1-Stretch	0.4	22	4699	984	35	124	3.688093	24.8					
Failure	1-Stretch	0.41	22	4699	985	36	124	3.793467	24.8					
Failure	1-Stretch	0.42	22	4699	986	37	124	3.898841	24.8					
Failure	1-Stretch	0.43	22	4699	987	38	124	4.004215	24.8					
Failure	1-Stretch	0.44	22	4699	988	39	124	4.109589	24.8					
Failure	1-Stretch	0.45	22	4699	989	40	124	4.214963	24.8					
Failure	1-Stretch	0.46	22	4699	990	41	124	4.320337	24.8					
Failure	1-Stretch	0.47	22	4699	991	42	124	4.425711	24.8					
Failure	1-Stretch	0.48	22	4699	992	43	124	4.531085	24.8					



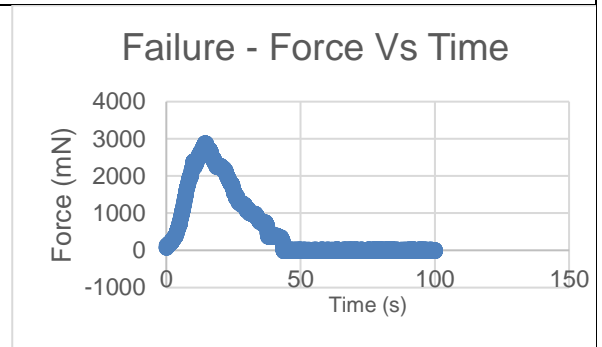
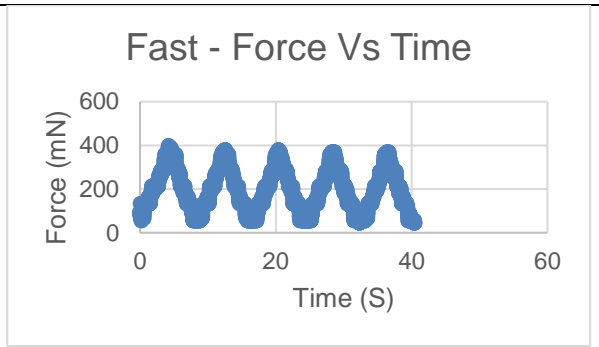
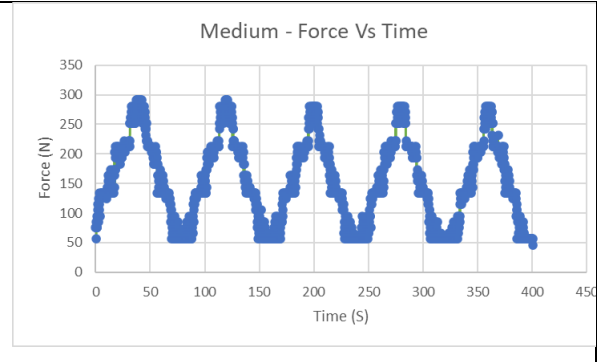
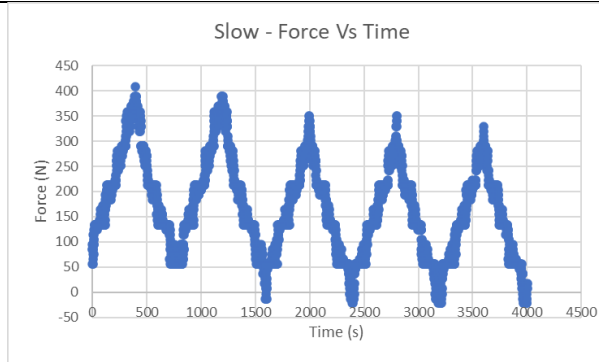
Appendix D

Testing curves (formal test) : Slow, Medium, Fast and Failure for all specimens and regions

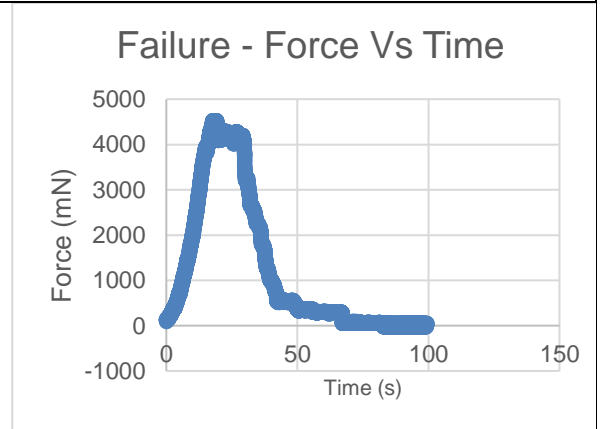
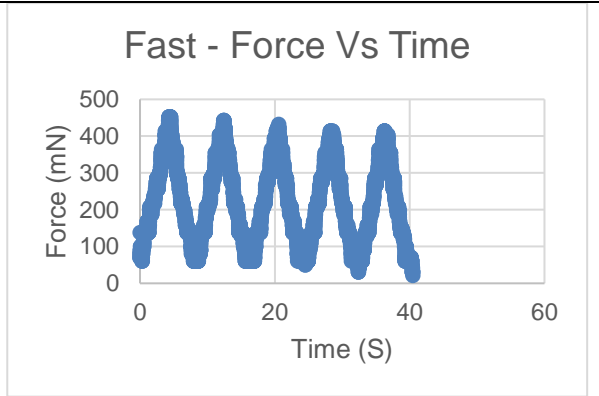
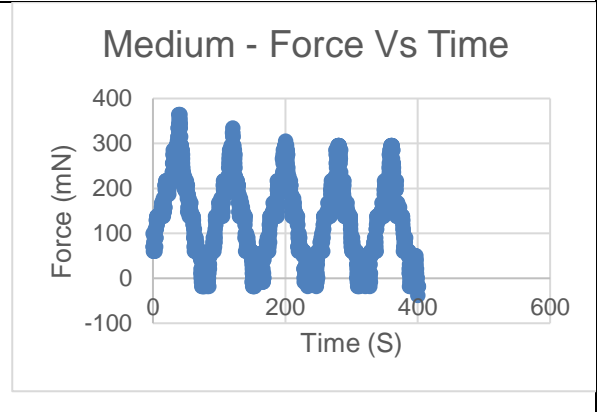
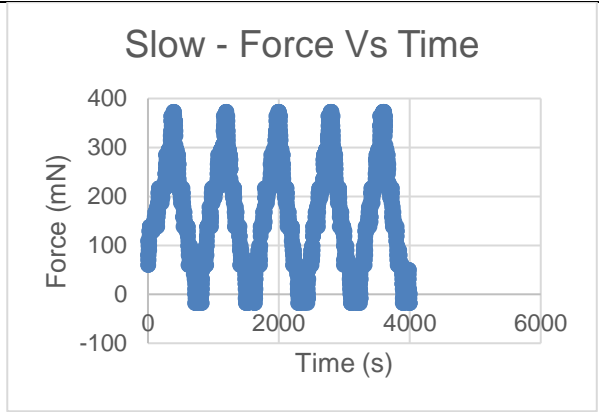
1) Human Test 1 (Grade 4,L4-5) - GL1911471 – Tensile

POS		
PLT		

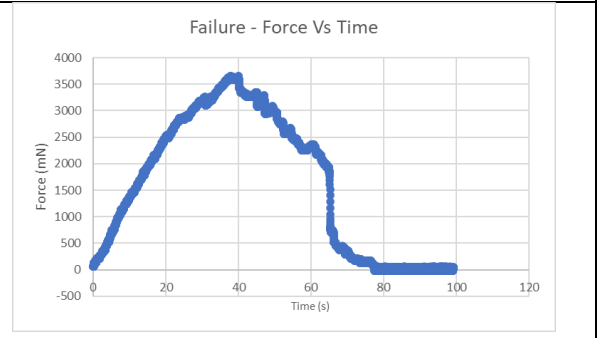
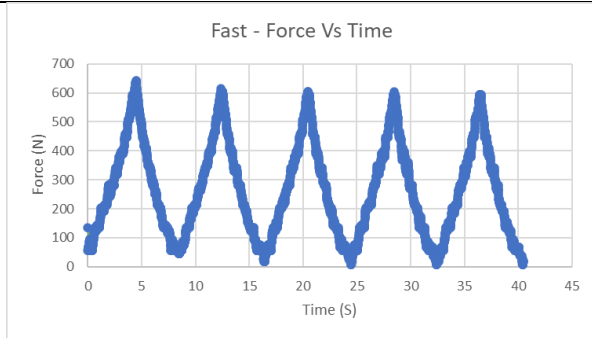
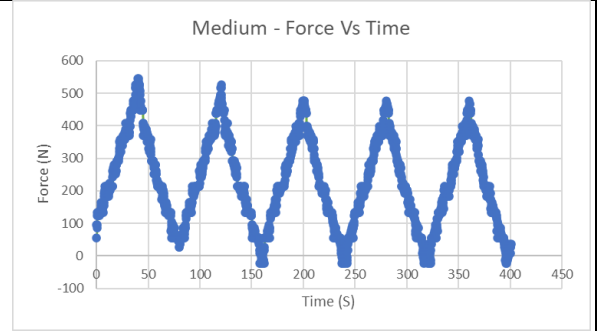
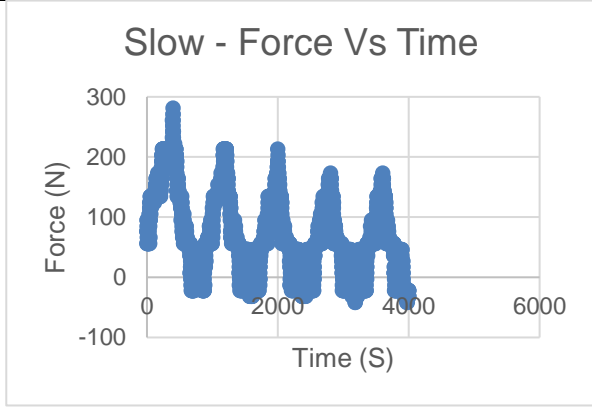
LAT



ANT

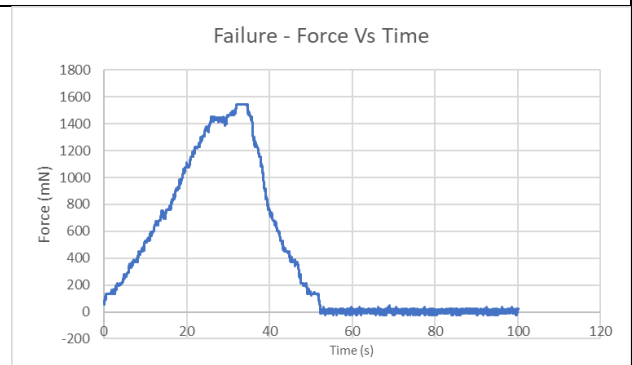
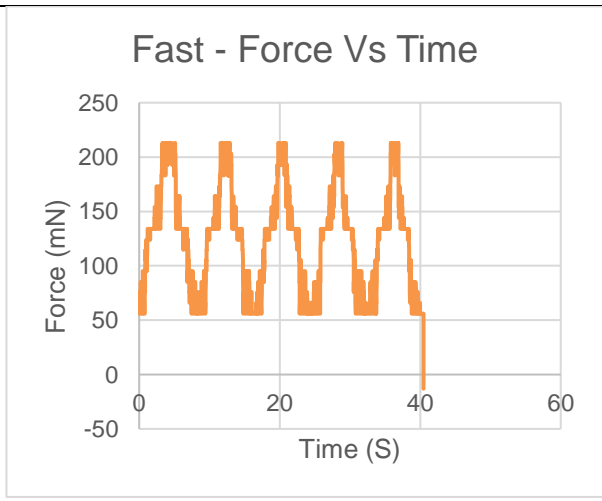
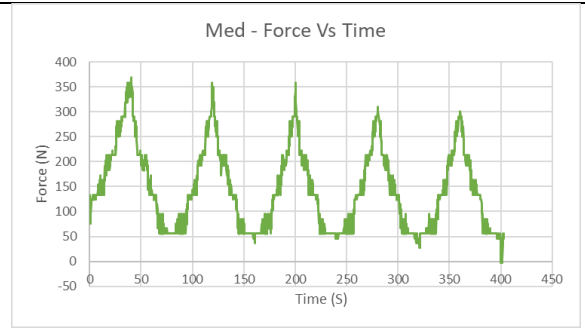
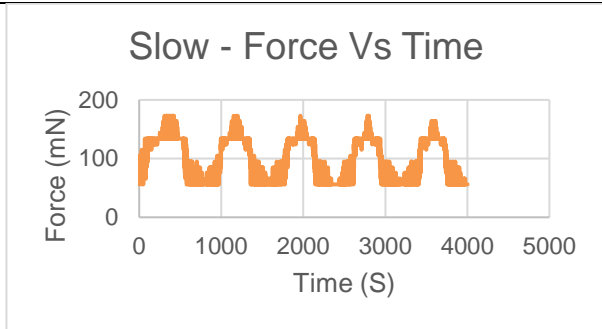


ALT

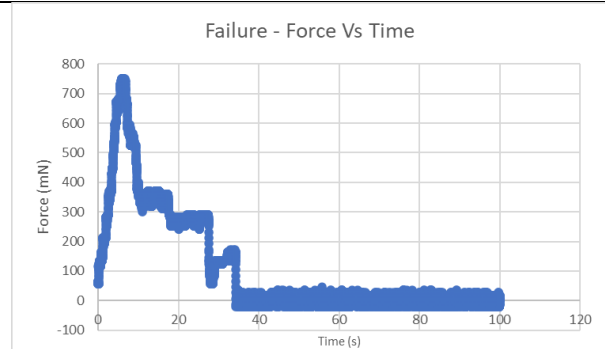
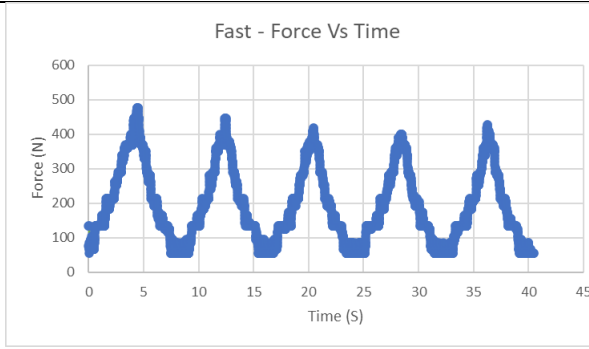
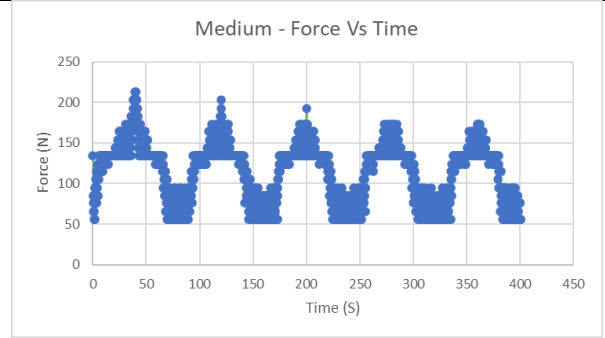
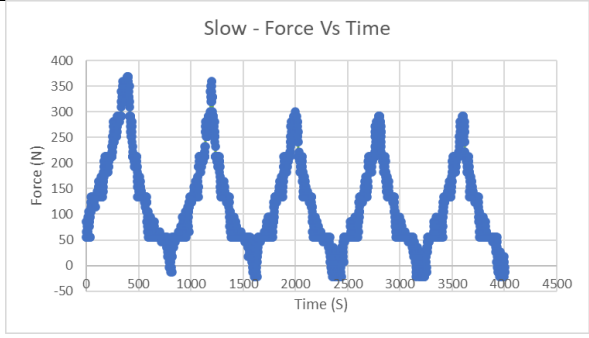


2) Human Test 1 (Grade 4,L4-5) - GL1911471 – Shear

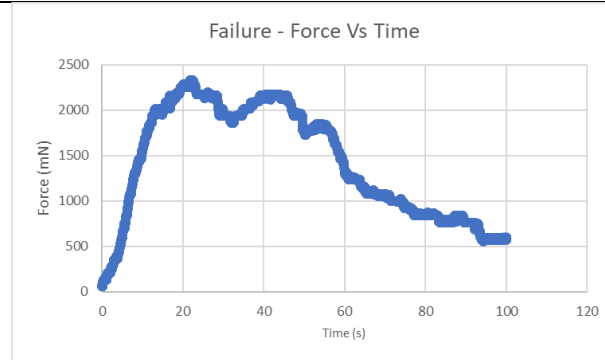
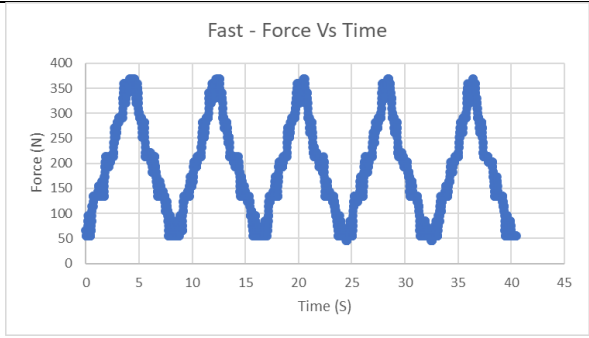
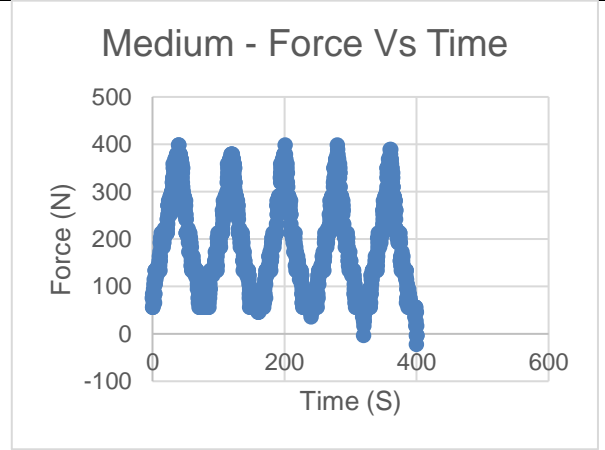
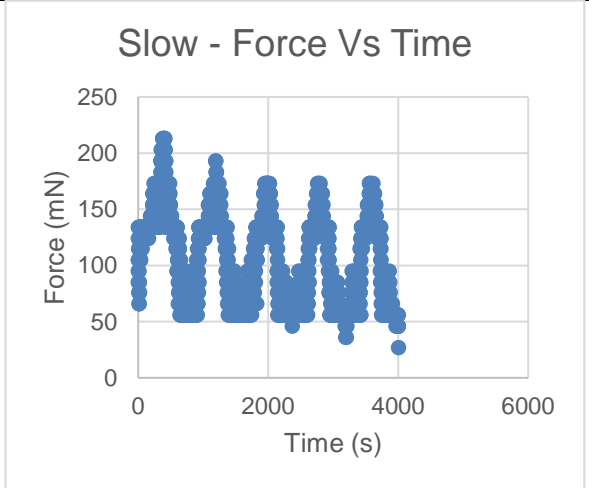
POS



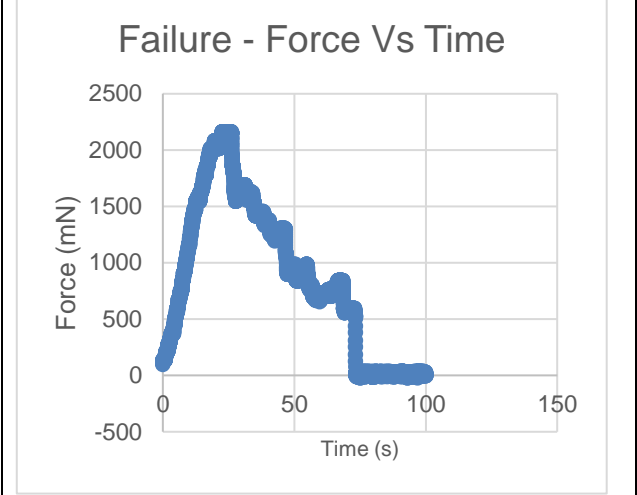
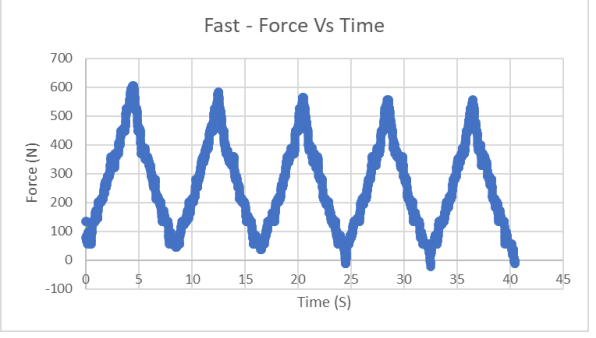
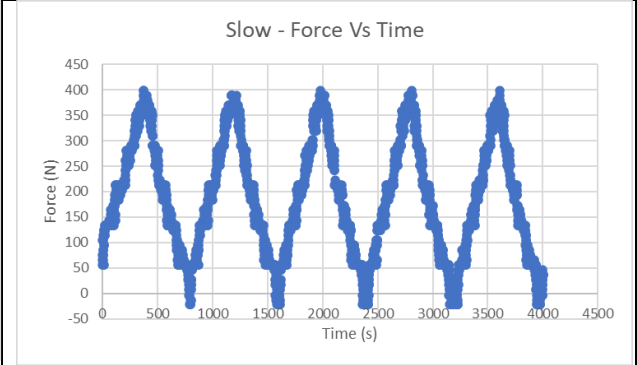
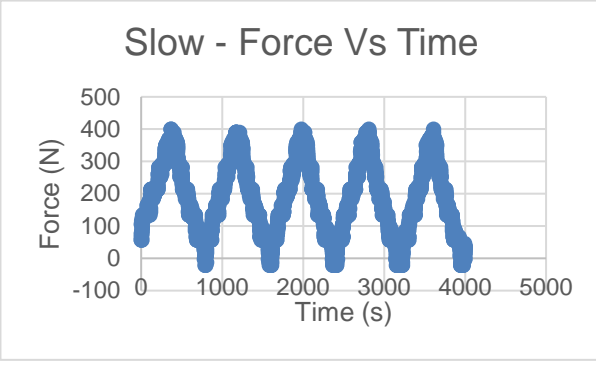
PLT



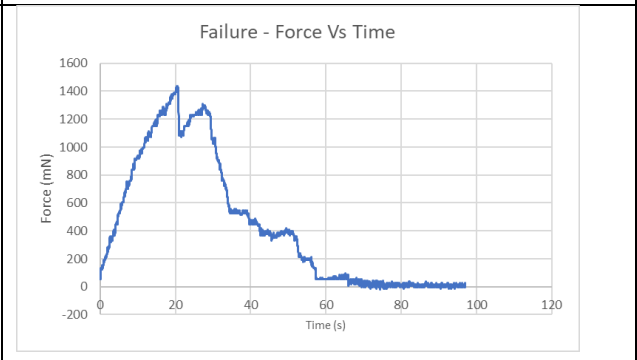
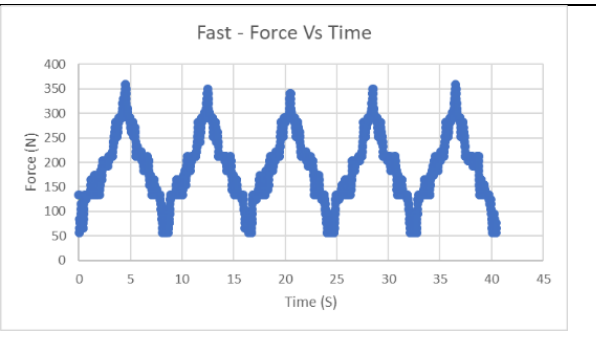
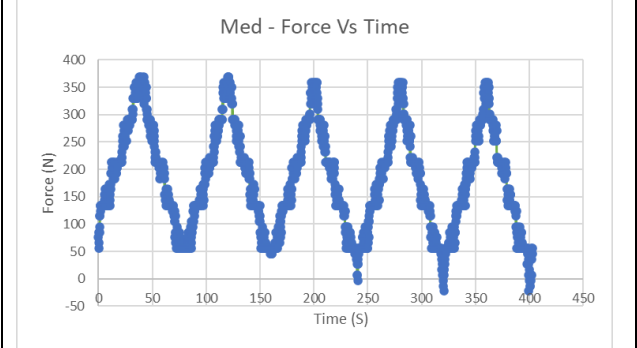
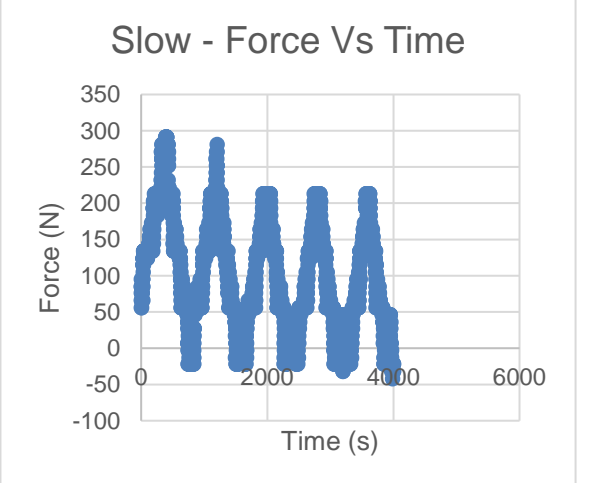
LA
T



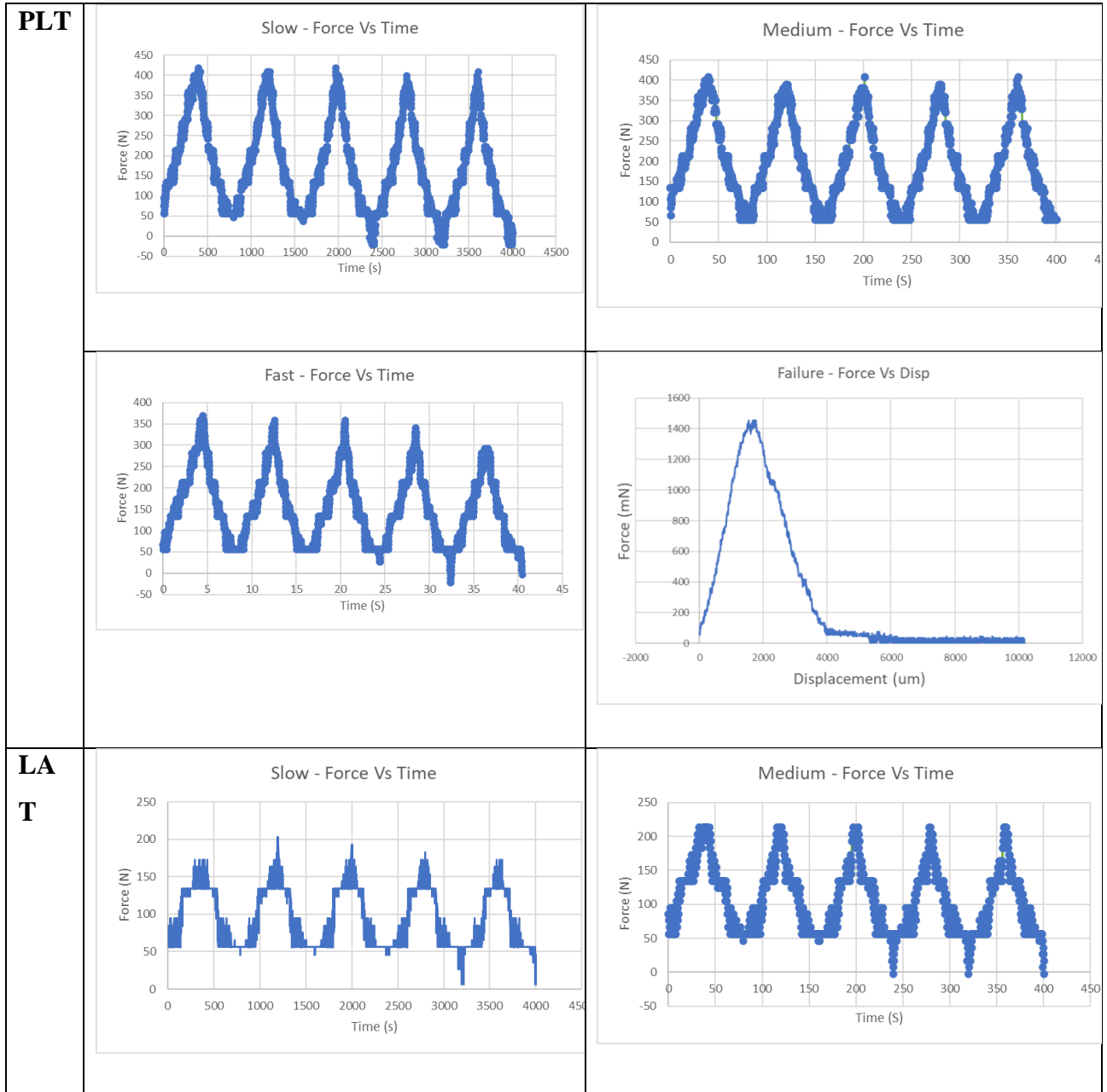
ANT

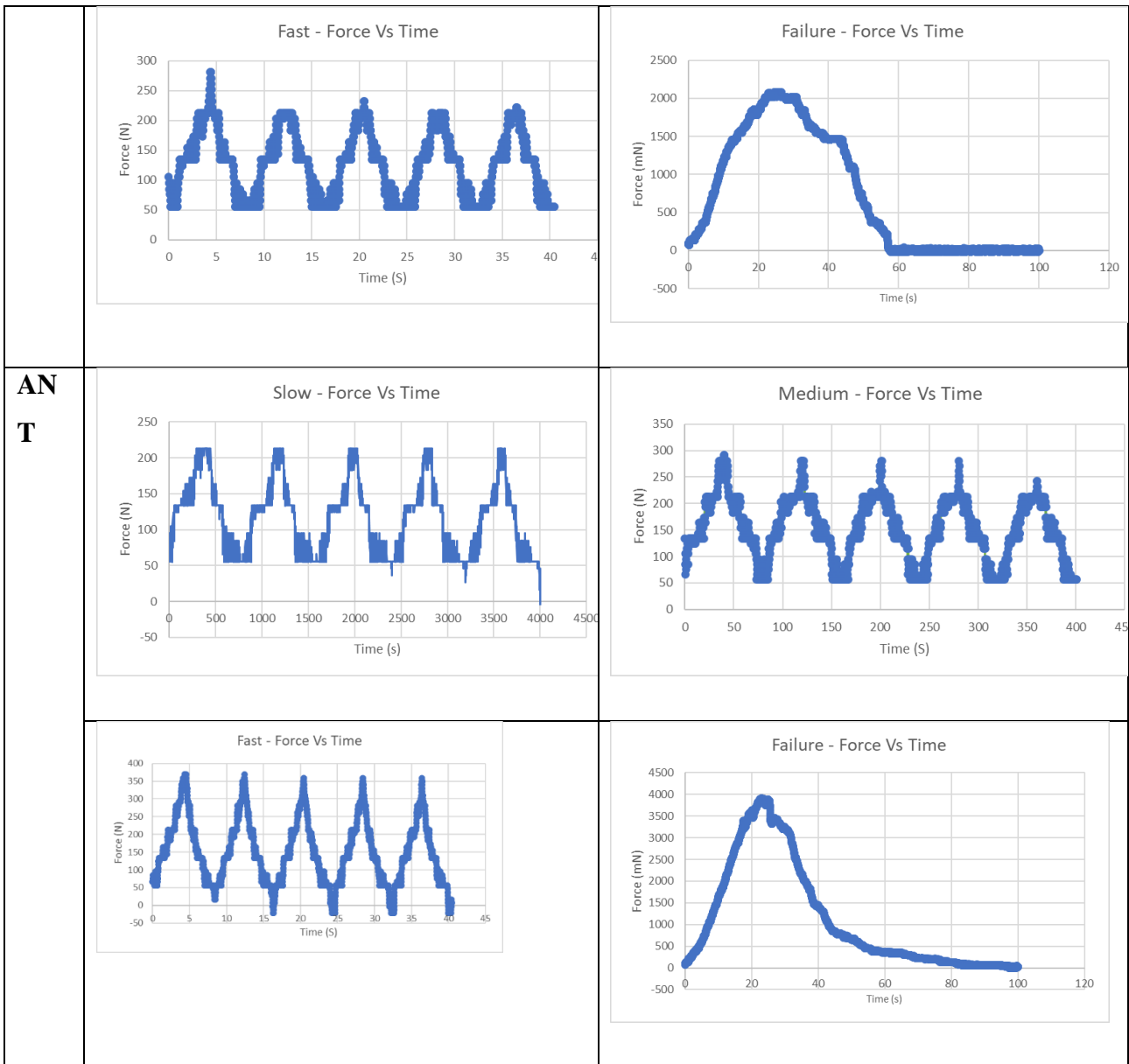


ALT

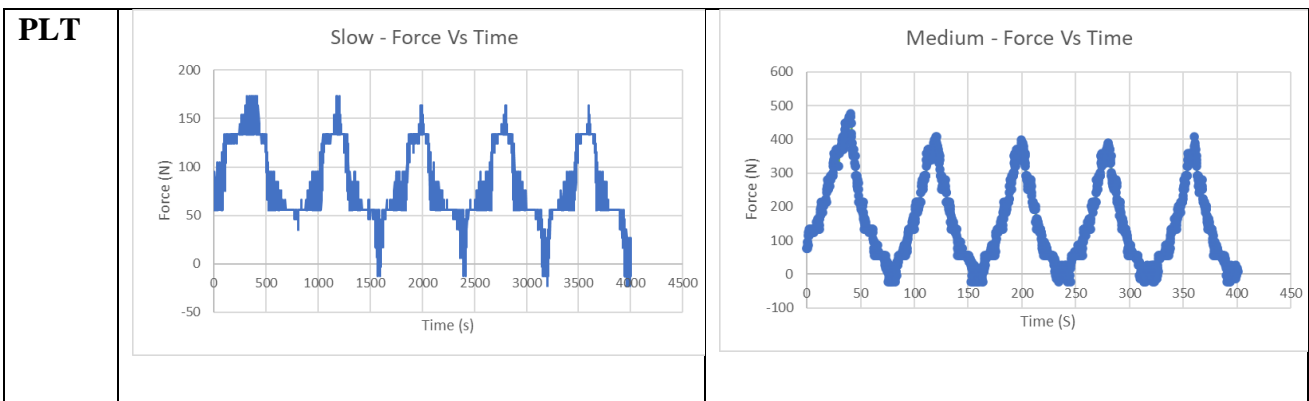


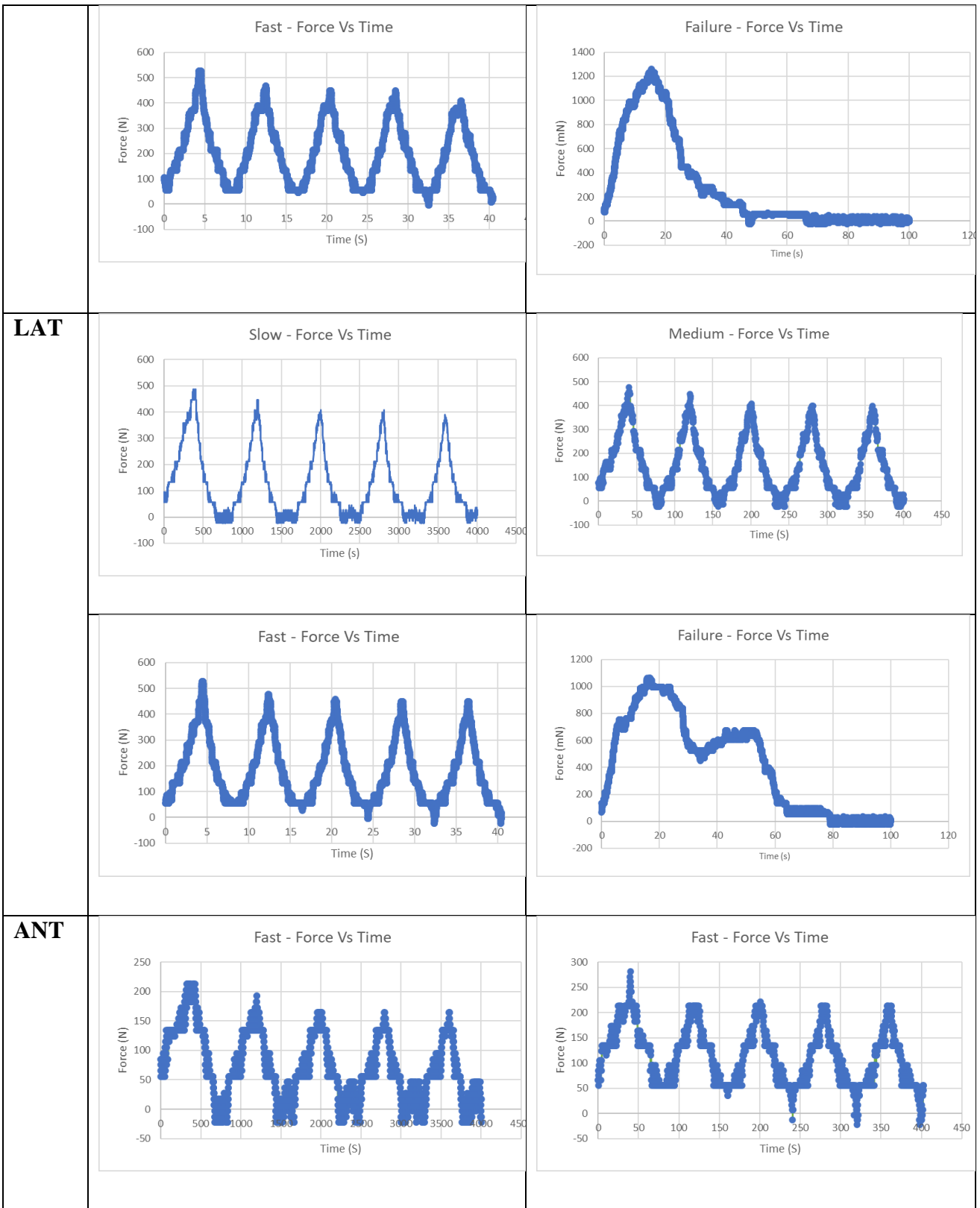
3) Human Test 2 (Grade 2, L3-4) - GL1706406– Tensile

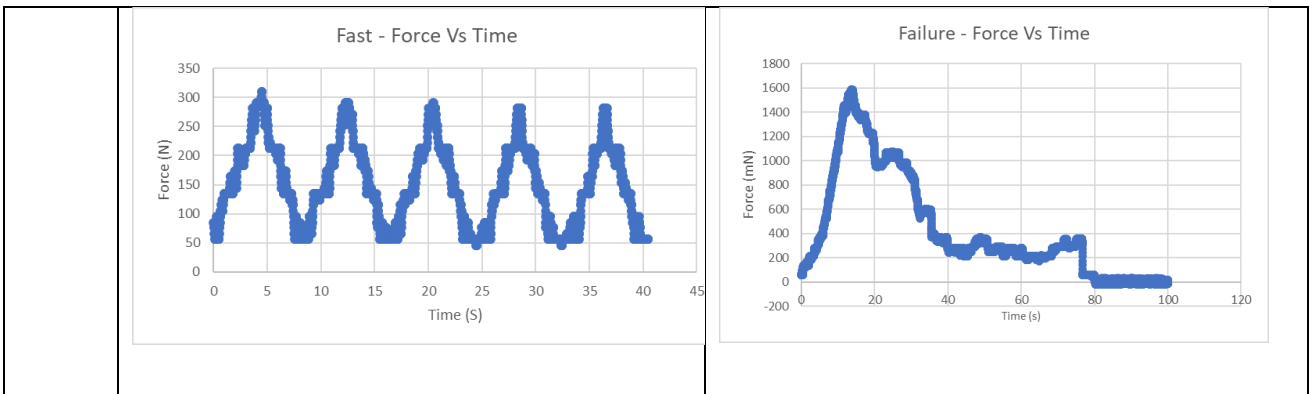




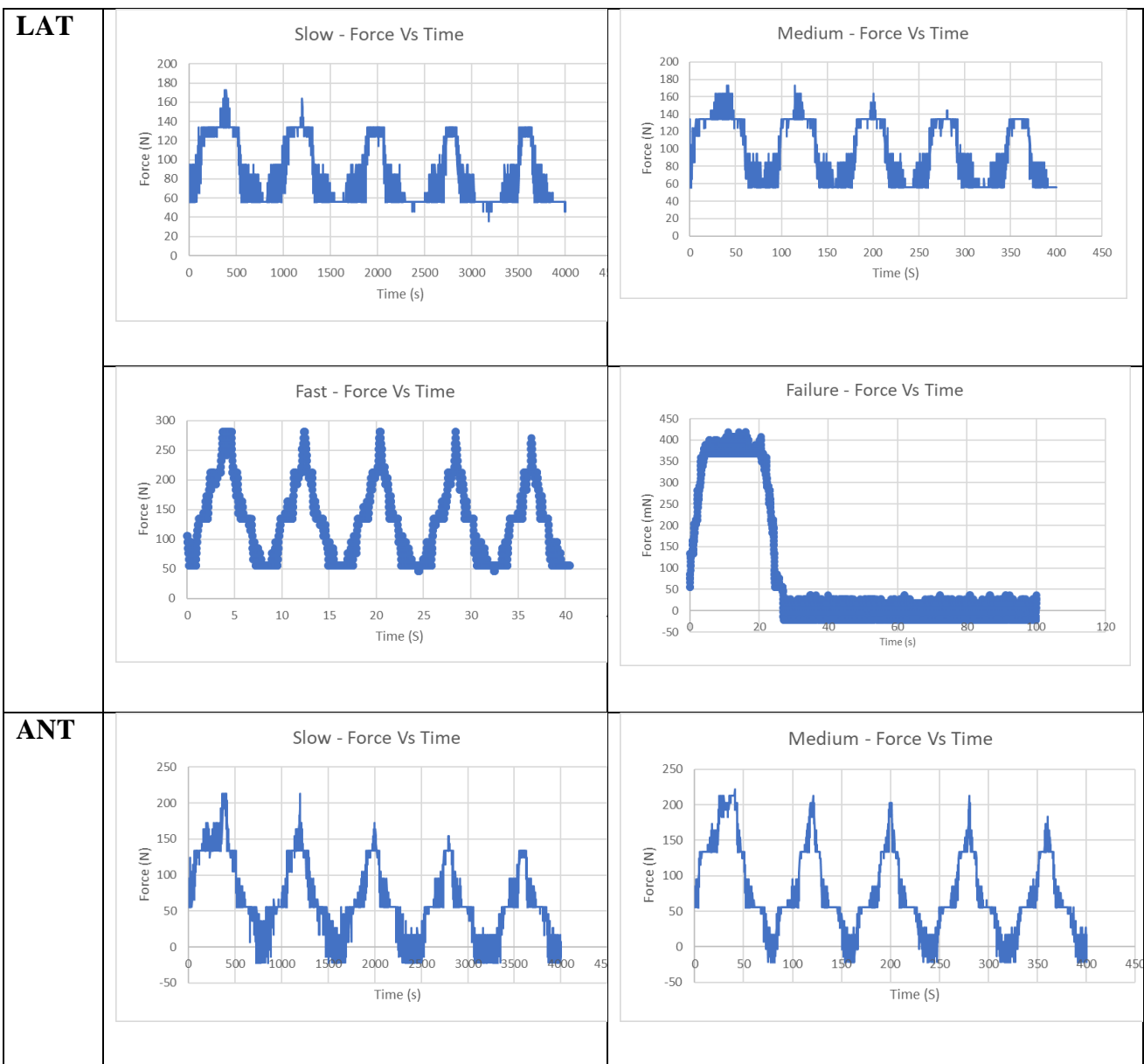
4) Human Test 2 (Grade 2, L3-4) - GL1706406- Shear

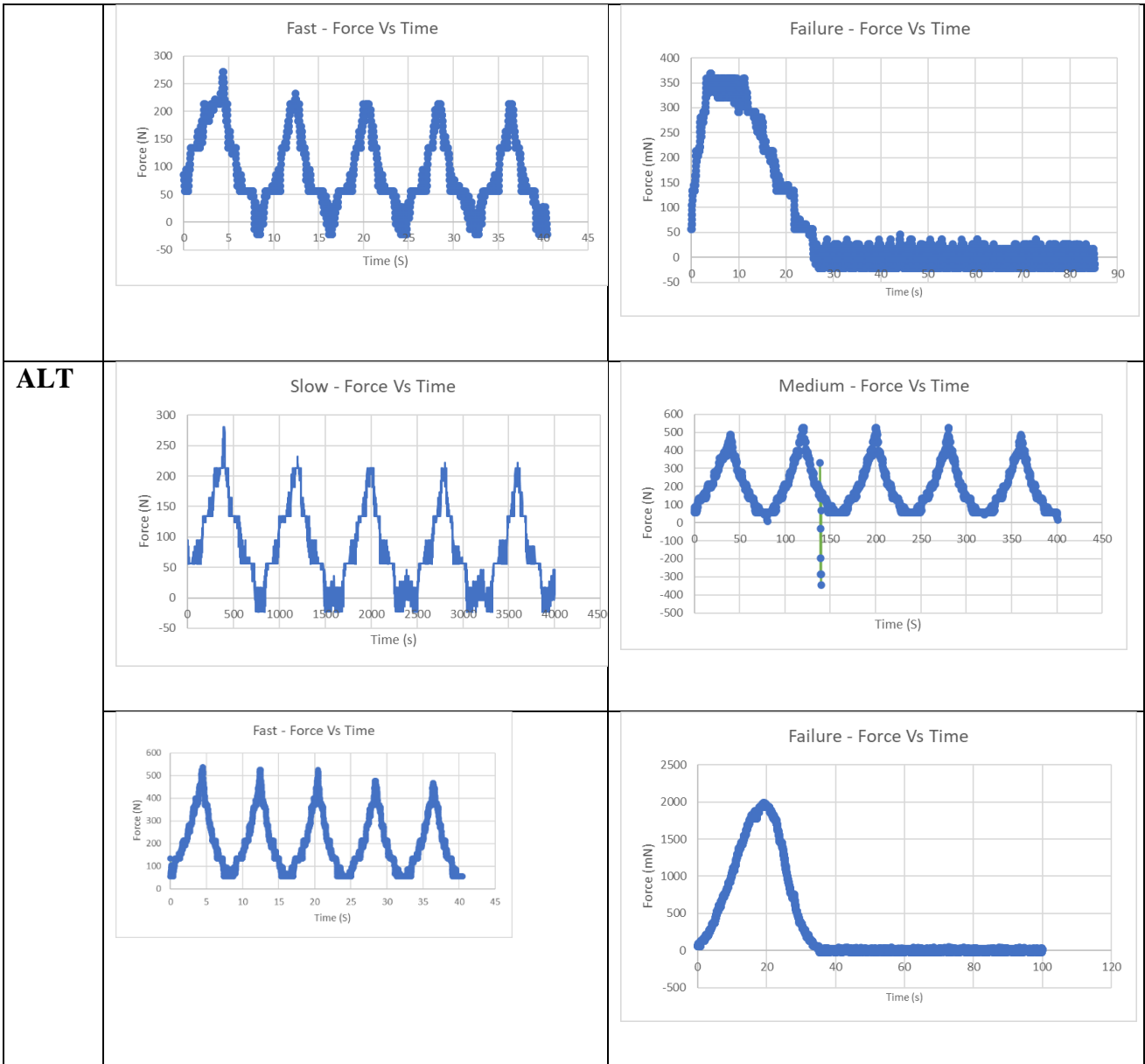




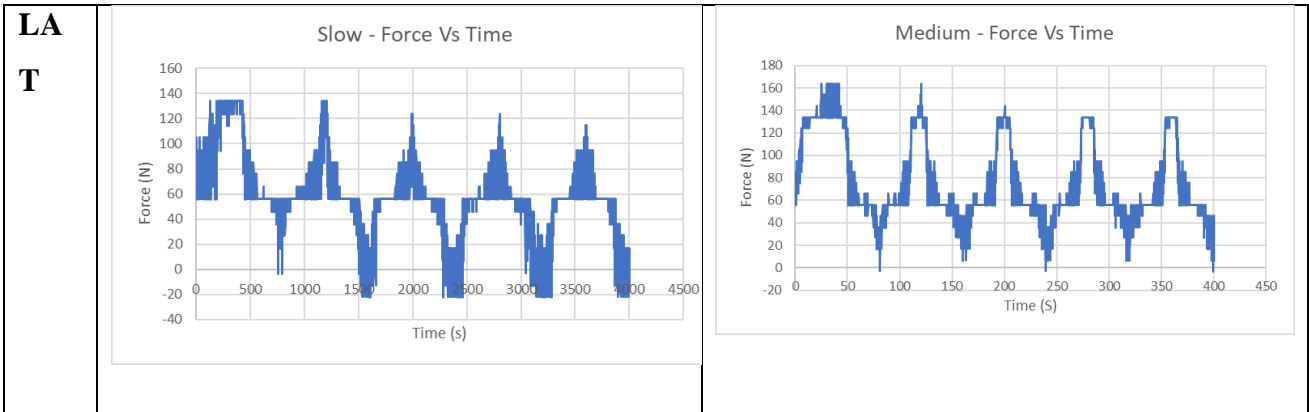


5) Human Test 3 (Grade 4, L4-L5) - W3W39 - 5194

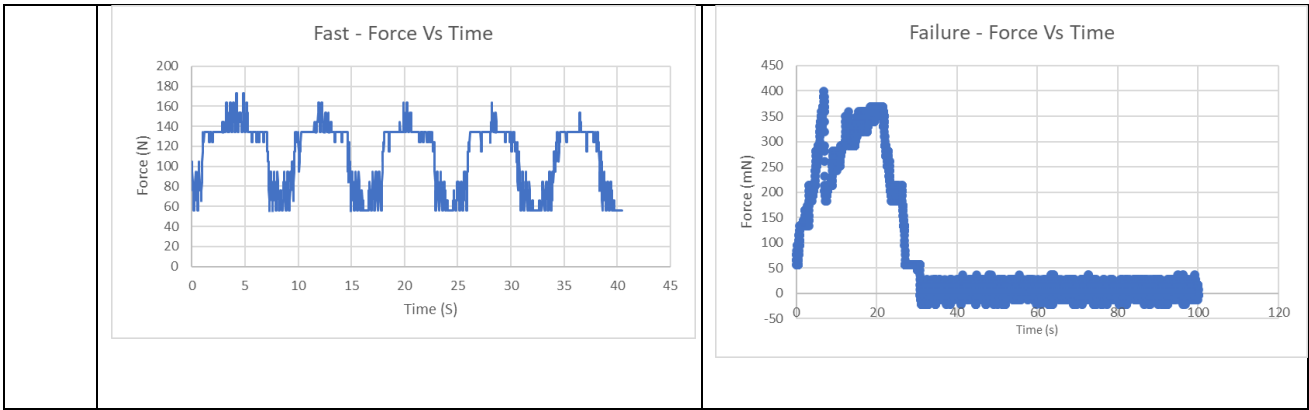




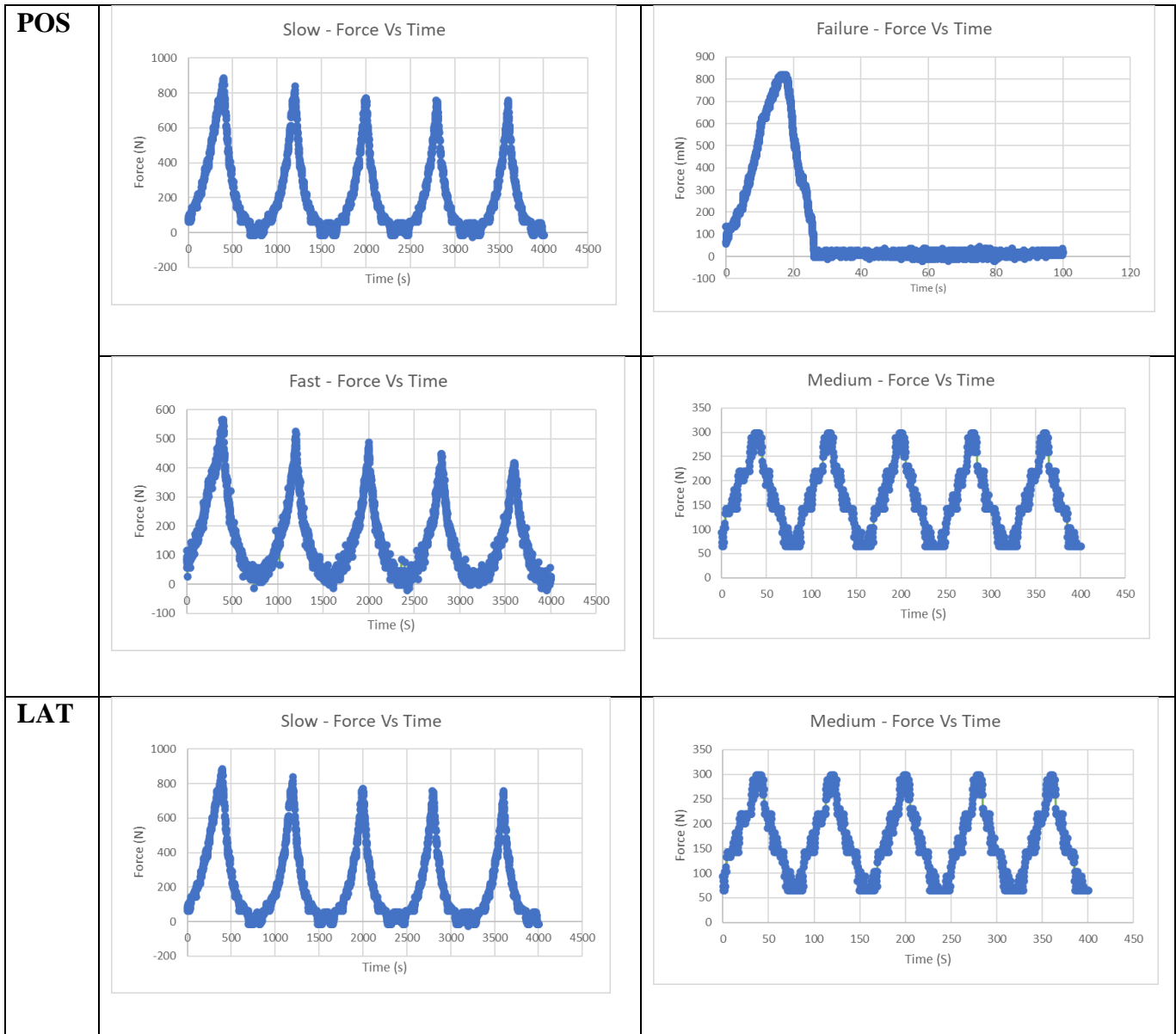
6) Human Test 2 (Grade 2, L3-4) - GL1706406- Shear

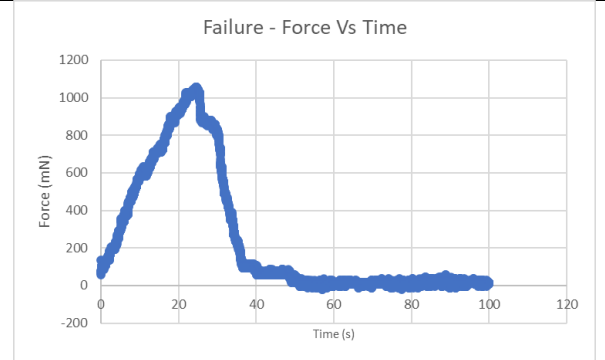
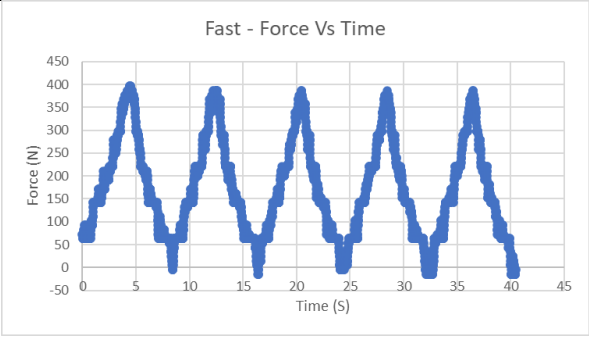


	<p>Fast - Force Vs Time</p>	<p>Failure - Force Vs Time</p>
AN T	<p>Slow - Force Vs Time</p>	<p>Medium - Force Vs Time</p>
	<p>Fast - Force Vs Time</p>	<p>Failure - Force Vs Time</p>
AL T	<p>Slow - Force Vs Time</p>	<p>Medium - Force Vs Time</p>

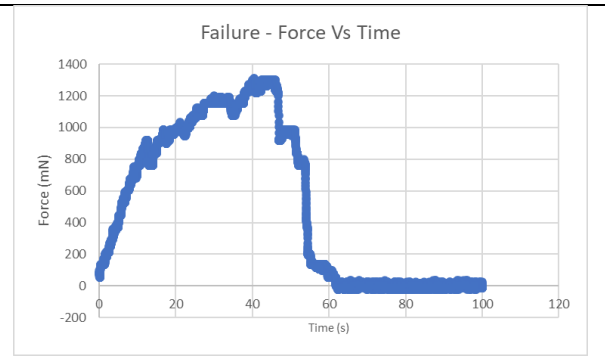
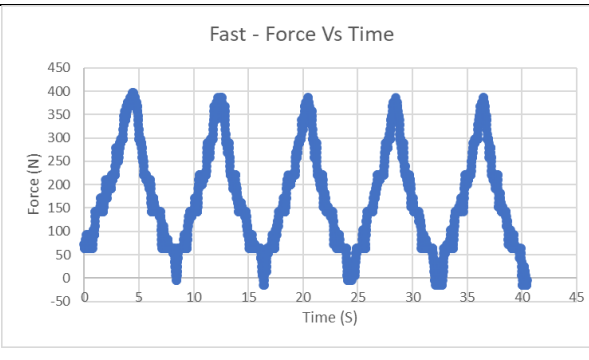
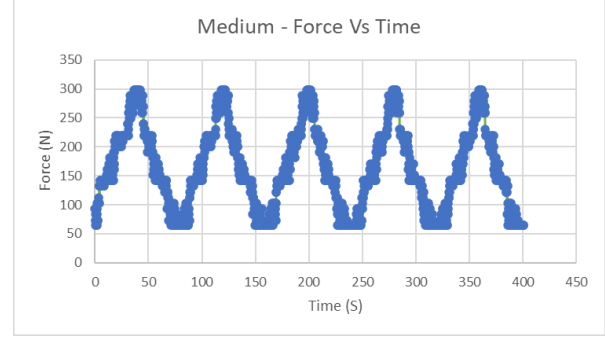
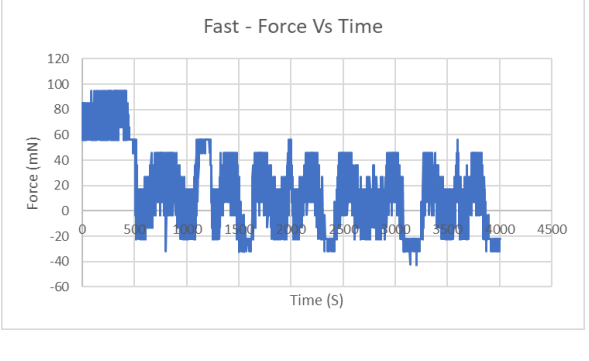


7) Human Test 4 (Grade 2, L5-S1) - W24W25 – 4696 – Tensile



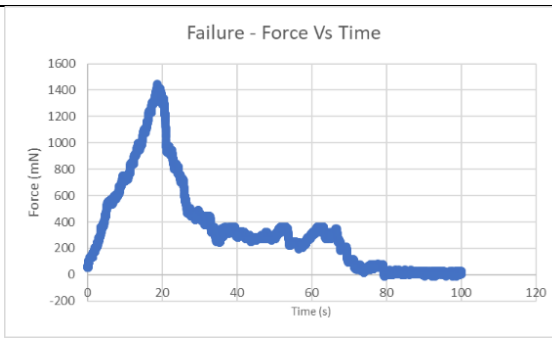
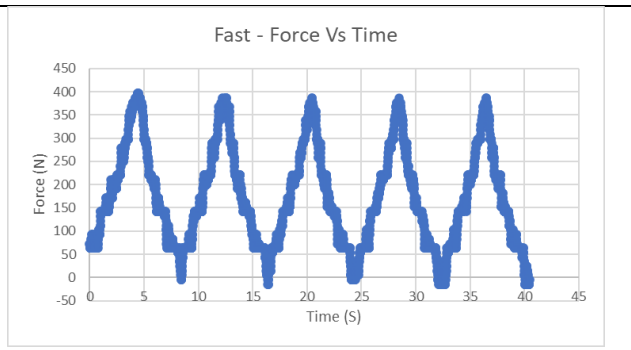
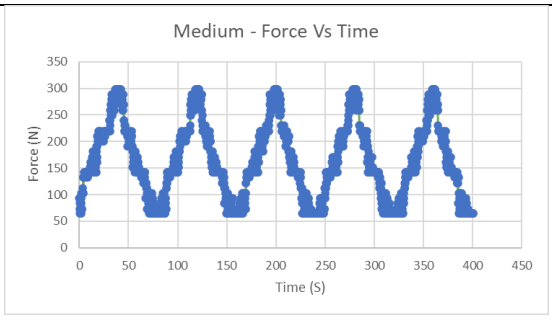
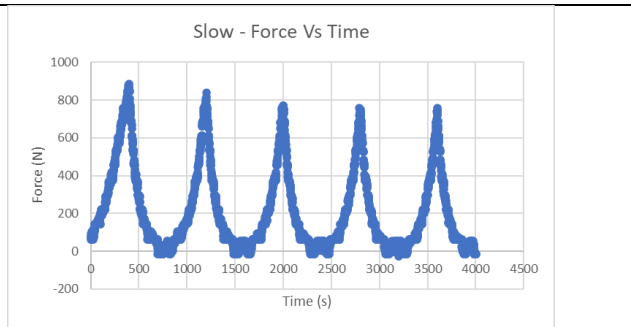


ALT

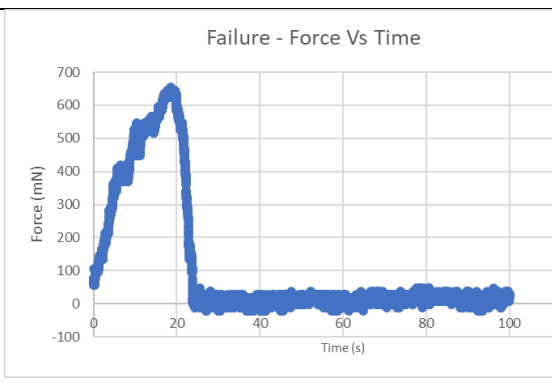
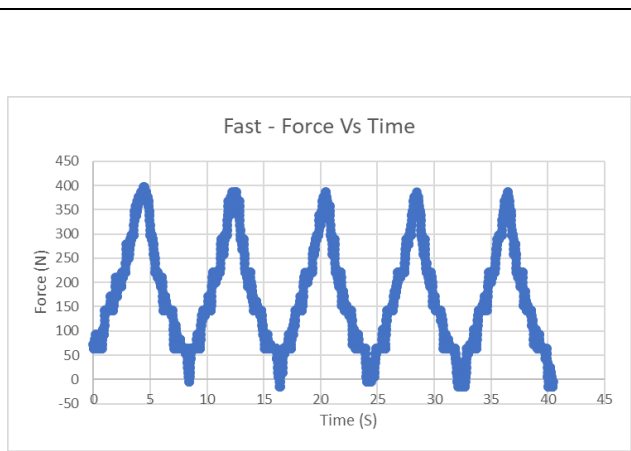
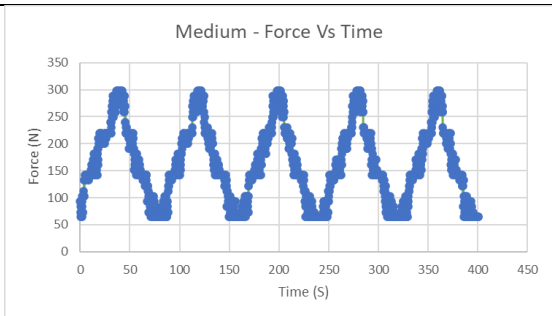
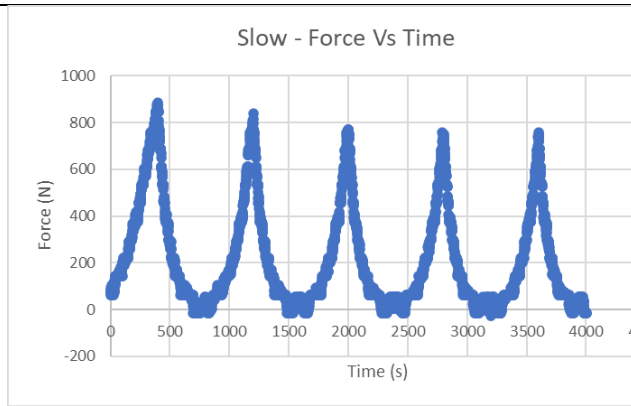


8) Human Test 4 (Grade 2, L5-S1) - W24W25 – 4696 - Shear

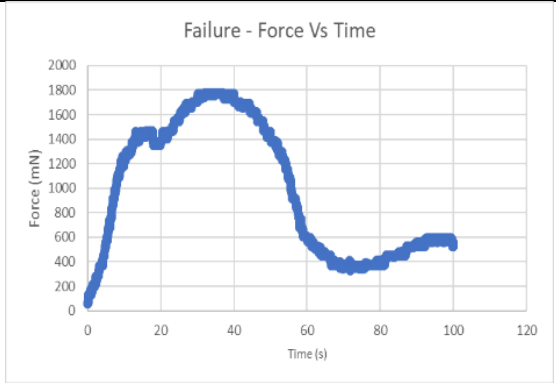
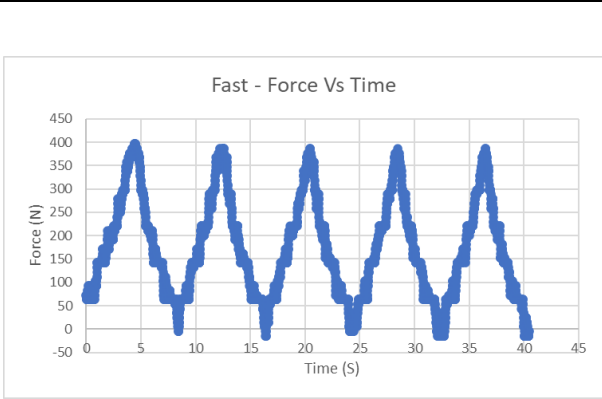
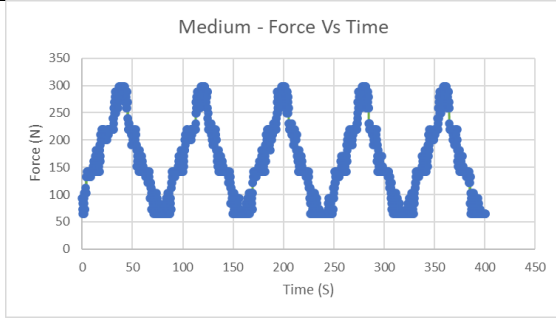
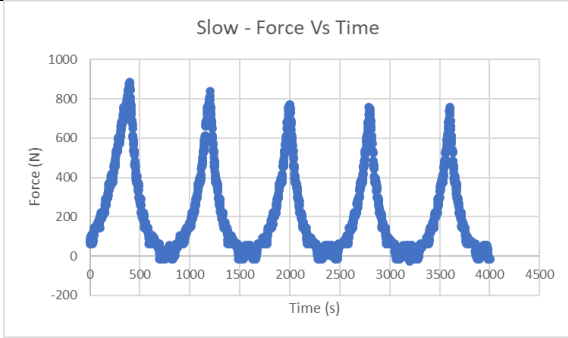
POS



LAT



ALT



Appendix E

Table of energy failure load and energy absorbed for all specimen :

1) Table of stiffness and hysteresis loss coefficient for all healthy specimen

Specim	Directic	Region	Status	Test	Stiffnes	Hysters
4696	TEN	ALT	H	SLW	0.124	-0.07107
4696	TEN	ALT	H	MED	1.76	0.09154
4696	TEN	ALT	H	FST	1.3	0.076145
4696	TEN	LAT	H	SLW	0.73	0.191974
4696	TEN	LAT	H	MED	1.143	0.09154
4696	TEN	LAT	H	FST	2.06	0.07555
4696	TEN	POS	H	SLW	2.71	0.272714
4696	TEN	POS	H	MED	1.388	0.09154
4696	TEN	POS	H	FST	1.73	0.138002
4696	SHR	ALT	H	SLW	1.379	0.196539
4696	SHR	ALT	H	MED	2.87	0.09154
4696	SHR	ALT	H	FST	1.533	0.088056
4696	SHR	LAT	H	SLW	0.7	0.286406
4696	SHR	LAT	H	MED	1.02	0.09154
4696	SHR	LAT	H	FST	1.422	0.139484
4696	SHR	POS	H	SLW	1.23	0.296108
4696	SHR	POS	H	MED	1.6	0.09154
4696	SHR	POS	H	FST	2.84	0.158893
GL406	TEN	ANT	H	SLW	0.957	0.258696
GL406	TEN	ANT	H	MED	0.214	0.146669
GL406	TEN	ANT	H	FST	1.595	0.201207
GL406	TEN	LAT	H	SLW	0.266	0.139016
GL406	TEN	LAT	H	MED	0.47	0.070731
GL406	TEN	LAT	H	FST	1.369	0.067418
GL406	TEN	PLT	H	SLW	2.395	0.198436
GL406	TEN	PLT	H	MED	2.48	0.131213
GL406	TEN	PLT	H	FST	1.76	0.132971
GL406	SHR	ANT	H	SLW	1.67	0.409205
GL406	SHR	ANT	H	MED	0.667	0.126904
GL406	SHR	ANT	H	FST	1.577	-0.04408
GL406	SHR	LAT	H	SLW	3.12	0.26634
GL406	SHR	LAT	H	MED	1.97	0.190051
GL406	SHR	LAT	H	FST	3.473	0.151639
GL406	SHR	PLT	H	SLW	1.03	0.258347
GL406	SHR	PLT	H	MED	3.44	0.263169
GL406	SHR	PLT	H	FST	2.66	0.153968

2) Table of stiffness and hysteresis loss coefficient for all healthy specimen

Specim	Directic	Region	Status	Test	Stiffnes	Hysters
5194	TEN	ANT	D	SLW	0.43	0.166769
5194	TEN	ANT	D	MED	1.65	0.1679
5194	TEN	ANT	D	FST	1.65	0.14673
5194	TEN	ALT	D	SLW	1.82	0.211668
5194	TEN	ALT	D	MED	3.16	0.159343
5194	TEN	ALT	D	FST	3.15	0.074471
5194	TEN	LAT	D	SLW	1.533	0.13174
5194	TEN	LAT	D	MED	0.71	0.094118
5194	TEN	LAT	D	FST	1.58	0.076776
5194	SHR	ANT	D	SLW	0.079	0.324479
5194	SHR	ANT	D	MED	1.75	0.289716
5194	SHR	ANT	D	FST	0.874	0.141534
5194	SHR	ALT	D	SLW	0.64	0.261766
5194	SHR	ALT	D	MED	1.36	0.096656
5194	SHR	ALT	D	FST	0.0438	0.064093
5194	SHR	LAT	D	SLW	0.41	0.175376
5194	SHR	LAT	D	MED	1.32	0.123096
5194	SHR	LAT	D	FST	0.63	0.08693
GL471	TEN	ANT	D	SLW	2.35	0.314463
GL471	TEN	ANT	D	MED	1.64	0.239152
GL471	TEN	ANT	D	FST	1.82	0.104909
GL471	TEN	ALT	D	SLW	1.67	0.299617
GL471	TEN	ALT	D	MED	2.22	0.162003
GL471	TEN	ALT	D	FST	2.98	0.083934
GL471	TEN	LAT	D	SLW	1.387	0.185907
GL471	TEN	LAT	D	MED	0.439	0.054365
GL471	TEN	LAT	D	FST	1.96	-0.0035
GL471	TEN	PLT	D	SLW	2.916	0.185907
GL471	TEN	PLT	D	MED	5.23	0.054365
GL471	TEN	PLT	D	FST	2.93	0.109784
GL471	TEN	POS	D	SLW	0.78	0.227577
GL471	TEN	POS	D	MED	2.12	0.156566
GL471	TEN	POS	D	FST	2.98	0.083934
GL471	SHR	ANT	D	SLW	2.26	0.18735
GL471	SHR	ANT	D	MED	2.24	0.142849
GL471	SHR	ANT	D	FST	2.22	0.042034
GL471	SHR	ALT	D	SLW	1.11	0.161296
GL471	SHR	ALT	D	MED	2.01	0.0718
GL471	SHR	ALT	D	FST	1.64	0.071388
GL471	SHR	LAT	D	SLW	0.258	0.146701
GL471	SHR	LAT	D	MED	2.51	0.153846
GL471	SHR	LAT	D	FST	2.279	0.097442
GL471	SHR	PLT	D	SLW	1.8	0.229828
GL471	SHR	PLT	D	MED	0.373	0.056504
GL471	SHR	PLT	D	FST	2.908	0.107537
GL471	SHR	POS	D	SLW	0.14	0.089135
GL471	SHR	POS	D	MED	1.689	0.09154
GL471	SHR	POS	D	FST	1.16	0.106968

3) Table of failure load and energy absorbed for all specimen

Specimen	Direction	Region	Status	Test	Failure load	Energy absorbed
4696	TEN	ALT	Healthy	FAL	403.4	32,754.437
4696	TEN	LAT	Healthy	FAL	243.7	27,702.717
4696	TEN	POS	Healthy	FAL	161.5	14,019.857
4696	SHR	ALT	Healthy	FAL	319.8	49,720.132
4696	SHR	LAT	Healthy	FAL	403.5	24,977.905
4696	SHR	POS	Healthy	FAL	186.3	26,338.858
5194	TEN	ANT	Degenerated	FAL	39.9	1,967.199
5194	TEN	ALT	Degenerated	FAL	191.5	38,665.811
5194	TEN	LAT	Degenerated	FAL	110.3	7,183.393
5194	SHR	ANT	Degenerated	FAL	109.7	8,375.390
5194	SHR	ALT	Degenerated	FAL	68	2,753.071
5194	SHR	LAT	Degenerated	FAL	146	5,147.854
GL406	TEN	ANT	Healthy	FAL	230.8	90,251.466
GL406	TEN	LAT	Healthy	FAL	245.7	48,807.984
GL406	TEN	PLT	Healthy	FAL	155	24,726.677
GL406	SHR	ANT	Healthy	FAL	139.6	20,118.401
GL406	SHR	LAT	Healthy	FAL	157	21,115.299
GL406	SHR	PLT	Healthy	FAL	155	24,726.677
GL471	TEN	ANT	Degenerated	FAL	178	70,126.663
GL471	TEN	ALT	Degenerated	FAL	327.6	55,526.421
GL471	TEN	LAT	Degenerated	FAL	143	41,692.770
GL471	TEN	PLT	Degenerated	FAL	174.43	32,386.798
GL471	TEN	POS	Degenerated	FAL	229.6	74,359.318
GL471	SHR	ANT	Degenerated	FAL	233.78	59,064.534
GL471	SHR	ALT	Degenerated	FAL	287.2	35,501.149
GL471	SHR	LAT	Degenerated	FAL	221	64,246.364
GL471	SHR	PLT	Degenerated	FAL	150	4,626.660
GL471	SHR	POS	Degenerated	FAL	147.43	32,386.798

4) Calculating median and IQR stiffness of degenerated and healthy - shear tests

Mean stiffness		Shear					
		Healthy			Degenerated		
		GL406	4696	Mean	5194	GL471	Mean
Anterior	Slow				0.079	2.26	1.169
	Medium				1.75	2.24	1.99
	Fast				0.874	2.22	1.54
Anterolateral	Slow				0.64	1.11	0.87
	Medium				1.36	2.01	1.68
	Fast				0.043	1.64	0.84
Lateral	Slow						
	Medium	1.97	1.02	1.49	1.32	2.51	1.91
	Fast	3.47	1.42	2.44	0.63	2.2	1.45
Posterolateral	Slow	1.03		1.03		1.8	1.8
	Medium	3.44		3.44		0.373	0.37
	Fast	2.66		2.66		2.9	2.9
Posterior	Slow		1.23	1.23		0.14	0.14
	Medium		1.6	1.6		1.68	1.68
	Fast		2.84	2.84		1.16	1.16

5) Calculating median and IQR of hysteresis loss coefficient of degenerated and healthy disc - shear tests

Mean Hysteresis loss coefficient		Shear					
		L406	Healthy	Mean	Degenerated	Degenerated	Mean
Anterior	Slow				0.324	0.187	0.259
	Medium				0.289	0.142	0.216
	Fast				0.141	0.042	0.091
Anterolateral	Slow				0.261	0.161	0.211
	Medium				0.096	0.071	0.08

	Fast				0.064	0.071	0.067
Lateral	Slow	0.266	0.28 6	0.276	0.175	0.146	0.161
	Medium	0.19	0.09 1	0.140	0.123	0.153	0.138
	Fast	0.15	0.13 4	0.145	0.086	0.097	0.092
Posterolateral	Slow	0.258		0.258		0.229	0.229
	Medium	0.263		0.263		0.056	0.056
	Fast	0.153		0.153		0.107	0.107
Posterior	Slow		0.29 6	0.296		0.089	0.089
	Medium		0.09 1	0.091		0.091	0.091
	Fast		0.15 8	0.15		0.106	0.106

6) Calculating median & IQR for stiffness – Shear test

Mean stiffness	Shear			Healthy			
		Healthy	Degenerated	Median	25% percentile	75% percentile	IQR
Anterior	Slow		1.16	2.024	1.42	2.70	
	Medium		1.99		0.595	0.681	0.086
	Fast		1.54				
Anterolateral	Slow		0.875				
	Medium		1.68				
	Fast		0.841				
Lateral	Slow						
	Medium	1.49	1.91				
	Fast	2.44	1.45				
					Unhealthy		
Posterolateral	Slow	1.03	1.8	Median	25% percentile	75% percentile	
	Medium	3.44	0.373	1.	0.946	1.77	IQR
	Fast	2.66	2.90		0.554	0.271	-0.283
Posterior	Slow	1.23	0.14				
	Medium	1.6	1.68				
	Fast	2.84	1.16				

7) Calculating median for stiffness – Shear test

Mean Hysteresis loss coefficient	Shear						
		L406	Healthy				
Anterior	Slow			Group 3	Healthy	25% percentile	IQR
	Medium						
	Fast						
Anterolateral	Slow				0.159	0.146	
	Medium					0.013	0.091
	Fast						
Lateral	Slow	0.266	0.286		Unhealthy		
	Medium	0.190	0.092				
	Fast	0.152	0.139				
Posterolateral	Slow	0.258		Median	25% percentile	75% percentile	IQR
	Medium	0.263		0.107	0.090	0.186	
	Fast	0.154			0.017	0.079	0.062686
Posterior	Slow		0.296				
	Medium		0.092				
	Fast		0.159				

8) Calculating Mean stiffness of degenerated and healthy tensile tests

Mean stiffness	Tensile	Healthy			Degenerated		
		GL406	4696	Mean	5194	GL471	Mean
Anterior	Slow	0.957		0.957	0.43	2.35	1.39
	Medium	0.214		0.214	1.65	1.64	1.64
	Fast	1.59		1.59	1.65	1.82	1.73
Anterolateral	Slow				1.82	1.67	1.74
	Medium				3.16	2.22	2.69
	Fast				3.15	2.98	3.06
Lateral	Slow	0.266	0.73	0.5	1.53	1.5	1.53
	Medium	0.47	1.14	0.8	0.71	0.71	0.71
	Fast	1.36	2.06	1.71	1.58	1.58	1.58
Posterolateral	Slow	2.3		2.39		2.91	2.91
	Medium	2.48		2.48		5.23	5.23
	Fast	1.76		1.76		2.93	2.93
Posterior	Slow		2.71	2.71		0.78	0.78
	Medium		1.388	1.38		2.12	2.12

	Fast		1.73	1.73		2.98	2.98
--	------	--	------	------	--	------	------

9) Calculating Mean stiffness of degenerated and healthy tensile tests

Mean Hysteresis loss coefficient	Tensile						
		L406	Healthy	Mean	Degenerated	Degenerated	Mean
Anterior	Slow	0.259		0.259	0.167	0.314	0.241
	Medium	0.147		0.147	0.168	0.239	0.204
	Fast	0.201		0.201	0.147	0.105	0.126
Anterolateral	Slow				0.212	0.300	0.256
	Medium				0.159	0.162	0.161
	Fast				0.074	0.084	0.079
Lateral	Slow	0.139	0.192	0.165	0.132	0.186	0.159
	Medium	0.071	0.092	0.081	0.094	0.054	0.074
	Fast	0.067	0.076	0.071	0.077	-0.004	0.037
Posterolateral	Slow	0.198		0.198		0.186	0.186
	Medium	0.131		0.131		0.054	0.054
	Fast	0.133		0.133		0.110	0.110
Posterior	Slow		0.273	0.273		0.228	0.228
	Medium		0.092	0.092		0.157	0.157
	Fast		0.138	0.138		0.084	0.084

10) Calculating median & IQR for stiffness –tensile test

Mean stiffness	Tensile				Healthy		
				Median	25% percentile	75% percentile	IQ
		Healthy	Degenerated	1.65	0.919	1.91	
Anterior	Slow	0.957	1.39		0.735	0.264	0.471
	Medium	0.214	1.6				
	Fast	1.5	1.7				
Anterolateral	Slow	0	1.7				
	Medium	0	2.69				
	Fast	0	3.06				
Lateral	Slow	0.498	1.533		Degenerated		
	Medium	0.8	0.71	Median	25% percentile	75% percentile	IQR
	Fast	1.7	1.58	1.74	1.55	2.92	
Posterolateral	Slow	2.3	2.91		0.18	1.17	0.989
	Medium	2.48	5.23				
	Fast	1.76	2.93				
Posterior	Slow	2.71	0.78				
	Medium	1.38	2.12				
	Fast	1.73	2.98				

11) Calculating median & IQR for hysteresis loss coefficient – tensile test

Mean Hysteresis	Tensile						
					Healthy		
		Healthy	Degenerated	Median	25% percentile	75% percentile	IQR
Anterior	Slow	0.259	0.241	0.142	0.121	0.199	
	Medium	0.147	0.204		0.02	0.056	0.035
	Fast	0.201	0.126				
Anterolateral	Slow		0.256				
	Medium		0.161				
	Fast		0.079				
Lateral	Slow	0.165	0.159				
	Medium	0.081	0.074				
	Fast	0.071	0.037				
Posterolateral	Slow	0.198	0.186		Degenerated		
	Medium	0.131	0.054	Median	25% percentile	75% percentile	IQR
	Fast	0.133	0.110	0.156	0.081	0.194	
Posterior	Slow	0.273	0.228		0.074	0.038	0.036
	Medium	0.092	0.157				
	Fast	0.138	0.084				